Thèse

Présentée et soutenue publiquement pour l'obtention du titre de

DOCTEUR DE L'UNIVERSITE DE LORRAINE

Mention : Énergie et Mécanique

by **Muhammad Shoaib Ahmed KHAN**

under the supervision of Prof. Riad BENELMIR

Modeling of a pilot installation for the recovery of residual sludge from olive oil extraction, for the production of biofuel by catalytic pyrolysis, integrating a sorption machine driven by solar energy and / or waste heat recovered from pyrolysis gas

January 11, 2022

Jury Members :

Directeur de thèse :	Mr. Riad BENELMIR	Professeur, Université de Lorraine, France
Co-directeur de thèse :	Mr. André DONNOT	Maitre de Conférences, Université de Lorraine, France
Président de jury :	Mr. Mohammed LACHI	Université de Reims Champagne Ardenne, Reims, France
Rapporteurs :	Mme. Fadila MAROTEAUX	Professeur, Université Versailles-Saint-Quentin-en-Yvelines, France
	Mr. Mohammed LACHI	Université de Reims Champagne Ardenne, Reims, France
Examinateurs :	Mr. Philippe ANDRE	Professeur, Université de Liège, Belgique
	Mr. Frank SCHOLZEN	Professeur, Université du Luxembourg, Luxembourg
	Mr. Kamel HALOUANI	Professeur, Université de Sfax, Tunisie
Membres invités :	Mr. Mohammed ELGANAOUI	Professeur, Université de Lorraine, France
	Mr. Stefan MAAS	Professeur, Université du Luxembourg, Luxembourg

Acknowledgment

This work was carried out in LERMAB and I would like to pay my regards to the director of laboratory Philippe GERARDIN and director of doctoral school SIMPPE Christine GERARDIN for approving my application for doctoral thesis.

Prof. Riad BENELMIR has accepted to supervise this thesis. His experience, unfailing support and his daily advice constituted a great contribution for me, not only scientific but above all human. He is a passionate thesis supervisor who gave me valuable advice and a taste for research. I also thank him for his meticulous proofreading of the manuscript.

I would like to express my respectful gratitude to André DONNOT, Senior Lecturer at LERMAB, for monitoring my work, for his infinite availability, his countless hours of technical discussion and guidance and interest and enthusiasm with which he has followed my work. I also thank him for helping out in administrative procedures.

I would like to pay my regards to Higher Education Commission, Islamabad Pakistan (HEC) which sponsored my stay in France during the whole period of my doctorate. Without this scholarship, it was not possible to join a university in France. My thanks go to Lorraine University of Excellence (LUE) for providing me an opportunity for international mobility in Sfax, Tunisia under the mechanism of DrEAM. I would also like to thank Prof. Kamel HALOUANI and Najla GRIOUI for making my stay comfortable in Tunisia and their active participation in experimental data collection and guidance for thermodynamic simulations. It was their utmost support and kindness that kept me afloat during the first confinement in Tunisia.

Thank you also to all those who, in one way or another, supported me and allowed me to have a good time in the laboratory. My second family is therefore made up of: Yassine MASMOUDI, Dalila ABBAZ, Allaoua SOUDANI, Ayoub CHADILI, Muhamed Elyas SAFI, Alaa HAJLAOUI, Lydia LAMHENE and Said SABRI. I would like to extend my gratitude to Corrine COURTEHOUX who helped me in the administrative errands during all the period of my doctorate.

I would also like to thank my international friends and community with whom I spent these three years and shared multi-cultural values and had a wonderful time specially with Nurhidayah, Wahid, Mahdi, Shaheen, Krupali, Asma and Anil.

Finally, I cannot forget my family, more particularly my parents and my siblings who were able to support me in any way they could, which I love so much. This work is also, in its own way, theirs. I present them my infinite gratitude.

Nomenclature

A	Pre-exponential factor (1/s)
AAD	Absolute average deviation
BWI	Bond work index (kWh/ton)
C_i	Concentration of solids in inlet gas
C_o	Concentration of solids in outlet cleaned gas
C_{pg}	Heat capacity of dry gas (kJ/kg.K)
C_{pl}	Heat capacity of moisture in solids (kJ/kg.K)
C_{ps}	Heat capacity of dry solids (kJ/kg.K)
C_{py}	Heat capacity of vapor in gas (kJ/kg.K)
COP	Coefficient of performance
DCF	Discounted cash flow
d_p	Diameter of particle (m)
E	Activation energy (kJ/mol/K)
E	Outlet emission flow rate of solids in cleaned gas (kg/s)
E_{fan}	Heat added due to mechanical work done by fans (kW)
E_{mech}	Heat added by mechanical conveying of material through dryer (kW)
FCI	Fixed capital investment
f_i	Stoichiometric factor
GGE	Gasoline gallon equivalent
HGI	Hardgrove grindability index
h_g	Enthalpy of dry gas (kJ/kg)
h_l	Enthalpy of moisture in liquids (kJ/kg)
h_s	Enthalpy of dry solids (kJ/kg)
h_y	Enthalpy of vapor in gas (kJ/kg)
IC	Indirect cost
h_{ga}	Enthalpy of inlet gas and associated vapor (kJ/kg)
h_{go}	Enthalpy of outlet gas and associated vapor (kJ/kg)
h_{si}	Enthalpy of inlet solids and associated vapor (kJ/kg)
h_{so}	Enthalpy of outlet solids and associated vapor (kJ/kg)
k	Rate constant (1/s)

LF	Location factor
MFSP	Minimum fuel selling price
n	Order of reaction
NPV	Net present value
OMWS	Olive mill waste water sludge
P	Power required (Watt)
Q_i	Inlet gas flow rate (kg/s)
Q_g	Heat provided at the generator of absorption machine (KW)
Q_h	Heat input from heater (kW)
Q_{wl}	Wall heat loss from dryer (kW)
R	Reaction rate (kg/m^3.s)
R	Gas constant (J/mol/K)
R_e	Reynolds number
TDIC	Total direct and indirect cost
TIC	Total installed cost
TPEC	Total purchase equipment cost
TPI	Total project investment
u_{mf}	Minimum fluidization velocity (m/s)
V_p	Volume of spherical particle (m^3)
W_c	Work of compression (kW)
W_g	Mass flow rate of the dry gas (kg/s)
W_s	Mass flow rate of dry solids (kg/s)
W_s	Mass of solids in fluidized bed reactor (kg)
X_F	Diameter larger than 80% of feed particle mass (m)
X_P	Diameter larger than 80% of product particle mass (m)
X_i	Moisture content of entering solids, dry basis (kg/kg)
X_o	Moisture content of exhaust solids, dry basis (kg/kg)
Y_i	Absolute humidity of inlet gas (kg/kg)
Y_o	Absolut humidity of exhaust gas (kg/kg)
e	Absolute average deviation
ε	Void fraction
ε_{mf}	Void fraction at minimum fluidization velocity
ρ_c	Density of particle (kg/m^3)

ρ_g	Density of gas (kg/m^3)
λ_o	Latent heat of evaporation (kJ/kg)
λ	Circulation ratio
Ψ	Sphericity of particle

Table of Contents

CHAPTER 1: LITERATURE REVIEW 18
1.1 Introduction 18
1.2 Fundamentals of pyrolysis process 20
1.2.1 Process Description 20
1.2.2 Feedstock for pyrolysis 21
1.2.3 Types of pyrolysis 22
1.2.4 Applications of bio-oil 25
1.2.5 Importance of biochar 25
1.3 Pyrolysis reactors 25
1.4 Modeling of pyrolysis 28
1.5 Exergy 31
1.6 Cost of bio-oil 35
1.7 Waste heat for Process cooling 39
1.7.1 Absorption cooling system 40
1.7.1.1 Process description 41
1.7.1.2 Generator 43
1.7.1.3 Condenser 43
1.7.1.4 Evaporator 43
1.7.1.5 Absorber 43
1.7.2 Important Features 44
1.8 Modeling of absorption chiller in Aspen Plus 44
1.9 Life cycle assessment (LCA) 45
1.9.1 Introduction 46
1.9.2 LCA of biofuel production systems 47

1.9.3 Previous studies 48
1.9.4 Methodology 49
1.9.4.1 The system function and the functional unit 49
1.9.4.2 Description of the scenarios 50
1.9.4.3 The limits and boundaries of the system 50
1.9.4.4 Data and assumptions 50
1.9.4.5 Life Cycle Inventory Analysis 50
1.9.4.6 Environmental impact assessment 51
1.9.4.7 Interpretation and recommendations 52
1.9.4.8 Rules of allocation 52
CHAPTER 2: METHODOLOGY 54
2.1 Experimental process overview 54
2.1.1 Feedstock handling and preparation 55
2.1.2 Pyrolysis 55
2.1.3 Solids preparation 55
2.1.4 Vapor Condensation 56
2.1.5 Product Yields 56
2.1.5.1 Bio-oil Composition 56
2.1.5.2 Non-condensable gases (NCG) 57
2.2 Lab-scale model development 58
2.2.1 Feedstock pretreatment 59
2.2.2 Pyrolysis 59
2.2.3 Condensers 61
2.3 Scaling up from lab to industrial scale 64
2.3.1 Industrial Scale 65
2.3.2 Industrial scale model development 66
2.3.2.1 Feedstock preparation (Area 100) 66

2.3.2.2 Crushing 68
2.3.2.3 Pyrolysis (Area 200) 70
2.3.2.4 Solids removal (Area 300) 73
2.3.2.5 Bio-oil Condensation (Area 400) 74
2.3.2.6 Refrigeration machine (Area 500) 74
2.3.2.7 Heat Generation (Area 600) 82
2.3.2.8 Electricity generation (Area 700) 83
2.4 Performance parameters 86
2.5 Economic analysis 86
2.6 Life cycle assessment 90
2.6.1 Goal and scope definition 90
2.6.2 Functional unit 90
2.6.3 System boundaries 90
2.6.4 Inventory analysis 91
CHAPTER 3: RESULTS AND DISCUSSION 94
3.1 Model validation 94
3.2 Industrial scale 99
3.2.1.1 Feedstock drying 99
3.2.1.2 Grinding 100
3.2.1.3 Fluidized bed reactor 100
3.2.1.4 Condensation 101
3.2.1.5 Heat Generation 101
3.3 Exergy analysis 105
3.4 Process performance 107
3.5 Economic assessment 108
3.5.1 Total project investment and operating cost 108
3.5.2 Sensitivity analysis 110

3.5.3 Monte Carlo sensitivity analysis 112
3.6 Life cycle assessment 113
Annex I 138
Annex II 139
Annex III 149
Annex IV 151
Annex V 152

List of Tables

Table 1.1. Modes of pyrolysis 23
Table 1.2. The comparison of bio-oil produced from fast pyrolysis of OMWWS and diesel [1][19] 24
Table 1.3. Overview of fast pyrolysis reactors for bio-oil production [16,20] 26
Table 1.4. Summary of advantages and disadvantages of different reactors for biomass pyrolysis 26
Table 1.5. Developed pyrolysis reaction models and kinetics [36,37] 30
Table 1.6. Standard chemical exergies and standard entropies of compounds. 34
Table 1.7. Commercial worldwide bio-oil productions technologies [61] 36
Table 2.1. OMWS attributes 55
Table 2.2. OMWS product yields 56
Table 2.3. Bio-oil composition 57
Table 2.4. NCG composition 58
Table 2.5. fi determined from experimental data of Agblevor et. al. [1] 60
Table 2.6. Components used in Aspen Plus 61
Table 2.7. Aspen Plus unit models 64
Table 2.8. State point assumptions 80
Table 2.9. Operating cost parameters 88
Table 2.10. Inputs for DCF analysis 88
Table 2.11. Variation in different parameters 88
Table 2.12. Total project investment estimation method 89
Table 2.13. Inventory data for energy inputs associated with different processes for 100 tonnes/day of OMWS 91
Table 2.14 type and distance of transport 92
Table 3.1. Comparison of simulation and experimental results 94
Table 3.2. Absolute average deviation for different temperatures 94
Table 3.3. Absorption refrigeration machine operating parameters 101
Table 3.4. Ultimate analysis of biochar (ash free) 102
Table 3.5. Energy balance 102
Table 3.6 Mass flows for different streams in Aspen Plus model 103

Table 3.7. Standard chemical exergy of some gases at 25°C, 0.1 MPa 105
Table 3.8. Exergy analysis 106
Table 3.9. Mass and energy flowrates 108
Table 3.10. Non-renewable energy demand (NRE) and global warming potential (GWP) for 1-kg bio-oil produced in different scenarios 116

List of Figures

Figure 1.1. Olive mill wastewater evaporation pond 19
Figure 1.2. Pyrolysis of biomass 21
Figure 1.3. A glance at feedstock availability and energy products from biomass pyrolysis .. 22
Figure 1.4. Influence of residence time, temperature and heating flux on gas, bio-oil and biochar produced by pyrolysis of wood 24
Figure 1.5. A common schematic of bubbling fluidized bed reactor 28
Figure 1.6. Aspen plus flowsheet of reactor model 32
Figure 1.7. Absorption cooling system 41
Figure 1.8. Process diagram of absorption cooling system 42
Figure 1.9. The phases of a life cycle assessment (ISO 14044, 2006) 47
Figure 1.10. Classification of impact categories according to the Impact 2002+ method 51
Figure 2.1. Schematic diagram of pyrolysis of OMWS 54
Figure 2.2. Schematic diagram of shell and tube type heat exchanger 56
Figure 2.3. Coupling of external user sub-routine with Aspen Plus 59
Figure 2.4. Aspen Plus flowsheet of catalytic fast pyrolysis process of OMWS 63
Figure 2.5. Upscaling from lab to industrial scale fluidized bed reactor 65
Figure 2.6. Process overview of industrial plant 66
Figure 2.7. Hammer mill 69
Figure 2.8. Fluidized bed reactor 70
Figure 2.9. Cyclone 73
Figure 2.10. Standard vapor compression system 75
Figure 2.11. Compression refrigeration machine modelled in Aspen Plus 76
Figure 2.12. Single effect absorption cycle 77
Figure 2.13. Absorption machine model implemented in Aspen Plus 80
Figure 2.14. Process flow diagram with compression refrigeration machine 84
Figure 2.15. Process flow diagram with absorption refrigeration machine 85
Figure 2.16. Methodology flow chart 87
Figure 2.17. System boundaries for bio-oil production via fast pyrolysis 91
Figure 3.1. Comparison between simulation and experimental yields at different temperatures 96
Figure 3.2. Gas composition of OMMWS at different temperatures 97
Figure 3.3. Composition of bio-oil for catalytic fast pyrolysis at 450°C. 98
Figure 3.4. Overall mass balance 99

Figure 3.5. Exergy destruction in different processes 107
Figure 3.6. Total capital cost investment proportions for scheme-1 109
Figure 3.7. Total capital cost investment proportions for scheme-2 109
Figure 3.8. Operating cost proportions 110
Figure 3.9. Scheme-1: Sensitivity of MFSP 111
Figure 3.10. Scheme-2: Sensitivity of MFSP 112
Figure 3.11. Monte Carlo sensitivity analysis for scheme-1 113
Figure 3.12. Monte Carlo sensitivity analysis for scheme-2 113
Figure 3.13. Non-renewable energy demand for three scenarios 115
Figure 3.14. Global warming potential for three scenarios 115
Figure 3.15. Non-renewable energy demand and global warming potential for different countries for scheme-1 117
Figure 3.16. Non-renewable energy demand and global warming potential for different countries for scheme-2 118
Figure 3.17. Non-renewable energy demand (NRE) for baseline scenario for compression machine 119
Figure 3.18. Global warming potential (GWP) for baseline scenario for compression machine 120
Figure 3.19. Non-renewable energy demand for ‘recycling heat and electricity’ scenario for absorption machine 121
Figure 3.20. Global warming potential (GWP) for scenario ‘recycling heat and electricity’ for absorption machine 122

Abstract

The socio-economic importance of the olive oil production is significant in the Mediterranean region, both in terms of wealth and tradition. Unfortunately, the production of olive oil generates massive amounts of waste, which, due to their high phytotoxicity, may have a significant influence on the soil and water habitat. Especially olive mill wastewater (OMWW) is one of the major environmental pollutants in olive oil industry. Waste2Fuel project is a European project to design a smart and sustainable integrated thermochemical catalytic processes of residues from olive mills by hydrothermal carbonization (HTC) of olive mill wastewater (OMWW) and fast pyrolysis of olive mill wastewater sludge (OMWS). The byproducts resulting from OMWW-HTC treatment are a solid phase enriched in carbon, called biochar and a liquid phase (residual water with less dissolved organic and phenolic compounds). HTC biochar can be tested as a fuel in combustion systems and will also be utilized in high-value applications, such as soil bio-fertilizer and as catalyst or/and catalyst support. The HTC residual water is characterized, treated and used in soil irrigation since the organic and the toxic compounds will be reduced under the permitted limits. Waste2Fuel project's concept includes also the conversion of OMWS to a green diesel through a catalytic pyrolysis process. The green diesel is then used as biofuel in an internal combustion engine (IC-Engine) for automotive application to be used for clean transportation. In this work, a theoretical study is considered for the use of heat from the pyrolysis non-condensable gases in a sorption-refrigeration machine for pyrolysis gases cooling and condensation of bio-oil vapors.

Olive oil extraction is one of the most traditional crops utilization in the Mediterranean region; unfortunately related with a number of adverse environmental problems such as increased amounts of wastewater and solid residues. The derived wastewater is a dark liquid, with an intense smell, highly organically charged, with moderately acidic pH, a high conductivity, rich in phenolic compounds and therefore not easily bio-degradable. OMWW shows a low biodegradability and phytotoxic properties. Phyto-toxicity is mainly attributed to the relatively high concentration of polyphenols, which are also known to possess antibacterial properties. After a period of disposal in evaporation ponds, a sufficient quantity of water is evaporated and a sludge called Olive Mill Wastewater Sludge (OMWS) is formed.

Different disposal methods based on evaporation ponds, thermal concentration, physio-chemical and biological treatments as well as direct application to agricultural soils as organic fertilizers have been proposed. The most frequent disposal practices are storage ponds, where the majority of the water evaporates and the leftover sludge (olive mill wastewater sludge,

OMWS) is subsequently disposed of in landfills. This approach requires a significant amount of land, emits a foul stench, causes soil penetration, and insect infestation. Every year, OMWS disposal in the Mediterranean area leads to serious ecological problems, rendering it a toxic waste that needs to be treated. Several reported research efforts aimed for the valorization of this waste for chemical ingredients used in cosmetics and pharmaceutical products, or the production of liquid fuel.

Fast pyrolysis is a suitable choice for the exploitation of this food-waste biomass feedstock. Since bio-oil produced from thermal pyrolysis is a low-quality product, heterogeneous catalysts are employed to produce an upgraded de-oxygenated liquid product. The produced green diesel can be used in an internal combustion engine for automotive application and clean transportation. On the other hand, conventional diesel is strongly related with environmental pollution, starting from its production till its emissions during combustion.

Pyrolysis is an energy-intensive process that produces a high energy content products. The main energy consuming processes in a commercial plant are drying and grinding of biomass, heating the fluidized bed reactor and condensing the bio-oil vapors. Drying of biomass and heating the fluidized bed reactor can be achieved by combusting the biochar and non-condensable gases produced in the process. Condensing the bio-oil requires a cooling machine with a large capacity. In usual practice, a compression refrigeration machine is employed for this purpose but fortunately, there is a possibility to recover the heat from the process and use this heat to drive a sorption machine to condense the bio-oil. This integration of sorption machine will improve the efficiency of pyrolysis process by reducing the electricity consumption and reduce CO_2 emissions. If waste heat recovery is not enough to meet the cooling demand of the process, solar thermal system can be integrated to completely eliminate the use of compression refrigeration machine. To minimize dependency on fossil fuels, it makes sense to employ solar thermal as a sustainable primary heat source to satisfy cooling demands (through sorption process).

This study aims to explore the possibility of integrating an absorption machine for cooling the pyrolysis products of olive mill wastewater sludge (OMWS) in a fluidized bed reactor in the presence of red mud. In Aspen Plus, a steady state model of pyrolysis of OMWS is developed under typical pyrolysis conditions. A global reaction with kinetic parameters is written in an external Fortran user-subroutine and coupled with Aspen Plus. The model is validated against the experimental results of Agblevor et. al. The experiments were carried out at three different

temperatures 400, 450 and 500°C. A good agreement between simulation and experimental yields is observed.

The simulation model of the biochar and water yield distribution correlates better with experimental data of Agblevor et. al. particularly at temperatures 400 and 500°C (Absolute average deviation (AAD) < 3%). At temperature 400°C, water yield in the simulation is 11.4% while in the experiment is 11.3% resulting the AAD about 0.88%. Correlation between the model and experimental data reported by Agblevor et. al. was found to be satisfactory for bio-oil and gas yield results at different pyrolysis temperatures in the range of 400 – 500°C showing that the AAD is lower than 4.2%. However, the overall AAD values of products yields at temperatures 400, 450 and 500°C are 2.97%, 3.27% and 2.56%, respectively and the global AAD value comes out to be 2.36%. The composition of fast catalytic pyrolysis product gases predicted from Aspen plus-based simulation is also investigated and compared with the experimental data. The yield of CO_2 decreased from 78% at 400 °C to 66.1% at 500°C whereas the CO, H_2, and CH_4 increased from 6.45%, 2.1%, and 1.6% at 400 °C to 11.8% 3.9% and 3.8% at 500°C, respectively.

After validation, the model is extrapolated to industrial scale to process 100 tonnes of OMWS per day. Mass and energy balances are established for each component in the process. The plant produces 1,150 kg/hr bio-oil, 972 kg/hr biochar (ash free) and 770 kg/hr non-condensable gases (NCG). The yields are based on dry and ash free OMWS. The bio-oil vapors are condensed using two different cooling mechanisms: one with compression refrigeration machine (Scheme-1) and the other with absorption refrigeration machine (Scheme-2). Since the reactor temperature for both process schemes was set to 400°C, there is no difference in fuel yields between the two process schemes. The performance of the two process configurations is assessed on the basis of exergetic efficiency and minimum fuel selling price (MFSP) of bio-oil. The process produced 303 kW of electricity, hence for scheme-1 with compression refrigeration machine, the plant requires 242 kW of electricity from external sources while for scheme-2 with absorption refrigeration machine, the plant is self-sufficient.

The process is divided into seven major technical parts (i) Pre-processing of feedstock (ii) Bio-oil production via catalytic fast pyrolysis (iii) Solids removal (iv) Bio-oil condensation (v) Compression/absorption machine (vi) Combustion of biochar and NCG (vii) Electricity generation.

Flue gases from the combustion of biochar and NCG are used to heat the air for drying the OMWS. The feedstock is dried in a convective dryer by hot air at 120°C. Process demands

17,000 kg/hr of hot air to dry about 4 tons of feedstock per hour from 10% wt. moisture to 4% wt. moisture content. The exit temperature of the gases is 60°C. The direct contact during drying transfers 260 kg of water from wet biomass to the hot air thus increasing the moisture content of hot air from 10 inlet (10 g/kg dry solid) to 25.5 outlet (25.5 g/kg dry solid). Heat required to heat the air from 20 to 120°C is found to be 486 kW.

After drying, the biomass is ground from 10 mm to 2 mm using a hammer mill. The product particles are filtered and if size is greater than 2 mm they are sent back to the crusher to be ground again. The power required for the crusher is calculated to be 53.55 kW. The pyrolysis takes place at 400°C and entrained biochar and red mud particles are separated in a cyclone. The exiting products pass through a series of condensers where bio-oil and water are separated from NCG. The heat removed in the first condenser from vapors is found to be 803 kW and in the second condenser 384 kW. With a COP of 3.0, the electricity needed to operate a compression refrigeration machine is 395 kW. For absorption machine with a COP of 0.61, the heat required at generator is 632 kW to cool down the products in the second condenser.

The separated NCG and biochar are combusted to provide heat for pyrolysis, drying of biomass and steam generation for electricity production. The combustion air is preheated by recovering heat from flue gases after steam generation and biomass drying. The air required for combustion of biochar is calculated to be 20,115 kg/hr and for NCG is 2,600 kg/hr. Based on the ultimate analysis of biochar, lower heating value is calculated to be 29 MJ/kg.

After upscaling, an exergy analysis is performed to assess the performance of the process. The chemical exergy for OMWS is found to be 26,256 kW, for biochar 8,400 kW and for bio-oil 14,839 kW. The chemical exergy of a gas mixture and is found to be 2,162 kW. The exergy associated with electrical power is equivalent to electrical energy and is calculated to be 545 kW for scheme-1 and 145 kW for scheme-2. The overall exergetic efficiency for scheme-1 (compression machine) is 55.9% and for scheme-2 (absorption machine) 57% when only bio-oil is considered the desired product. The difference in the exergetic efficiencies of two schemes is due to the excessive electricity used for compression refrigeration machine. The two sources of exergy input in the drying process are the chemical exergy of biomass and the heat required by the drying process. About 88% of physical exergy in dryer is destroyed while chemical exergy destruction is negligible as water has negligible chemical exergy.

The maximum exergy destruction (65%) takes place in the combustion of biochar and non-condensable gases. The exergy destruction in this process is caused by the combustion of the

char and NCG to produce CO_2 with the low standard chemical exergy. Pyrolysis accounts for only 18% exergy destruction. The main part of exergy destruction is lost in the heat exchanger to heat the fluidizing gas to a higher temperature. The analysis shows the heat losses in the heat exchangers are major part of the exergy destruction. Total physical exergy destruction accounts for 43.6% in the whole system while 54.3% consists of chemical exergy destruction. Electrical exergy only constitutes 2.1% of exergy destruction. To conclude, physical exergy destruction can be minimized by improving the effectiveness of heat exchangers. The exergetic efficiency of plant indicates that pyrolysis is a viable energy conversion process.

The production of bio-oil from fast pyrolysis of OMWS has been investigated from an economic aspect also. In terms of energy consumption and MFSP/GGE, two process schemes (scheme-1 and scheme-2) were examined and compared. The pyrolysis unit accounted for the maximum cost (about €5.67 million) while solids separation section constitutes the minimum capital cost (about €0.11 million). Overall, the total capital costs of the process is estimated to be €17.9 million for scheme-1 and €14.9 million for scheme-2. The higher capital cost observed in scheme-1 compared to scheme-2 is attributable to cost of vapor compression refrigeration machine which is significantly bigger than the absorption refrigeration machine. The total operating costs of scheme-1 and scheme-2 were estimated at €4.9 million and €3.6 million respectively. Scheme-1 has higher operating cost than scheme-2 due to the compression refrigeration machine's high electricity consumption. The MFSP for scheme-1 is €3.63/GGE, based on a capital investment of €17.9 million and operational expenses of €4.6 million. Scheme-2, on the other hand, had a capital cost of €14.9 million and an operating cost of €3.6 million and MFSP is found to be €2.99/GGE.

The impact of 30% difference in economic parameters was analyzed on the MFSPs of the two process schemes. A 30% reduction in fuel yield resulted in a 44% increase in MFSP for scheme-1 and scheme-2 (scheme-1: €5.24; scheme-2: €4.31). In contrast, a 30% rise in fuel yield resulted in a 22% decrease in MFSP for scheme-1 and a 26% decrease in MFSP for scheme-2 (scheme-1: €2.34; scheme-2: €2.31). This means that yield losses, which can occur as a result of events like operating and servicing issues, will hurt the profitability of both process schemes.
Scaling up the plant capacity, on the other hand, would make both process schemes more financially viable. Increased plant capacity is one way to increase fuel yield, but it will give rise to capital and operating costs. Both designs' MFSPs were also highly sensitive to changes in their operating costs. A 30% rise in operating costs resulted in 21% increase in the MFSP for scheme-

1 and scheme-2 (scheme-1: €4.39; scheme-2: €3.61). In contrast, a 30% reduction in operating costs resulted in MFSP reductions of 19% for scheme-1 and 26% for scheme-2 (scheme-1: €2.93; scheme-2: €2.21). Since biomass feed costs account for a large portion of the operating expense, finding a less expensive option would be a safer economic decision. Variations in income tax had a major impact on the profitability of both method schemes.

A 20% rise in income tax resulted in a 50% increase in MFSPs (scheme-1: €5.45; scheme-2: €4.50), while a 30% decline in income tax resulted in an 33% decrease in MFSPs (scheme-1: €2.43; scheme-2: €2.01). This means that income tax reductions or deductions would be beneficial to the both operation schemes' profitability. As compared to the parameters discussed above, the MFSPs demonstrated less exposure to capital cost, with a 30% rise in capital cost triggering a 10% increase in scheme-1 and a 9% increase in scheme-2 (scheme-1: €4.01; scheme-2: €2.71), and vice versa (scheme-1: €3.29; scheme-2: €2.71). The small impact of higher capital investment on MFSPs, compared to the strong impact of higher bio-oil yield, indicates that the profitability could be scaled up by increasing plant capacity.

In the above sensitivity analysis, only single point variations of a parameter were considered while other parameters were maintained constant. In order to understand the fluctuation of several parameters at the same time, a Monte Carlo sensitivity analysis was conducted using ModelRisk software. The spider plot describes how sensitive the value of an output variable is to the input variable of the model. The plot is generated using 10,000 samples so each mean MFSP is calculated from 1,000 samples. The mean MFSP is calculated to be €4.18/GGE for scheme-1 and €3.48/GGE for scheme-2.

A comparative life cycle assessment of three scenarios is performed for production of 1 kg bio-oil from pyrolysis of OMWS in SimaPro 9.0. The scenarios differ in the fact if the heat and electricity provided to the system are produced in the process or provided from external sources. The baseline scenario is based on the Tunisian electricity which is produced mainly from natural gas. Another scenario is proposed depending upon the geographic location of the plant. Therefore, France and Greece are considered which are collaborative partners in this research project.

The non-renewable energy demand (NRE) and global warming potential (GWP) are maximum for baseline scenario i.e. 9.85 MJ/kg bio-oil and 5.27 kg CO_2 eq./ kg-bio-oil for compression refrigeration machine. For the same scenario, just by replacing compression refrigeration machine by absorption refrigeration machine, NRE and GWP are reduced by 43% and 4% respectively. By introducing thermal energy recycling scenario for absorption machine, the

environmental impacts are further reduced by 82% for NRE and 76% for GWP (NRE: 1.72MJ, GWP: 1.26 kg CO2 eq.). The production of electricity with absorption refrigeration machine allows to produce more electricity than what is consumed by the process, thus GWP is reduced by 94% and NRE by 116%. Almost all non-renewable energy demand is because of the Tunisian electricity production and heat generation from gas. The transport sector does not have a significant effect on the investigated environmental impacts.

The analysis of the geographical impact on the production of bio-oil on the basis of electricity generation sources by a country shows that the process is favorable for France (NRE: 2.24 MJ, 0.466 kg CO_2 eq.) whose main source of electricity production is nuclear power (scheme-1). Greece has slightly higher environmental impacts than France as its major sources of electricity are fossil fuels i.e. natural gas (30%), lignite (29.3%), oil (9%) and renewable energy resources (31.7%) while for Tunisia, electricity is produced mainly from natural gas (95%).

For scheme-2, Greece has the minimum environmental impacts (NRE: -4.12; GWP: 0.134) as we are producing more electricity in the process than it is utilized by the process so excess electricity is provided to the external sources.

Key words: Pyrolysis, Olive mill wastewater sludge, Aspen Plus, absorption machine, exergy, economic analysis, life cycle analysis

Résumé

L'importance socio-économique de la production d'huile d'olive est considérable dans la région méditerranéenne, tant en termes de richesse que de tradition. Cependant, l'extraction de l'huile d'olive génère d'énormes quantités de déchets qui peuvent avoir un impact important sur l'environnement terrestre et aquatique en raison de leur forte phytotoxicité. Les eaux usées des moulins à huile sont l'un des principaux polluants environnementaux de l'industrie oléicole. Le projet Waste2Fuel est un projet européen qui vise à concevoir un processus catalytique thermochimique intégré intelligent et durable pour les résidus des moulins à huile, par carbonisation hydrothermique (HTC) des eaux usées des moulins à huile (OMWW) et par pyrolyse rapide des boues d'eaux usées des moulins à huile (OMWS). Les sous-produits résultant du traitement des OMW-HTC sont une phase solide enrichie en carbone, appelée biochar, et une phase liquide (eau résiduelle avec moins de composés organiques et phénoliques dissous). Le biochar HTC peut être testé comme combustible dans les systèmes de combustion et sera également utilisé dans des applications à haute valeur ajoutée, comme le bio-engrais pour le sol et comme catalyseur ou/et support de catalyseur. L'eau résiduelle du HTC est caractérisée, traitée et utilisée pour l'irrigation des sols puisque les composés organiques et toxiques seront réduits dans les limites autorisées. Le concept du projet Waste2Fuel comprend également la conversion des OMWS en un diesel vert par un processus de pyrolyse catalytique. Le diesel vert est ensuite utilisé comme biocarburant dans un moteur à combustion interne (IC-Engine) pour une application automobile afin d'être utilisé pour un transport propre. Dans ce travail, une étude théorique est envisagée pour l'utilisation de la chaleur des gaz non condensables de la pyrolyse dans une machine de sorption-réfrigération pour le refroidissement des gaz de pyrolyse et la condensation des vapeurs de bio-huile.

L'extraction de l'huile d'olive est l'une des cultures les plus traditionnelles de la région méditerranéenne ; elle est malheureusement liée à un certain nombre de problèmes environnementaux négatifs tels que l'augmentation des quantités d'eaux usées et de résidus solides. Les eaux usées dérivées sont un liquide foncé, avec une odeur intense, fortement chargé organiquement, avec un pH modérément acide, une conductivité élevée, riche en composés phénoliques et donc difficilement biodégradable. Les OMW présentent une faible biodégradabilité et des propriétés phytotoxiques. La phytotoxicité est principalement attribuée à la concentration relativement élevée de polyphénols, qui sont également connus pour leurs propriétés antibactériennes. Après une période d'élimination dans des bassins d'évaporation,

une quantité suffisante d'eau est évaporée et une boue appelée boue d'eaux usées du moulin à huile (OMWS) est formée.

Différentes méthodes d'élimination basées sur les bassins d'évaporation, la concentration thermique, les traitements physiochimiques et biologiques ainsi que l'application directe sur les sols agricoles comme engrais organiques ont été proposées. Les méthodes d'élimination les plus courantes comprennent les bassins de stockage, où la plus grande partie de l'eau est évaporée, tandis que la boue résiduelle (boue résiduelle de moulin à huile, OMWS) est ensuite envoyée dans des décharges. Cette méthode nécessite de grandes surfaces, produit de mauvaises odeurs, provoque des infiltrations dans le sol et une infestation d'insectes. Chaque année, l'élimination des OMWS dans la région méditerranéenne entraîne de graves problèmes écologiques, ce qui en fait un déchet toxique qui doit être traité. Plusieurs efforts de recherche ont été signalés pour la valorisation de ces déchets en ingrédients chimiques utilisés dans les cosmétiques et les produits pharmaceutiques, ou pour la production de carburant liquide.

La pyrolyse rapide est un choix approprié pour l'exploitation de cette matière première de biomasse issue de déchets alimentaires. La bio-huile produite par pyrolyse thermique étant un produit de faible qualité, des catalyseurs hétérogènes sont utilisés pour produire un produit liquide désoxygéné amélioré. Le diesel vert produit peut être utilisé dans un moteur à combustion interne pour des applications automobiles et des transports propres. D'autre part, le diesel conventionnel est fortement lié à la pollution de l'environnement, depuis sa production jusqu'à ses émissions pendant la combustion.

La pyrolyse est un processus à forte intensité énergétique, mais qui permet d'obtenir un contenu énergétique élevé. Les principaux processus consommateurs d'énergie dans une usine commerciale sont le séchage et le broyage de la biomasse, le chauffage du réacteur à lit fluidisé et la condensation des vapeurs de bio-huile. Le séchage de la biomasse et le chauffage du réacteur à lit fluidisé peuvent être réalisés en brûlant le biochar et les gaz non condensables produits au cours du processus. La condensation de la bio-huile nécessite une machine de refroidissement de grande capacité. Dans la pratique habituelle, une machine frigorifique à compression est utilisée à cette fin, mais heureusement, il est possible de récupérer la chaleur du processus et de l'utiliser pour faire fonctionner une machine à sorption pour condenser la bio-huile. Cette intégration de la machine à sorption améliorera l'efficacité du processus de pyrolyse en réduisant la consommation d'électricité et les émissions de CO_2. Si la récupération de la chaleur résiduelle ne suffit pas à répondre à la demande de refroidissement du processus, un système solaire thermique peut être intégré pour éliminer complètement l'utilisation de la

machine de réfrigération à compression. Afin de réduire la dépendance aux combustibles fossiles, il est logique d'utiliser le solaire thermique comme source de chaleur primaire renouvelable afin de répondre aux besoins de refroidissement (par des processus de sorption).

Cette étude a pour but d'explorer la possibilité d'intégrer une machine à absorption pour refroidir les produits de pyrolyse des boues résiduaires du moulin à huile (OMWS) dans un réacteur à lit fluidisé en présence de boue rouge. Un modèle de pyrolyse des OMWS en régime permanent est développé dans Aspen Plus dans des conditions de pyrolyse standard. Une réaction globale avec des paramètres cinétiques est employée dans un sous-programme utilisateur Fortran externe et couplée à Aspen Plus. Le modèle est validé par rapport aux résultats expérimentaux d'Agblevor et al. Les expériences ont été réalisées à trois températures différentes 400, 450 et 500°C. Un bon accord entre la simulation et les rendements expérimentaux est observé.

Le modèle de simulation de la distribution du biochar et du rendement en eau présente une meilleure corrélation avec les données expérimentales d'Agblevor et al. en particulier aux températures de 400 et 500°C (écart moyen absolu (AAD) < 3%). À la température de 400 °C, le rendement en eau dans la simulation est de 11,4 %, alors que dans l'expérience, il est de 11,3 %, ce qui donne un écart moyen absolu d'environ 0,88 %. La corrélation entre le modèle et les données expérimentales rapportées par Agblevor et. al. s'est avérée satisfaisante pour les résultats de rendement de bio-huile et de gaz à différentes températures de pyrolyse dans la gamme de 400 - 500°C montrant que l'AAD est inférieur à 4.2%. Cependant, les valeurs globales de DAA des produits obtenus aux températures de 400, 450 et 500°C sont respectivement de 2,97%, 3,27% et 2,56%, et la valeur globale de DAA est de 2,36%. La composition des gaz produits par la pyrolyse catalytique rapide prédite par la simulation basée sur Aspen plus est également étudiée et comparée aux données expérimentales. Le rendement du CO2 a diminué de 78 % à 400 °C à 66,1 % à 500 °C, tandis que le CO, le H2 et le CH4 ont augmenté de 6,45 %, 2,1 % et 1,6 % à 400 °C à 11,8 %, 3,9 % et 3,8 % à 500 °C, respectivement.

Après validation, le modèle est extrapolé à l'échelle industrielle pour traiter 100 tonnes d'OMWS par jour. Les bilans de masse et d'énergie sont établis pour chaque composant du processus. L'usine produit 1 150 kg/h de bio-huile, 972 kg/h de biochar (sans cendres) et 770 kg/h de gaz non condensables (GNC). Les rendements sont basés sur des OMWS sèches et sans cendres. Les vapeurs de bio-huile sont condensées à l'aide de deux mécanismes de refroidissement différents : l'un avec une machine frigorifique à compression (Schéma-1) et l'autre avec une machine frigorifique à absorption (Schéma-2). Comme la température du réacteur pour les deux schémas de traitement a été fixée à 400°C, il n'y a pas de différence dans

les rendements en combustible entre les deux schémas de traitement. La performance des deux configurations de processus est évaluée sur la base de l'efficacité énergétique et du prix de vente minimum du combustible (MFSP) de la bio-huile. Le procédé a produit 303 kW d'électricité, donc pour le schéma-1 avec la machine de réfrigération par compression, l'usine a besoin de 242 kW d'électricité provenant de sources externes alors que pour le schéma-2 avec la machine de réfrigération par absorption, l'usine est autosuffisante.

Le processus est divisé en sept parties techniques majeures (i) Prétraitement de la matière première (ii) Production de bio-huile par pyrolyse rapide catalytique (iii) Elimination des solides (iv) Condensation de la bio-huile (v) Machine de compression/absorption (vi) Combustion du biochar et du NCG (vii) Production d'électricité.

Les gaz de combustion du biochar et des NCG sont utilisés pour chauffer l'air pour le séchage des OMWS. La matière première est séchée dans un séchoir convectif par air chaud à 120°C. Le procédé nécessite 17 000 kg/h d'air chaud pour sécher environ 4 tonnes de matière première par heure, de 10 % d'humidité en poids à 4 % d'humidité en poids. La température de sortie des gaz est de 60°C. Le contact direct pendant le séchage transfère 260 kg d'eau de la biomasse humide à l'air chaud, ce qui augmente la teneur en humidité de l'air chaud de 10 à l'entrée (10 g/kg de matière sèche) à 25,5 à la sortie (25,5 g/kg de matière sèche). La chaleur nécessaire pour chauffer l'air de 20 à 120°C est de 486 kW.

Après séchage, la biomasse est broyée de 10 mm à 2 mm à l'aide d'un broyeur à marteaux. Les particules produites sont filtrées et si leur taille est supérieure à 2 mm, elles sont renvoyées dans le broyeur pour être broyées à nouveau. La puissance requise pour le broyeur est calculée à 53,55 kW. La pyrolyse a lieu à 400°C et les particules de biochar et de boue rouge entraînées sont séparées dans un cyclone. Les produits sortants passent par une série de condenseurs où la bio-huile et l'eau sont séparées des NCG. La chaleur retirée des vapeurs dans le premier condenseur est de 803 kW et dans le deuxième condenseur de 384 kW. Avec un COP de 3,0, l'électricité nécessaire pour faire fonctionner une machine frigorifique à compression est de 395 kW. Pour une machine à absorption dont le COP est de 0,61, la chaleur nécessaire au générateur est de 632 kW pour refroidir les produits dans le deuxième condenseur.

Le NCG et le biochar séparés sont brûlés pour fournir de la chaleur pour la pyrolyse, le séchage de la biomasse et la production de vapeur pour la production d'électricité. L'air de combustion est préchauffé en récupérant la chaleur des gaz de combustion après la production de vapeur et le séchage de la biomasse. On calcule que l'air nécessaire à la combustion du biochar est de 20

115 kg/h et de 2600 kg/h pour le NCG. Sur la base de l'analyse ultime du biochar, le pouvoir calorifique inférieur est calculé à 29 MJ/kg.

Après la mise à l'échelle, une analyse exergique est effectuée pour évaluer la performance du processus. L'exergie chimique des OMWS est de 26 256 kW, celle du biochar de 8 400 kW et celle de la biohuile de 14 839 kW. L'exergie chimique d'un mélange de gaz et est de 2162 kW. L'exergie associée à l'énergie électrique est équivalente à l'énergie électrique et est calculée à 545 kW pour le schéma-1 et 145 kW pour le schéma-2. L'efficacité énergétique globale pour le schéma-1 (machine de compression) est de 55,9 % et pour le schéma-2 (machine d'absorption) de 57 % lorsque seule la bio-huile est considérée comme le produit souhaité. La différence dans les rendements énergétiques des deux schémas est due à la consommation excessive d'électricité pour la machine de réfrigération à compression. Les deux sources d'apport d'exergie dans le processus de séchage sont l'exergie chimique de la biomasse et la chaleur requise par le processus de séchage. Environ 88% de l'exergie physique dans le séchoir est détruite tandis que la destruction de l'exergie chimique est négligeable car l'eau a une exergie chimique négligeable.

La destruction maximale d'exergie (65%) a lieu lors de la combustion du biochar et des gaz non condensables. La destruction d'énergie dans ce processus est causée par la combustion du charbon et des gaz non condensables pour produire du CO_2 avec une faible exergie chimique standard. La pyrolyse ne représente que 18% de la destruction d'énergie. La plus grande partie de la destruction d'énergie est perdue dans l'échangeur de chaleur pour chauffer le gaz de fluidisation à une température plus élevée. L'analyse montre que les pertes de chaleur dans les échangeurs de chaleur constituent la majeure partie de la destruction d'exergie. La destruction totale d'exergie physique représente 43,6 % de l'ensemble du système, tandis que 54,3 % sont des pertes d'exergie chimique. L'exergie électrique ne constitue que 2,1% de la destruction d'exergie. En conclusion, la destruction d'exergie physique peut être minimisée en améliorant l'efficacité des échangeurs de chaleur. L'efficacité énergétique de l'usine indique que la pyrolyse est un processus de conversion énergétique viable.

D'un point de vue économique, la production de bio-huile à partir de la pyrolyse rapide de boues d'eaux usées de moulin à huile a été étudiée. En termes de consommation d'énergie et de PSFM/GGE, deux schémas de procédé (schéma-1 et schéma-2) ont été examinés et comparés. L'unité de pyrolyse a représenté le coût maximal (environ 5,67 millions d'euros) tandis que la section de séparation des solides constitue le coût d'investissement minimal (environ 0,11 million d'euros). Globalement, les coûts d'investissement totaux du procédé sont estimés à 17,9

millions d'euros pour le schéma 1 et à 14,9 millions d'euros pour le schéma 2. Le coût d'investissement plus élevé observé dans le schéma-1 par rapport au schéma-2 est attribuable au coût de la machine de réfrigération par compression de vapeur, qui est beaucoup plus grande que la machine de réfrigération par absorption. Les coûts d'exploitation totaux des systèmes 1 et 2 ont été estimés à 4,9 millions € et 3,6 millions € respectivement. Le coût d'exploitation plus élevé du système 1 par rapport au système 2 est dû à la consommation d'électricité relativement plus élevée de la machine frigorifique à compression. Le PSFM du régime 1 est de 3,63 €/GGE, sur la base d'un investissement en capital de 17,9 millions d'euros et de dépenses d'exploitation de 4,6 millions d'euros. Le schéma-2, quant à lui, a un coût d'investissement de 14,9 millions d'euros et un coût d'exploitation de 3,6 millions d'euros, et le PSFM est de 2,99 €/GGE.

L'impact d'une différence de 30 % dans les paramètres économiques a été analysé sur les MFSP des deux schémas de traitement. Une réduction de 30 % du rendement du combustible s'est traduite par une augmentation de 44 % du PSFM pour le schéma 1 et le schéma 2 (schéma 1 : 5,24 € ; schéma 2 : 4,31 €). En revanche, une augmentation de 30 % du rendement en combustible a entraîné une diminution de 22 % du MFSP pour le régime 1 et de 26 % pour le régime 2 (schéma-1 : 2,34 € ; schéma-2 : 2,31 €). Cela signifie que les pertes de rendement, qui peuvent survenir à la suite d'événements tels que des problèmes d'exploitation et d'entretien, affecteront la rentabilité des deux systèmes de traitement.

En revanche, l'augmentation de la capacité de l'usine serait commercialement plus rentable pour les deux procédés. L'augmentation de la capacité de l'usine est un moyen d'accroître le rendement en combustible, mais elle entraîne des coûts d'investissement et d'exploitation. Les PSFM des deux conceptions étaient également très sensibles aux changements de leurs coûts d'exploitation. Une augmentation de 30 % des coûts d'exploitation a entraîné une hausse de 21 % du PSFM pour le schéma-1 et le schéma-2 (schéma-1 : 4,39 € ; schéma-2 : 3,61 €). En revanche, une réduction de 30 % des coûts d'exploitation a entraîné une diminution du MFSP de 19 % pour le régime 1 et de 26 % pour le régime 2 (schéma-1 : 2,93 € ; schéma-2 : 2,21 €). Comme les coûts d'alimentation en biomasse représentent une grande partie des frais d'exploitation, trouver une option moins coûteuse serait une décision économique plus sûre. Les variations de l'impôt sur le revenu ont eu un impact majeur sur la rentabilité des deux schémas de méthode.

Une hausse de 20 % de l'impôt sur le revenu a entraîné une augmentation de 50 % des MFSP (régime 1 : 5,45 € ; régime 2 : 4,50 €), tandis qu'une baisse de 30 % de l'impôt sur le revenu a entraîné une diminution de 33 % des PSFM (régime 1 : 2,43 € ; régime 2 : 2,01 €). Cela signifie

que les réductions ou déductions de l'impôt sur le revenu seraient bénéfiques à la rentabilité des deux régimes d'exploitation. Par rapport aux paramètres examinés ci-dessus, les MFSP sont moins exposés au coût du capital, une augmentation de 30 % du coût du capital entraînant une augmentation de 10 % pour le régime 1 et de 9 % pour le régime 2 (schéma-1 : 4,01 € ; schéma-2 : 2,71 €), et vice versa (schéma-1 : 3,29 € ; schéma-2 : 2,71 €). Le faible impact d'un investissement en capital plus élevé sur les PSFM, comparé au fort impact d'un rendement plus élevé en bio-huile, indique que la rentabilité pourrait être accrue en augmentant la capacité des usines.

L'analyse de sensibilité ci-dessus n'a pris en compte que la variation ponctuelle d'un paramètre sur le PSFM, les autres paramètres étant maintenus constants. Pour comprendre la variation de plus d'un paramètre à la fois, une analyse de sensibilité Monte Carlo a été réalisée à l'aide du logiciel ModelRisk. Le graphique en araignée décrit la sensibilité de la valeur d'une variable de sortie par rapport à la variable d'entrée du modèle. Le graphique est généré à partir de 10000 échantillons, de sorte que chaque PSFM moyen est calculé à partir de 1000 échantillons. Le PSFM moyen est calculé comme étant de 4,18 €/GGE pour le schéma-1 et de 3,48 €/GGE pour le schéma-2.

Une analyse comparative du cycle de vie de trois scénarios est réalisée pour la production de 1 kg de bio-huile à partir de la pyrolyse des OMWS dans SimaPro 9.0. Les scénarios diffèrent par le fait que la chaleur et l'électricité fournies au système sont produites dans le processus ou fournies par des sources externes. Le scénario de base est basé sur l'électricité tunisienne qui est produite principalement à partir de gaz naturel. Un autre scénario est proposé en fonction de l'emplacement géographique de l'usine. Ainsi, la France et la Grèce sont considérées comme des partenaires de collaboration dans ce projet de recherche.

La demande d'énergie non renouvelable (NRE) et le potentiel de réchauffement global (GWP) sont maximaux pour le scénario de base, c'est-à-dire 9,85 MJ/kg de bio-huile et 5,27 kg d'équivalent CO2/kg de bio-huile pour la machine de réfrigération par compression. Pour le même scénario, en remplaçant simplement la machine de réfrigération par compression par une machine de réfrigération par absorption, le NRE et le GWP sont réduits de 43% et 4% respectivement. En introduisant un scénario de recyclage de l'énergie thermique pour la machine à absorption, les impacts environnementaux sont encore réduits de 82% pour le NRE et de 76% pour le GWP (NRE : 1,72MJ, GWP : 1,26 kg CO_2 eq.). La production d'électricité avec une machine frigorifique à absorption permet de produire plus d'électricité que ce qui est consommé par le processus, le PRP est donc réduit de 94 % et le NRE de 116 %. La quasi-

totalité de la demande d'énergie non renouvelable est due à la production d'électricité tunisienne et à la production de chaleur à partir de gaz. Le secteur des transports n'a pas d'effet significatif sur les impacts environnementaux étudiés.

L'analyse de l'impact géographique de la production de bio-huile sur la base des sources de production d'électricité d'un pays montre que le processus est favorable à la France (NRE : 2,24 MJ, 0,466 kg eq. CO_2) dont la principale source de production d'électricité est l'énergie nucléaire (schéma-1). La Grèce a des impacts environnementaux légèrement plus élevés que la France car ses principales sources d'électricité sont les combustibles fossiles, à savoir le gaz naturel (30 %), le lignite (29,3 %), le pétrole (9 %) et les ressources énergétiques renouvelables (31,7 %), tandis que pour la Tunisie, l'électricité est produite principalement à partir du gaz naturel (95 %). Pour le schéma 2, la Grèce a les impacts environnementaux les plus faibles (NRE : -4,12 ; GWP : 0,134) car nous produisons plus d'électricité dans le processus qu'elle n'en utilise, l'électricité excédentaire est donc fournie aux sources externes.

Mots clés : Pyrolyse, boues d'eaux usées de moulin à huile, Aspen Plus, machine à absorption, exergie, analyse économique, life cycle analysis

General Introduction

The waste-to-Energy market has grown considerably since incineration first started in 1874. However, concerns over harmful by-products of the incineration process, both pollution and health related led to widespread regulatory tightening of particulate and fuel emissions forcing some plants out of business and increasing public opposition. Advances in thermochemical technologies to convert waste to gas, liquid and solid fuels have emerged recently. Among them, biomass catalytic fast pyrolysis (CFP) and hydrothermal carbonization (HTC) are ones of the most promising technologies as they offer significant logistical and economic advantages. Indeed, the liquid product 'bio-oil' from catalytic fast pyrolysis can be stored until required or readily transported to where it can be most effectively used. The most promising application is seen in the automotive field without the need of its extensive upgrading.

Olive mill wastewater (OMWW), on the other hand, has been a major environmental concern for the majority of olive oil producing countries. Various disposal strategies have been introduced including evaporation ponds, thermal concentration, physio-chemical and biological processes and direct application to agricultural soils as biofertilizers. After a certain period of disposal in evaporation ponds a significant quantity of water is evaporated and a sludge called olive mill wastewater sludge (OMWS) rests there.

The main objective of the Waste2Fuel project is to design an integrated process of HTC and CFP of OMWW (liquid) and OMWS (sludge) wastes from olive mills. The major products of HTC treatment are a carbon-rich solid phase known as biochar and a residual liquid phase containing dissolved organic molecules. The biochar is investigated as fuel in solid combustion systems for heat generation as well as soil bio-fertilizer. The bio-oil produced from CFP of OMWS finds its application in internal combustion engine (IC-Engine) for clean automotive application. The biochar produced in CFP can be used as solid fuel for heat generation for electricity production or soil bio fertilizer.

This study aims to explore the possibility of integrating an absorption machine for cooling the pyrolysis products of olive mill wastewater sludge (OMWS) in a fluidized bed reactor in the presence of red mud. The process is modelled in Aspen Plus and validated against experimental data of Agblevor et. al. [1]. The experiments were performed at three different temperatures 400, 450 and 500°C. After validation, the model is extrapolated to industrial scale to process 100 tonnes/day of OMWS. The plant produces 1,150 kg/hr bio-oil, 972 kg/hr biochar (ash free) and 770 kg/hr non-condensable gases (NCG). The yields are based on dry and ash free OMWS.

The bio-oil vapors are condensed using two different cooling mechanisms: one with compression refrigeration machine (Scheme-1) and the other with absorption refrigeration machine (Scheme-2). The performance of the two process configurations is assessed on the basis of exergetic efficiency and minimum fuel selling price (MFSP) of bio-oil.

The first chapter 'Literature Review' is divided into four parts. The first section gives an introduction to OMWS, different methods to dispose off OMWS, pyrolysis, fluidized bed reactor and application of Aspen Plus for modeling pyrolysis process. The second section talks about energy and exergy analysis of pyrolysis and third section represents the economic analysis for production of bio-oil on industrial scale. Section four is about the use of absorption cooling machine for condensation of bio-oil.

The second chapter 'Methodology' provides the data collection for lab scale and its validation with experimental data. The extrapolation of lab scale to industrial scale is carried out and mass and energy balances are established. The performance of the system is assessed by performing an exergy analysis of the whole system. Finally, an economic analysis is conducted to determine the minimum fuel selling price of bio-oil.

The third chapter starts with the simulation results of the process modelled in Aspen Plus validated against experimental data. The model is then extrapolated to industrial scale and mass and energy balances are established. The exergy analysis of the whole process deduces the aspects where process can be improved. The economic analysis helps to determine the minimum fuel selling price by taking into account the total project investment, operating cost, quantity of bio-oil produced, taxes and discounted rate.

CHAPTER 1: LITERATURE REVIEW

1.1 Introduction

The socio-economic relevance of olive oil production in the Mediterranean area is substantial, both in terms of income and tradition. However, the extraction of olive oil creates massive amounts of wastes that, due to their high phytotoxicity, may have a significant influence on land and aquatic habitats. Especially olive mill wastewater (OMWW) is one of the major environmental pollutants in olive oil industry. Waste2Fuel project is a European project to design a smart and sustainable integrated thermochemical catalytic processes of residues from olive mills: hydrothermal carbonization (HTC) of olive mill wastewater (OMWW) and fast pyrolysis of olive mill wastewater sludge (OMWS). Indeed, the byproducts resulting from OMWW-HTC treatment are a solid phase enriched in carbon, called biochar and a liquid phase (residual water with less dissolved organic and phenolic compounds). HTC biochar will be tested as fuel in combustion systems and will also be utilized in high-value applications, such as soil bio-fertilizer and as catalyst or/and catalyst support. The HTC residual water will be characterized, treated and used in soil irrigation since the organic and the toxic compounds will be reduced under the permitted limits. Waste2Fuel project's concept includes also the conversion of OMWS to a green diesel through a catalytic pyrolysis process. The green diesel is then used as biofuel in an internal combustion engine (IC-Engine) for automotive application to be used for clean transportation. In this work, a theoretical study is considered for the use of a fraction of the heat from the pyrolysis non-condensable gases (alternatively to a solar collector) in a sorption-refrigeration machine for pyrolysis gases cooling and condensation to produce bio-oil.

Olive oil extraction is one of the most traditional crops utilization in the Mediterranean region; unfortunately related with a number of adverse environmental problems such as increased amounts of wastewater and solid residues. Olive mill wastewater (OMWW) has been a critical environmental problem concern for the most olive oil producing countries. The derived wastewater is a dark liquid, with an intense smell, highly organically charged, with moderately acidic pH, a high conductivity, rich in phenolic compounds and therefore not easily bio-degradable (Figure 1.1). OMWW shows a low biodegradability and phytotoxic properties. Phyto-toxicity is mainly attributed to the relatively high concentration of polyphenols, which are also known to possess antibacterial properties. After a period of disposal in evaporation

ponds, a sufficient quantity of water is evaporated and a sludge called Olive Mill Wastewater Sludge (OMWS) is formed.

Different disposal methods based on evaporation ponds, thermal concentration, physio-chemical and biological treatments as well as direct application to agricultural soils as organic fertilizers have been proposed. The most frequent disposal techniques are storage ponds, where the majority of the water evaporates and the leftover sludge (olive mill wastewater sludge, OMWS) is subsequently disposed off in landfills. This approach necessitates a significant amount of land, emits a foul stench, causes soil penetration, and insect infestation. Every year, OMWS disposal in the Mediterranean area leads to serious ecological problems, rendering it a toxic waste that needs to be treated. Several reported research efforts aimed for the valorization of this waste for chemical ingredients used in cosmetics and pharmaceutical products, or the production of liquid fuel [2].

Figure 1.1. Olive mill wastewater evaporation pond

Fast pyrolysis is a suitable choice for the exploitation of this food-waste biomass feedstock. Since bio-oil produced from thermal pyrolysis is a low-quality product, heterogeneous catalysts are employed to produce an upgraded de-oxygenated liquid product. The produced green diesel can be used in an internal combustion engine for automotive application and clean transportation. On the other hand, conventional diesel is strongly related with environmental pollution, starting from its production till its emissions during combustion.

Pyrolysis is an energy intensive process but at the same time it produces high energy content products. The main energy consuming processes in a commercial plant are drying and grinding of biomass, heating the fluidized bed reactor and condensing the bio-oil vapors. Drying of biomass and heating the fluidized bed reactor can be achieved by combusting the biochar produced in the process. Condensing the bio-oil requires a cooling machine with a large capacity. In usual practice, a compression refrigeration machine is employed for this purpose but fortunately, there is a possibility to recover the heat from the process and use this heat to drive a sorption machine to condense the bio-oil. This integration of sorption machine will improve the efficiency of pyrolysis process by reducing the electricity consumption and reduce CO_2 emissions. If waste heat recovery is not enough to meet the cooling demand of the process, solar thermal system can be integrated to completely eliminate the use of compression refrigeration machine. To minimize dependency on fossil fuels, it makes sense to employ solar thermal as a sustainable primary heat source to satisfy cooling demands (through sorption process) [3].

1.2 Fundamentals of pyrolysis process

Pyrolysis is the thermal decomposition of organic materials at elevated temperatures in the absence of oxygen. Large complex organic materials are decomposed into smaller molecules and it is common to classify the product into:

- Biochar
- Bio-oil
- Non-condensable gases at atmospheric temperature and pressure

Pyrolysis produces mostly biochar at low temperatures, less than 400 °C, when the heating rate is slow, and mostly gases at high temperatures, higher than 550 °C, when the heating rate is fast. At moderate temperatures and rather high heating rates, bio-oil is the key product.

1.2.1 Process Description

The pyrolysis process starts with drying of biomass and then ground to size of about 2 mm. The biomass particles are then sent to pyrolysis reactor where pyrolysis reactions take place and products are passed through high efficiency cyclones where entrained biochar and catalyst particles are separated. The bio-oil vapors and non-condensable gases (NCG) are passed through condensers where bio-oil is quenched and separated. In some cases, electrostatic precipitator has been employed to remove the remaining bio-oil aerosols from the NCG.

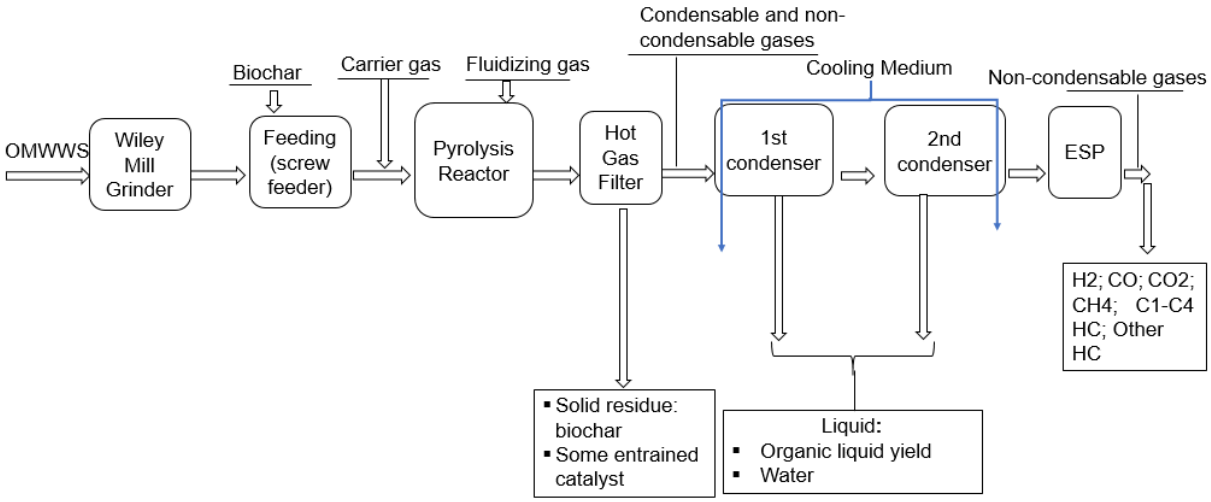

Figure 1.2. Pyrolysis of biomass

Pyrolysis may be conducted on a small scale and in remote places, increasing the energy density of biomass resources while lowering transportation and handling costs. Because the pyrolysis process is endothermic, adequate heat transfer surface area must be given to fulfill the process requirements. Pyrolysis is a versatile and appealing method of turning solid biomass into an easily stored and transportable liquid that may be used to generate heat, electricity, and chemicals.

1.2.2 Feedstock for pyrolysis

In the pyrolysis process, a broad variety of biomass feedstocks may be utilized. Bagasse (from sugar cane), rice husk, rice straw, peanut hulls, oat hulls, switchgrass, wheatstraw, sludge, and wood are examples of waste biomass feedstocks [4]. The moisture content of the feedstock, which should be less than 10%, is critical to the pyrolysis process. High quantities of water are generated at greater moisture contents, while reducing too much moisture content could cause the evaporation of volatile matter during drying process thus reducing quantity of bio-oil. Drying is required for high-moisture waste streams, such as sludge and other wastes, before they can be pyrolyzed.

The particle size of feedstock affects the efficiency and nature of the pyrolysis process. Because of the necessity for rapid heat transmission through the particle, most pyrolysis methods can only handle tiny particles up to 2 mm in diameter. The need for tiny particle size necessitates size reduction of the feedstock prior to pyrolysis.

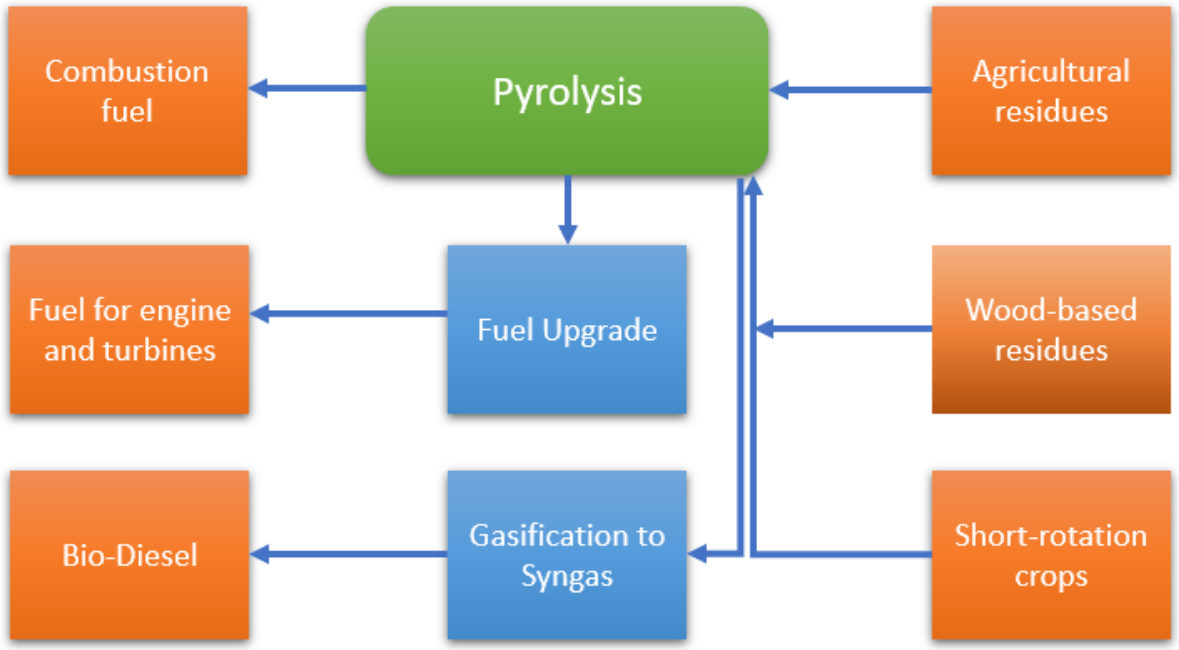

Figure 1.3. A glance at feedstock availability and energy products from biomass pyrolysis

1.2.3 Types of pyrolysis

Pyrolysis is classified into four types based on the heating rate and residence time of the feedstock in the reactor: slow, intermediate, fast, and flash pyrolysis [5,6]. Fast pyrolysis is the most often used pyrolysis technique nowadays. Slow pyrolysis takes many hours and yields biochar as the major product. Its process temperature may range from 300 to 700 °C, with biomass particle sizes ranging from 2 to 50 mm [7]. Fast pyrolysis, on the other hand, yields 60% of bio-oil and takes only seconds to complete. It also produces 20% biochar and 20% syngas. It has a different heating rate than slow pyrolysis (heating rate > 10–200 °C/s, residence duration = 0.5–10 s). A heating rate of 103–104 °C/s is employed in flash pyrolysis, with a biomass residence time of less than 0.5 seconds [8,9].

Fast pyrolysis is a well-known thermochemical conversion process capable of converting solid biomass into an intermediate liquid product (bio-oil), gas, and biochar in the absence of oxygen and at a high heating rate. Through hydroprocessing technology, bio-oil may be transformed to a transportation fuel, producing renewable diesel and gasoline. There have been several research studies on the conversion of biomass to bio-oil using fast pyrolysis [10–15].

Fast pyrolysis has been proved on a commercial scale, with global capacity rising. This procedure produces bio-oil, which may be used as a renewable heating oil in place of petroleum

oils. Co-processing crude bio-oil in petroleum refineries' fluidized catalytic cracking (FCC) units is a "low-CAPEX" (capital-expenditure ratio) upgrading solution.

A vast number of laboratory and pilot studies have been reported, with different feedstocks, reactor layouts, and catalysts being tested to increase product quality and yields. Some technologies have now reached maturity and are in commercial production.

Open-core fixed bed pyrolysis, ablative fast pyrolysis, cyclonic fast pyrolysis, and rotating core fast pyrolysis are all examples of rapid pyrolysis processes. The following are the fundamental characteristics of a fast pyrolysis process:

- Extremely high heating and heat transmission rates necessitate a finely ground feed.
- Carefully regulated reaction temperature of 500°C in the vapor phase
- Pyrolysis products have a residence time less than 2 seconds in the reactor.
- Quenching (rapid cooling) of pyrolysis vapors to produce bio-oil

The conversion of biomass into liquid products is favored by moderate temperature (350–500 °C) and low residence time, whereas high residence time and low temperature mostly transforms the biomass into biochar. Table 1.1 summarizes the conditions for the liquid and biochar generation processes [16]. Figure 1.4 illustrates the graphical representation of variation in yields of products with temperature, heating rate and residence time [17].

Table 1.1. Modes of pyrolysis

Mode	**Temperature (°C)**	**Residence time (s)**	**Yields (wt.%)**		
			Liquid	**Gas**	**Char**
Slow	450	Very long (>30)	30 (70% water)	35	35
Medium	500	Moderate (10–30)	50 (50% water)	25	25
Fast	500	Short (<2)	70 (30% water)	12	13
Flash	500	Very short (<0.5)	75 (25% water)	<12	<13
Gasification	>800	Long	5	85	10

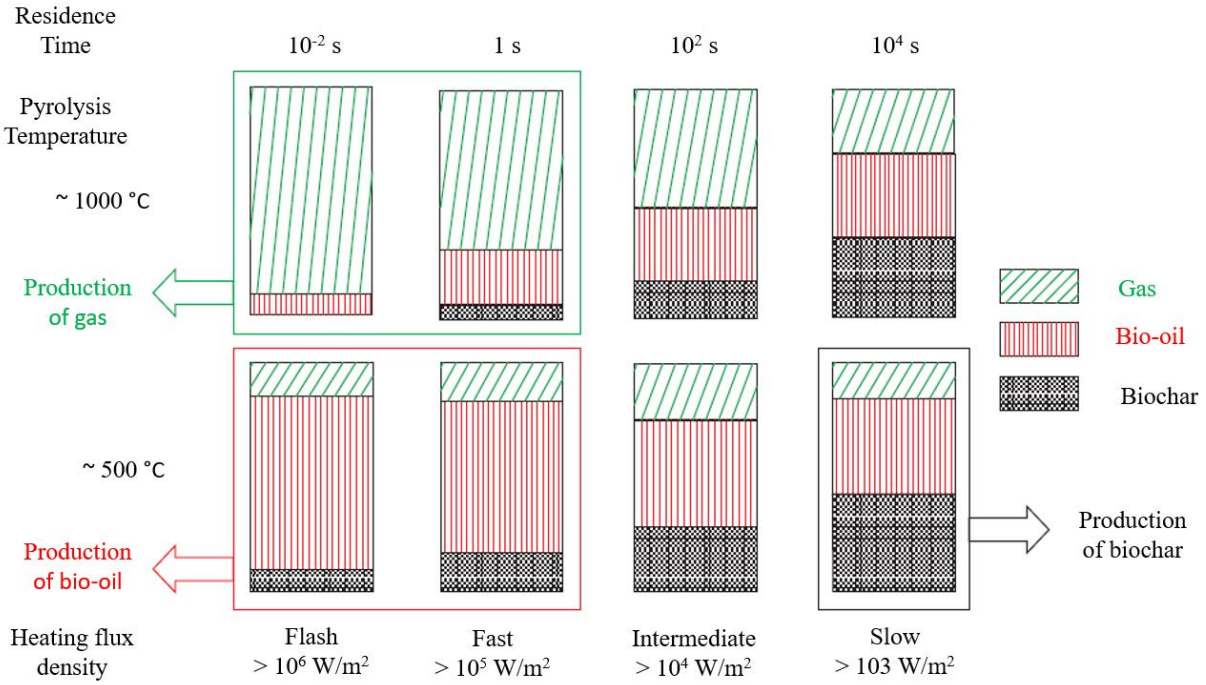

Figure 1.4. Influence of residence time, temperature and heating flux on gas, bio-oil and biochar produced by pyrolysis of wood

The typical characteristics of bio-oil produced from OMWS and diesel are compared in Table 1.2 [18].

Table 1.2. The comparison of bio-oil produced from fast pyrolysis of OMWWS and diesel [1][19]

Properties	**Bio-oil**	**Heavy fuel oil**
pH	6.25-7.4	Neutral
Specific gravity	1.20	0.81-0.96
C (wt.%)	77–82	86.50
H (wt.%)	11.0–11.8	13.20
O (wt.%)	3.0–8.1	0
N (wt%)	2.13-2.84	0
S (wt.%)	trace	0.3
Ash (wt.%)	0.0	0
Higher heating value (MJ/kg)	37.5–41.3	40
Viscosity (cP)	4.6-9.2 (at 500 °C)	2.4-2.7 (at 18°C)
Density (kg/m^3)	900-920	850

1.2.4 Applications of bio-oil

Bio-oil is a dark brown liquid, and its density is significantly higher than that of woody materials, reducing storage and transportation expenses. Bio-oil cannot be used directly in conventional internal combustion engines. Alternatively, the bio-oil can be converted to a specific engine fuel or a syngas and subsequently bio-diesel through upgrading procedures. Bio-oil is especially appealing for co-firing since it is easier to handle and burn than solid fuel, and it is also less expensive to carry and store. Because of the simplicity of handling, storage, and burning in an existing power plant where additional start-up procedures are not required, bio-oil can offer significant benefits over solid biomass in certain situations. Bio-oil is also an important source of a variety of organic molecules and chemicals.

1.2.5 Importance of biochar

The increased awareness about climate change has thrust biochar into the spotlight. The combustion and breakdown of woody biomass and agricultural leftovers emits a significant quantity of carbon dioxide. Biochar may store CO_2 in the soil, reducing greenhouse gas (GHG) emissions and increasing soil fertility. Aside from the potential for carbon sequestration, biochar offers various other advantages, which are outlined below.

- Biochar can improve available nutrients for plant development, retain water, and minimize fertilizer usage by limiting nutrient loss from the soil.
- Biochar lowers methane and nitrous oxide emissions from soil, hence lowering GHG emissions even further.
- Biochar may be used as a substitute for other biomass energy systems in a variety of applications.
- Biochar can be used as a soil amendment to boost the yield of plant growth.

1.3 Pyrolysis reactors

The reactor is the most important component of every pyrolysis operation. The heating system is a vital component of the manufacturing facilities. Several reactors have been built over the last two decades to accomplish this aim, depending on the heating system used. Table 1.3 summarizes the characteristics of fast pyrolysis reactors for bio-oil processing.

Researchers have investigated a variety of pyrolysis reactors, including fixed bed, bubbling bed, fluidized bed, cyclone bed, vacuum reactor, etc. [14,15]. Among these reactors, the fluidized bed reactor yields the most bio-oil because it can be used at lower temperature and high heating rate.

Table 1.3. Overview of fast pyrolysis reactors for bio-oil production [16,20]

Property	Status	Bio-oil yield on dry biomass (wt%)	Complexity	Feed size specification	Inert gas requirements	Specific reactor size	Scale up	Gas quality
Fluidised bed	Commercial	75	Medium	High	High	Medium	Easy	Low
CFB and transported bed	Commercial	75	High	High	High	Medium	Easy	Low
Rotating cone	Demonstration	70	High	High	Low	Low	Medium	High
Entrained flow	Laboratory	60	Medium	High	High	Medium	Easy	Low
Ablative	Laboratory	75	High	Low	Low	Low	Difficult	High
Screw or auger	Pilot	60	Medium	Medium	Low	Low	Medium	High
Vacuum	None	60	High	Low	Low	High	Difficult	Medium

Table 1.4 summarizes the benefits and drawbacks of several types of reactors used in biomass pyrolysis [16], [21].

Table 1.4. Summary of advantages and disadvantages of different reactors for biomass pyrolysis

Type	Advantages	Drawbacks
Bubbling fluidized bed	Elevated bio-oil yield	Limit of biomass particle size
	Even temperature distribution avoids hot spots	The risk of ash fusion
	Easy regeneration of catalyst	
	Good solids and gases mixture is achieved	
Circulating fluidized bed and transported bed	High throughput	Increased reactor vessel size
	Uniform particle mixing	Pumping requirements and pressure drop
	Uniform temperature gradients	Particle entrainment
	Ability to operate reactor in continuous state	Lack of current understanding
		Erosion of internal components
		Pressure loss scenarios

Type	Advantages	Drawbacks
Rotating cone	High efficiency of heat transferring	High energy consumption
	No inert gas needed	
Ablative pyrolysis	Large particle can be used	Reaction rates limited by heat transfer to the reactor
	Inert gas is not required	High cost to scale up
	Controllable residence time	High gas flow and production dilution
	System is more intensive	
	Good heat transfer	
Grinding pyrolysis	Ability to handle wide range of particle sizes	Plugging risk
	Easy to scale up	low bio-oil yield
		High water content in bio-oil
Auger	Low pyrolysis temperature	Plugging risk
	Compact, flexible design	Lower bio-oil yield
	No carrier gas, dilution	Moving parts in the hot zone
	High quality of char produced	Heat transfer limitation

Fluidized bed reactor

As illustrated in Figure 1.5, fluidization occurs when tiny solid particles are suspended in an upward moving stream of fluid. The fluid velocity is adequate to suspend the particles but insufficient to transport them out of the vessel. The solid particles rapidly swirl around the bed, resulting in efficient mixing. The fluidized substance is usually a solid, whereas the fluidizing medium is either a liquid or a gas. The qualities and behavior of a fluidized bed are substantially influenced by both solid and gas properties. Nearly all significant commercial applications of fluidized bed technology concern gas solid systems.

Fluidized beds outperform conventional process technologies in three ways: improved heat transmission, the capacity to transport materials like a fluid, and the ability to process with a wide particle size variation. Heat may be transported far more efficiently by moving particles than by gas alone. The catalyst in the reactor can be added or withdrawn without needing a shutdown.

The performance of bubbling fluidized bed pyrolyzers is consistent with high liquid yields of 30–65 wt.% from wood on a dry feed basis. To achieve high biomass heating rates, the particle sizes of the biomass should be tiny, less than 2–3 mm. The residence time of solids and vapors is controlled by the fluidizing gas flow rate. The biochar generated during pyrolysis should be removed from the bio-oil since it functions as an excellent vapor cracking catalyst. Typically, an ejection and entrainment system is installed for this purpose, followed by separation in one or more cyclones [4], [16]. A common schematic of bubbling fluidized bed reactor is shown in Fig. 1.5.

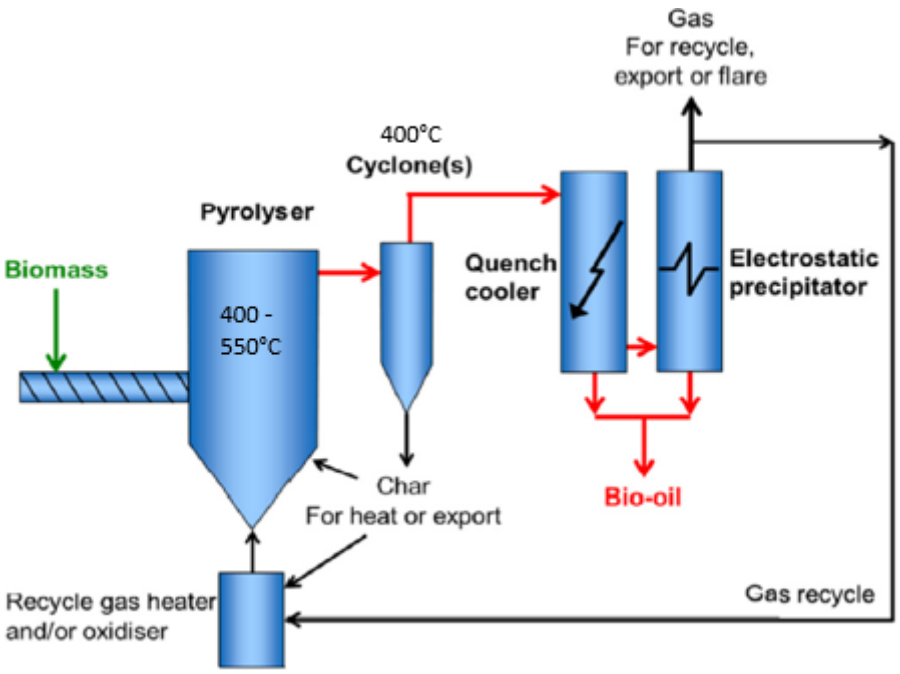

Figure 1.5. A common schematic of bubbling fluidized bed reactor

1.4 Modeling of pyrolysis

The use of the Aspen Plus modeling software in process engineering has grown significantly in recent years. It's a modeling software that calculates a process's physicochemical parameters. The tool is popular because it may be used for all phases of the process (solid, liquid, and vapor) [22]. A few recent studies have shown that the simulation tool may be used to analyze pyrolysis experiments and forecast the process yield(s) [23]. The tool is also effective in optimizing the pyrolysis process operating parameters such as heating rate, temperature, solid residence time, feedstock size, etc.

Aspen Plus contains a directory of different reactors suitable for pyrolysis process. For example, *RYield* reactor is used when product yield of the reaction is known. Similarly, *RCSTR* (Continuous stirred tank reactor) is employed when stoichiometry and kinetics of the reaction

are available. Reactions kinetics can be specified by built-in reaction models and user-defined external Fortran subroutines.

So far, pyrolysis models which have been studied and developed in Aspen Plus are based on the work of Ranzi et. al. [24] which target the cellulosic biomass. The biomass is first decomposed into cellulose, hemicellulose and lignin and then in the second reactor, pyrolysis reactions take place. The decomposition of biomass into basic building blocks (cellulose, hemicellulose and lignin) takes place in *RYield* reactor, followed by pyrolysis reactions in *RCSTR* and then secondary reactions in *RYield* reactor [25,26]. The decomposition of biomass is governed by Power Law type reactions [25,27].

$$r = k * T^n * e^{-E/RT} \quad 1.1$$

Where r is the rate of reaction, k is pre-exponential factor, T is the temperature, E is the activation energy and R is gas law constant.

Typical particles size of biomass ranges from 2-3 mm in a circulating fluidized bed reactor [26,28]. The bio-oil yield ranges from 28 wt.% to 64 wt.% of dry biomass [1,28,29]. Optimum temperature for maximum bio-oil yield can vary from 400 to 520°C depending upon the type of biomass [1,26–28,30–32]. For fluidizing purpose, nitrogen gas or non-condensable gases can be used [28,31]. Several catalysts have been employed for in-situ and ex-situ pyrolysis among which zeolites (HZSM-5) are gaining more ground [33–35].

Table 1.5. Developed pyrolysis reaction models and kinetics [36,37]

Reactions	**Kinetic constant** (1/s)	**Activation energy** (kJ/mol)
CELLULOSE -> CELLA	8.00E+13	192.5
CELLULOSE -> 5H2O + 6 Char	8.00E+07	125.5
CELLULOSE -> LVG	4T	41.8
CELLLOSE -> 0.95HAA + 0.25Glyoxal + 0.25HMFU +0.2Aceton + 0.16CO2	1.00E+9	133.9
HCE -> 0.4HCE1 + 0.6HCE2	1.00E+10	129.7
HCE1 -> 2.5H2 + 0.124H2O + CO + CO2 + 0.25Methanol + 0.5Formaldehyde + 0.125 Ethanol +2Char	3.00E+09	113
HCE1 -> Xylan	3T	46
HCE2 -> CO2 + 0.5 CH4 + 0.25 C2H4 + 0.8CO + 0.8H2 + 0.7Formaldehyde + 0.25 Methanol + 0.125Ethanol + 0.125H2O + Char	1.00E+10	138.1
LIG-C -> 0.35LIG_{CC} + 0.1pCoumaryl + 0.08Phenol + 0.41C2H4 + H2O + 0.495CH4	4.00E+15	202.9
LIG-H -> LIG_{OH} + Aceton	2.00E+13	156.9
LIG-O -> LIG_{OH} + CO2	1.00E+9	106.7
LIGCC ->> 0.3pCoumaryl + 0.2 Phenol + 0.35Acrylic + 0.7H2O + 0.65CH4 + 0.6C2H4 + 1.8CO + H2 + 6.4Char	5.00E+6	131.8
LIGOH -> LIG + H2O + Methanol + 0.45CH4 + 0.2C2H4 + 2CO + 0.7H2 + 4.15Char	3.00E+08	125.5
LIG -> Lomped-phenol	8T	50.2
LIG -> H2O + 2CO +0.2Aceton + 0.4 Methanol + 0.2Aceta + 0.2Formaldehyde + 0.6CH4 + 0.65C2H4+ 0.5H2+ 5.5Char	120E+09	125.5

1.5 Exergy

Exergy is a measure of a substance's maximal theoretical work available if it were to reach equilibrium with its surroundings. The use of exergy concept can be found in determining the potential of energy resources. The standard accepted reference values are 298 K and 1 atm. Exergy for unit mass can be expressed by the relation given below [38].

$$E_x = (h - h_o) - T_o(s - s_o) + \frac{V^2}{2} + gz + E_{xch} \quad \text{(kJ/kg)} \quad 1.2$$

The first four terms correspond to thermomechanical exergy and the last term indicates the chemical exergy. Input exergy consists of biomass exergy and electrical or thermal exergy to heat the reactor. The exergy of electricity is normally equivalent to electrical energy. Exergy of ash, water produced, exergy of nitrogen for fluidization and exergy associated with electrostatic precipitator being less than 1% of total exergy can be ignored.

Introduction

Environmental and economic concerns of reducing carbon dioxide and increasing fuel flexibility are the motivation for the utilization of biomass as a substitute for fossil fuels for electricity generation, transportation fuels and heat supply. It is critical to develop effective biomass conversion technologies in order to compete with fossil fuels in a biomass-based system [39]. Exergy analysis is the most frequent method for evaluating the performance of various processes. Exergy can clearly detect efficiency gains and reductions in thermodynamic losses, as well as assess the environmental and economic advantages of energy technologies [40]. One of the first stages in using exergy analysis is to calculate exergy.

As biomass is a scarce resource, it must be used as efficiently as possible. An evaluation of a process' operational efficiency is useful for both enhancing its performance and comparing it to other conversion processes. Exergetic analysis, which finds thermodynamic irreversibilities in energy conversion systems and may be utilized to enhance operational efficiency, is a useful technique for this purpose. Although exergetic analysis has been frequently used in power plants and other comparable processes [41], [42], it has only been applied to a traditional or even second generation biofuel processes [43–49].

Peters et. al. [50] conducted an exergy analysis of fast pyrolysis plant modelled in Aspen Plus. The feedstock hybrid poplar having 50% moisture was fed to a circulating fluidized bed reactor

operating at 520°C. Pyrolysis gases were used as fluidizing medium with a flow rate of 1.5 times the flow of feedstock resulting in a residence time of 2 seconds. Decomposition of feedstock takes place in *RYield* reactor, primary reactions occur in *RCSTR* reactor and secondary reactions take place in *RYield* reactor as shown in Figure 1.6. Reaction kinetics are based on the work of Ranzi et. al. [24]. The pyrolysis exergetic efficiency comes out to be 71.2%.

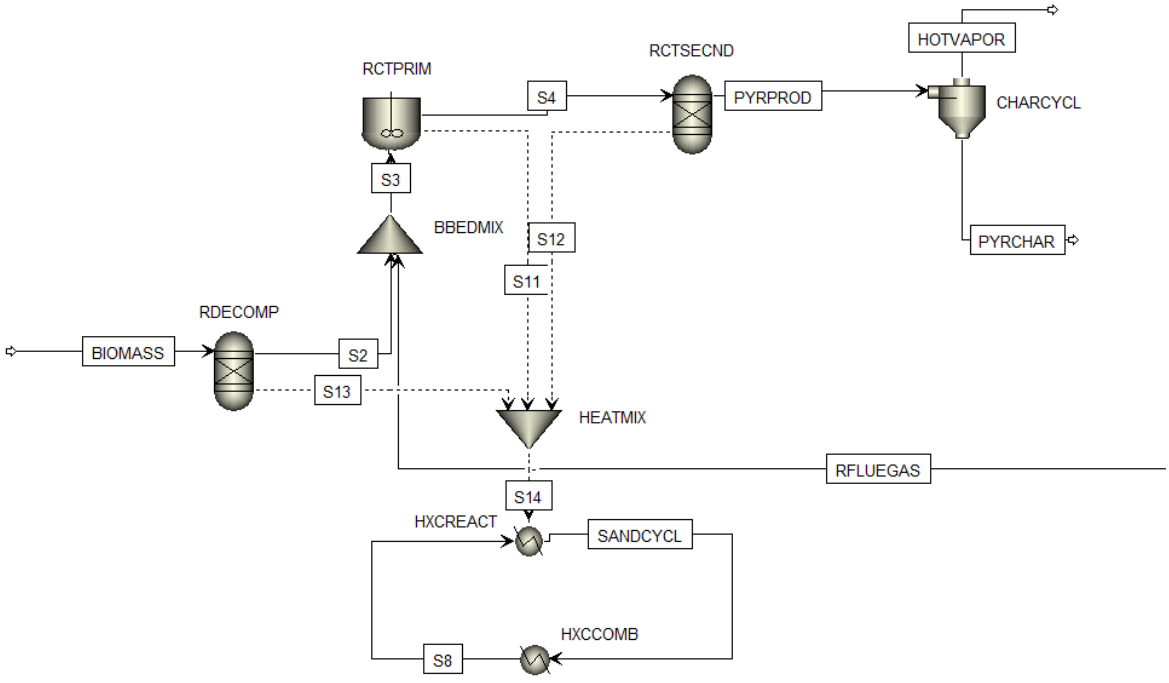

Figure 1.6. Aspen plus flowsheet of reactor model

Similarly, Boateng et. al. [38] performed a mass, energy and exergy analysis of pyrolysis of different biomasses for production of bio-oil. The system uses a bubbling fluidized bed reactor with a diameter of 7.62 cm operating in the range of 400-450°C. The biomass feed rate is 2.5 kg/h. The system includes two cyclones for biochar collection, four chilled water condensers connected in series and three electrostatic precipitators for collection of bio-oil. All the material streams are analyzed by their heat of combustion or high heating value (HHV). Hence energy of a material stream is given by

$$E = HHV \quad \text{(MJ/kg)} \qquad 1.3$$

Energy recovery is computed by following relation

$$Energy\ recovery = \frac{Useful\ energy\ output}{Energy\ input} \qquad 1.4$$

The chemical exergy of biomass, biochar and bio-oil is not well defined so statistical methods are applied and regression equations reported for a large number of organic compounds and fuels are employed [51]. The general form of exergy for dry substances on the basis of lower heating value (LHV) with negligible ash and sulfur is given by

$$E_{xch} = \beta\ (LHV) \quad \text{(MJ/kg)} \quad 1.5$$

where β is the ratio of mass fraction between H/C, O/C, N/C and S/C and chemical exergy. LHV is the lower heating value of the biomass. The following equation define β with z being the mass fraction [52].

$$\beta_{biomass} = \frac{1.0412 + 0.2160\frac{Z_H}{Z_C} - 0.2499\frac{Z_O}{Z_C}\left[1 + 0.7884\frac{Z_H}{Z_C}\right] + 0.0450\frac{Z_N}{Z_C}}{1 - 0.3035\frac{Z_O}{Z_C}} \quad 1.6$$

$$\beta_{biochar} = 1.0437 + 0.1896\frac{z_H}{z_C} + 0.0617\ \frac{z_O}{z_C} + 0.0428\frac{z_N}{z_C} \quad 1.7$$

$$\beta_{bio-oil} = 1.0401 + 0.1728\frac{z_H}{z_C} + 0.0432\ \frac{z_O}{z_C} + 0.2169\frac{z_S}{z_C}(1 - 2.0628\frac{z_H}{z_C}) \quad 1.8$$

Chemical exergies of non-condensable gases (NCG) are computed by following relation.

$$E_{xch} = e^{ch} + RT_o \ln(y) \quad \text{(kJ/mol)} \quad 1.9$$

The exergy associated with electrical power is equivalent to electrical energy [53]. Exergy efficiency can be defined as

$$\Psi = \frac{E_{x,biooil}}{E_{x,biomass} + E_{electricity}} \quad 1.10$$

The measured exergetic efficiency for switchgrass was 66.5% and model predicted efficiency of 88.3% if all the products were considered useful. If only bio-oil is considered as useful product, the measured exergetic efficiency comes out to be 52.4% while model gave the efficiency of 59.9% [38].

Estimation of chemical exergy is one of the fundamental stages in performance analysis and optimization of biomass conversion systems. Song et. al. [54] developed a practical method for estimating the chemical exergy of biomass on dry basis from the reference environment model

of Szargut et. al. [55]. The method was applied to 86 distinct types of biomass and statistical data showed that the chemical exergy of dry biomass varied between 11.5 to 24.2 MJ/kg. Chemical exergy is always slightly larger than HHV for biomass (db) and the ratio of chemical exergy to HHV is on average 1.047. Therefore, the following empirical correlation may be used to determine the specific chemical exergy of dry biomass.

$$E_{xch} = 1.047 \times HHV \quad \text{(MJ/kg)} \qquad 1.11$$

This equation is specifically useful in exergy analysis of processes while using commercial simulation softwares such as Aspen Plus.

The standard chemical exergies of related compounds of C, H, O, N, and S as well as oxides of Si, Ca, K, P, Al, Mg, Fe, S, Na and Ti on Szargut's R.E model are listed in Table 1.6. The standard chemical exergy of a compound was calculated by means of exergy balance of a reversible formation reaction [51,56].

Table 1.6. Standard chemical exergies and standard entropies of compounds.

Substance	e^o	s^o
	kJ/mol	*kJ/mol.K*
CO_2	19.87	0.214
H_2O *(l)*	0.95	0.070
O_2	3.97	0.205
N_2	0.72	0.192
SO_2	310.93	0.248
SiO_2	1.636	0.041
CaO	129.881	0.038
K_2O	412.544	0.102
P_2O_5	377.115	0.117
Al_2O_3	4.479	0.051
MgO	62.417	0.027
Fe_2O_3	17.656	0.087
SO_3	242.003	0.257
Na_2O	296.32	0.075
TiO_2	21.224	0.050

[a] Abreviations: *l* =liquid phase

1.6 Cost of bio-oil

Several prior studies have reported the cost of producing bio-oil using fast pyrolysis, with assumptions for feedstock cost, production volume, reactor type and other parameters [27,29,30,57–60]. Previous studies have estimated the cost of bio-oil to range between €1.75 and €8.67/GGE (gasoline gallon equivalent) (€0.014/MJ - €0.07/MJ). The capital cost for the study conducted by Wright et. al. [59] is €166 million for a pyrolysis plant of 2,000 tons/day. The production cost of green diesel for a system of 2,000 tons per day feedstock is €0.81 to €1.05 per litre. The economic analysis of a plant of 49 kg/hr Napier grass bagasse indicates that the capital cost is estimated to be €1.77 million and operating cost €0.25 million [27].

The following table 1.7 summarizes the existing commercial and demonstration facilities that are planned or in operation [61].

Table 1.7. Commercial worldwide bio-oil productions technologies [61]

Location	Technology	Feedstock	Primary product	Capacity	Capital Investment	Operation date	Scale	Status
Canada	Fast pyrolysis circulating fluidized bed reactor	Wood residues from Arbec saw-mill	Pyrolysis oil	38 *ML/y	EUR 67.5 M	2018	Commercial, TRL 8-9	Active
Brazil	Fast pyrolysis circulating fluidized bed reactor	Eucalyptus forest residues	Pyrolysis oil	83 ML/y	EUR 66.6 M	Unknown	Commercial Technology readiness level (TRL) 8	Under development
Canada	Hydrothermal liquefaction	Wood and pulp residues from Kraft pulping	Bio-crude	80 ML/y	EUR 27M	Unknown	Demonstration to commercial, TRL7-8	Under development
Canada	Fast pyrolysis circulating fluidized bed reactor	Mill and forest woody residues	Pyrolysis oil	11 ML/y	Unknown	2006	Commercial, TRL 9	Active
Finland	Fast pyrolysis VTT fluid riser reactor	Forest residues, sawdust	Pyrolysis oil	43 ML/y	EUR 38 M	2013	Commercial, TRL 8	Active
Finland	Fast pyrolysis, rotating cone reactor	Sawdust and wood residue	Pyrolysis oil	20 ML/y	EUR 25M	Q4 2020	Commercial, TRL 8	Active
Netherlands	Fast pyrolysis – rotating cone reactor	Clean woody biomass	Pyrolysis oil	20 ML/y	EUR 19M	2015	Commercial, TRL 8	Active
Sweden	Fast pyrolysis rotating cone reactor	Sawdust	Pyrolysis oil, oil refinery co feed	21 ML/y	EUR 12M	2021	Commercial, TRL 8	Under construction
USA	Fast pyrolysis, circulating fluidized bed reactor	Mill wood residues, forest residues	Pyrolysis oil	76 ML/y	EUR 60.6M	Unknown	Commercial, TRL 8	Late stage development
USA	Fast pyrolysis, circulating fluidized bed reactor	Wood residues	Specialty chemicals	9 ML/y	Unknown	1995	Commercial, TRL 9	Active
Australia	Hydrothermal liquefaction	Wood, agricultural residue, pulp and paper	HTL bio-crude	9 ML/y	EUR 48M	2012	Demonstration to commercial, TRL 6-7	Active

Australia	Hydrothermal liquefaction	Sewage sludge, microalgae, recycled tyres	HTL bio-crude	Unknown	EUR 7.5M	2014	Demonstration, TRL 7	Inactive
Canada	Fast pyrolysis, auger reactor	Woody residues	Pyrolysis oil	50 t of biomass/d Upto 6 ML bio-oil/y	EUR 4.7M	Unknown	Demonstration, TRL6	Active
China	Fast pyrolysis, downdraft circulating fluidized bed reactor	Rice husks	Pyrolysis oil	1-3 t of biomass/h 2-6 ML bio-oil/y	Unknown	2016	Demonstration, TRL6-7	Active
China	Fast pyrolysis, fluidized bed	Wood and agricultural waste	Pyrolysis oil	15 t of biomass/d 2 ML bio-oil/y	Unknown	2010	Demonstration plant, TRL6	Unknown
India	Integrated hydropyrolysis and hydroconversion	Forestry, agricultural and urban waste	Gas, jet and diesel fuels	5 t biomass/d Upto 0.5 ML fuel/y	Unknown	Commissioned 2018-2019	Demonstration, TRL6-7	Active
India	Pyrolysis	Waste materials, nuts, sewage sludge	Pyrolysis oil	Unknown	Unknown	Unknown	Demonstration, TRL7	Unknown
Norway	Hydrothermal liquefaction	Forest residues	HTL bio-crude	4000 L/d 1 ML/y	EUR 50M	2019	Demonstration, TRL7-8	Active
Turkey	Catalytic hydrothermal liquefaction	Various biomass sources	HTL bio-crude	15 t of biomass/hr Upto 20 ML bio-crude/y	Unknown	2016-2017	Demonstration, TRL7	Active
USA	Fast pyrolysis, Ablative reactor	Demolition wood, Bark beetle infested trees, forest and agricultural residues	Pyrolysis oil	500 kg biomass/hr Upto 1.3 bio-oil ML/y	Unknown	June 2020	Pilot to demonstration, TRL6-7	Under development

*ML/y Million liters per year

Economic Parameters

Economic analysis of large-scale model can be conducted in Aspen Process Economic Analyzer (APEA) or Aspen In-plant cost estimator [29][58]. The total plant investment cost is estimated by Peters and Timmerhaus method [62]. Once the equipment is purchased, it is installed at a cost of 3.02 times the total equipment purchased cost. Installation cost includes piping, electrical, yard improvement, building, equipment, installation etc. The indirect cost is 0.89 times the total purchase equipment cost and is made up of contractor's fee, legal expenses, construction expenses and engineering and supervision costs.

The cost of pyrolysis reactor and regenerators is evaluated from the scaling equation stated by Wright et. al. [59].

$$C_1 = C_o.\left(\frac{S_1}{S_o}\right)^{0.6} \qquad 1.12$$

Where C_1 is the estimated cost with the size of S_1 and C_o is the base cost with the size of S_o.

The profitability analysis is performed using discounted cash flow method (DCF). For DCF analysis, the plant can be assumed to operate for a 20-year period (t). In addition, income tax of 30% is applied to the DCF calculation. Minimum fuel selling price is computed by setting the NPV equal to zero in the equation while other variables were held constant.

The main factors effecting the MSF significantly are fuel yield, income tax and operating cost as observed by sensitivity analysis [58]. The energy analysis can be performed by assigning appropriate utilities in Aspen Energy Analyzer (AEA) tool [27].

Power requirements for biomass grinding are based on research by Mani et. al. [63]. This model employs a rule of thumb for calculating the drying energy requirement of 5 MJ per kg of water evaporated using a steam rotary dryer.

The cost of the heat exchange network can be derived by scaling from the design report [64] using the total heat duty. The total installed cost is obtained by employing installation cost to bare equipment costs. Bare equipment costs are computed from vendors, engineering consultants and Aspen Capital Cost Estimator (ACCE). Variable operating costs are calculated based on the materials and energy use whereas fixed operating costs are based on expenditures such as plant maintenance cost and personnel.

1.7 Waste heat for Process cooling

For the sake of this study, waste heat will be defined as heat generated in a process that would otherwise be rejected to the environment. The viability of utilizing waste heat in a process is determined by the temperature, amount, and availability of the waste heat, with the principal advantage being a reduction in the process's energy requirement. Increased energy efficiency has several advantages, including lower primary energy input, lower carbon dioxide and other emissions, and lower operational expenses. As a result, when practical, waste heat utilization is an appealing upgrade.

Many industrial processes discharge large amounts of heat into the environment as low/medium temperature effluents. These effluents may be gases (e.g. exhausts from furnaces) liquids (e.g. cooling water) or vapors (e.g. excess in process steam production). Obviously, attempts have been made to maximize the use of primary energy by exploiting heat in other process phases e.g. to pre-heat materials prior to entry into the production phase.

Numerous studies have been conducted to assess the viability of waste heat for a variety of applications, including water desalination, air conditioning, gas turbine performance increases, and vapor compression enhancements [65–68]. However, there have been few studies that have particularly explored waste heat management in pyrolysis plants.

The financial circumstances and environmental laws for industrial and agricultural cooling energy generation have shifted dramatically in recent years. With high electricity rates and stringent environmental regulations, an absorption chiller is the ideal option for using waste heat from industrial operations or power generation. It is more cost effective than traditional compression chillers.

Absorption chillers can be used to recover process waste heat to provide cooling which improves energy efficiency. An absorption chiller is a closed loop cycle that uses waste heat to provide cooling or refrigeration. The application of absorption chillers has been limited due to their comparatively low efficiency in delivering cooling when compared to vapor compression cycles. For comparison, coefficient of performance of an absorption chiller ranges from 0.5 to 1.5, based on heat input. The COP of modern vapor compression cycles is greater than 3.0. However, absorption chillers remain practical in some applications due to their ability to employ low temperature (<100°C) heat to produce cooling. In this respect, the COP of an absorption chiller cannot be compared to the COP of other cooling cycles since the input energy

for an absorption chiller might be basically free, such as waste heat, which would otherwise go unused in most processes. As a result, in processes where low temperature heat is accessible and cooling is necessary, it frequently makes sense to incorporate an absorption chiller to improve overall process efficiency [69,70]. As a working fluid, absorption chillers employ a refrigerant-absorbent pair. Water/lithium bromide (LiBr) and ammonia/water are the two most prevalent working fluid combinations. In addition, cycles might have a single, double, or even triple impact. Multi-effect cycles require more components and waste heat at higher temperatures but offer better COPs.

The following section explores the possibility of using absorption chillers to utilize waste heat in pyrolysis of olive mill wastewater sludge. The absorption cooling cycle is modelled in Aspen Plus and integrated with pyrolysis process.

1.7.1 Absorption cooling system

The cooling cycle of single effect absorption cooling system is given in Figure 1.7. A heat medium (hot water) ranging from 70°C to 95°C from an industrial process, cogeneration system, solar energy, or other heat source powers the absorption cycle. The nominal thermodynamic performance of absorption chillers is given by the coefficient of performance or EER/Energy efficiency ratio which is the ratio between cooling energy obtained and thermal energy used. This coefficient is 0.7 for a typical absorption chiller. There are different types of refrigerant-absorbent pairs which can be utilized for absorption refrigeration systems. The most familiar pairs that provide acceptable thermodynamic performance and are environment friendly are lithium bromide-water and ammonia-water pair.

In this work, the working fluid of the absorption chiller is a solution of lithium bromide and water. The refrigerant is water, while the absorbent is lithium bromide, a harmless salt.

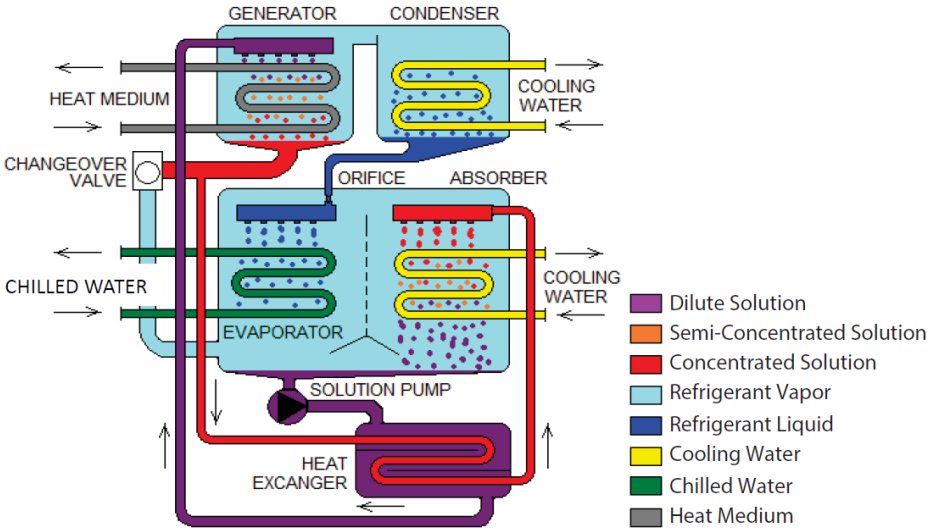

Figure 1.7. Absorption cooling system

1.7.1.1 Process description

The weak solution of lithium bromide and water is pumped into the generator where heat is supplied through a hot medium. The water is evaporated and passes to the condenser where it is condensed. The strong solution returns from the generator to the absorber and it passes through the heat exchanger where it pre-heats the weak solution of lithium bromide (LiBr) and water (H_2O), thus increasing the efficiency of the absorption chiller. Water is evaporated in the evaporator by absorbing heat from the environment or other fluid and is absorbed by strong solution of lithium bromide (LiBr) in the absorber.

The major steps involved in the absorption cooling process are presented in the pressure versus temperature chart as shown in the Figure 1.8.

1) Line 1-7 shows pumping of the weak solution from the absorber to the generator by passing through the heat exchanger. Properties of weak solution at the outlet of heat exchanger are represented by point 7 whereas concentration remains same for the solution.
2) The heating of the weak solution by hot water in the generator is indicated from route 7-2. It is sensible heating, because it raises the temperature of the solution. Line 2- 3 shows the latent heating causing boiling of water from the weak solution at the constant pressure of the condenser Pc. During this practice, the weak solution changes into a strong solution by evaporating water vapor.
3) Path 3-4 indicates that strong solution moves from the generator to the absorber by passing through the heat exchanger. Meanwhile the energy of strong solution is utilized

to preheat the weak solution coming from the absorber to the generator. The concentration of the strong solution of lithium bromide (LiBr) remains constant in this process.

4) The heat at the condenser is rejected in the cooling tower and this process is shown by line 2-5. During this process, the pressure of the condenser remains constant (Pc).
5) The water is condensed by rejecting its heat to the cooling medium usually cooling water. This condensed water then flows towards the evaporator. This process is indicated by line 5-6.
6) Low pressure evaporation takes place in the evaporator by absorbing heat from chilled water or the environment. It is represented by line form 6-1, and water vapor is absorbed by the absorber to complete the cycle.

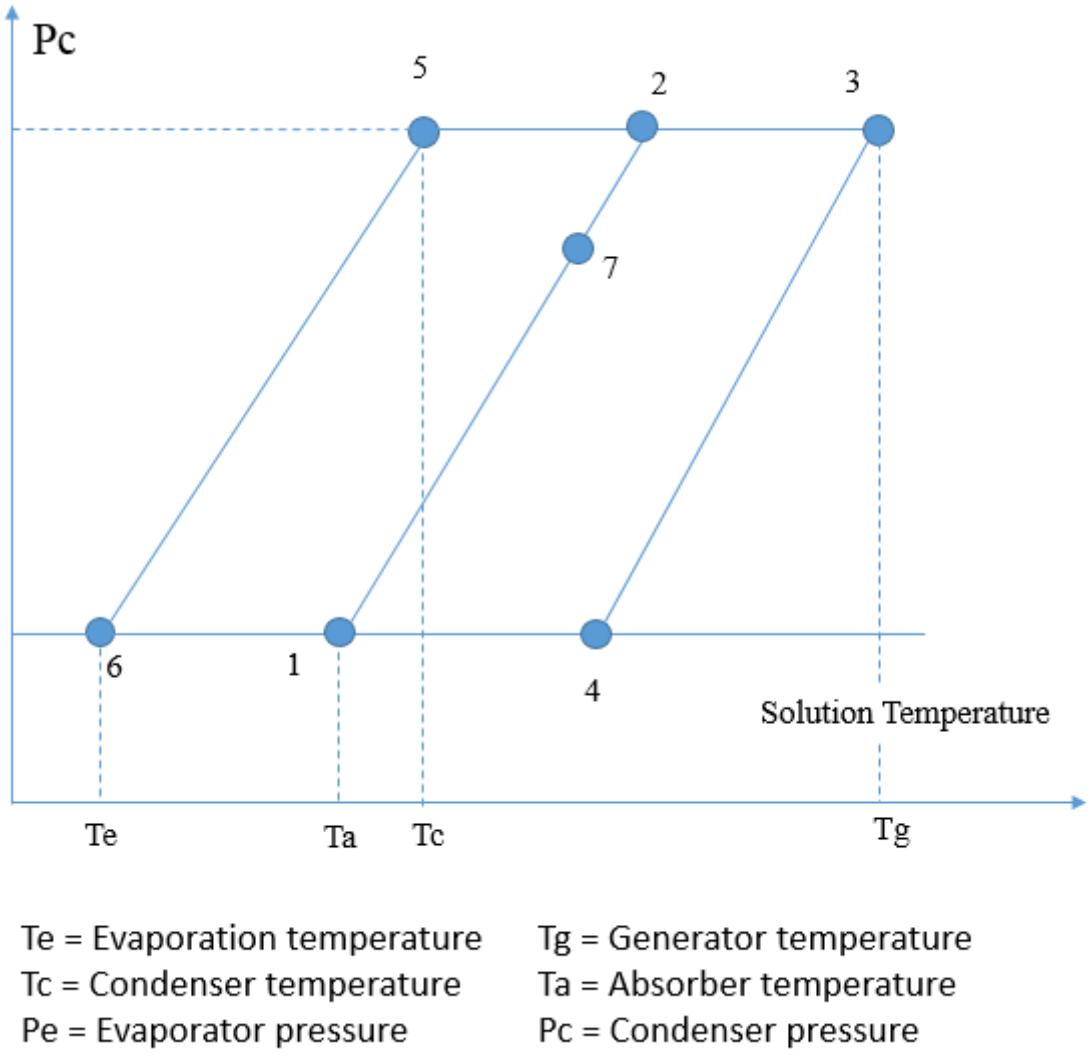

Figure 1.8. Process diagram of absorption cooling system

1.7.1.2 Generator

When the temperature of the heat medium input surpasses 70°C, the solution pump pumps a dilute lithium bromide solution into the generator. On the surface of the generator tubing bundle, the solution boils, producing refrigerant vapor. The vapor rises and enters the condenser. Consequently, the solution gets more concentrated, and the concentrated solution drains into the generator sump and through a heat exchanger before entering the absorper. The heat balance at the generator is given by

$$Q_g = m_v h_v + \left(m_{sol,s} - m_v\right) h_{sol,s} - m_{sol,w} h_{sol,w} \quad \text{(kW)} \quad 1.13$$

In the above equation, m_v is the mass flow rate of refrigerant vapor, $m_{sol,w}$ is the mass flow rate of diluted solution and $m_{sol,s}$ is the mass flow rate of strong solution while h denotes the enthalpy change for the respective state.

1.7.1.3 Condenser

In the condenser, the refrigerant vapor is condensed on the surface of the cooling coil and latent heat, removed by the cooling water, is rejected to a cooling water. Refrigerant liquid accumulates in the condenser sump and then passes through an orifice into evaporator. The heat balance at the condenser is given by

$$Q_c = m_v (h_v - h_l) \quad \text{(kW)} \quad 1.14$$

1.7.1.4 Evaporator

Due to the action of the absorber, the refrigerant liquid is subjected to a much deeper vacuum in the evaporator than in the condenser. The refrigerant liquid evaporates as it travels over the surface of the evaporator coil, removing heat from the chilled water circuit equal to the latent heat of vaporization. The refrigerant vapor is drawn to the absorber once the recirculating chilled water is cooled to the desired set temperature.

$$Q_e = m_v (h_l - h_v) \quad \text{(kW)} \quad 1.15$$

1.7.1.5 Absorber

The affinity of the concentrated solution from the generator for the refrigerant vapor generated in the evaporator maintains a deep vacuum in the absorber. The concentrated lithium bromide solution flowing across the surface of the absorber coil absorbs the refrigerant vapor. The cooling water removes the heat from condensation and dilution and sends it to a cooling tower.

The dilute solution is then heated in a heat exchanger before being returned to the generator to repeat the cycle.

$$Q_a = m_v h_v - m_{sol,w} h_{sol,w} + (m_{sol,s} - m_v) h_{sol,s} \quad \text{(kW)} \quad 1.16$$

1.7.2 Important Features

- The absorption cycle is energized by hot water. Hot water can be from any source including cogeneration, solar or any waste heat sources as long as it can be provided to the generator at a temperature between 70°C to 95°C.
- Lithium bromide and water working fluid functions in a vacuum at all times and is safe, odorless, and nontoxic.
- The hermetically sealed solution pump is the only revolving component. As a result, having a finite number of movable mechanical parts reduces the number of components that are vulnerable to wear and tear, requiring less monitoring and maintenance.
- CFCs and HCFCs, which are very harmful to the environment and have since been prohibited, are not used in absorption chillers. Furthermore, the primary energy utilized lowers emissions of toxic combustion products.
- They're designed to be installed outside, even in hostile environments like coastal and industrial applications. The refrigeration plant no longer needs to be housed in utility rooms.
- The primary energy used is thermal which can be waste heat from any origin. Only the auxiliary control, fluid circulation, and heat exhaust appliances need electricity.

1.8 Modeling of absorption chiller in Aspen Plus

In the past, absorption chillers have been modelled and simulated in a number of programs, such as the one developed by Lazzarin et al [71]. Modern models are commonly developed in one of two softwares: Absorption simulation (ABSIM), developed by Oak Ridge National Laboratory [72] and Engineering Equation Solver (EES), developed at the University of Wisconsin [73–75]. When compared to actual data, EES modeling allows the user to compute thermo-physical parameters of working fluids with high accuracy [76].

Models for single and double effect water/lithium bromide and ammonia/water chillers were developed in Aspen Plus by Somers et. al. [77]. The model was coupled with a gas turbine as a waste heat source, and parametric studies were carried out for a variety of part load circumstances, evaporator temperatures, and ambient temperatures. For the water/lithium

bromide solution, the ELECNRTL property technique was employed [78]. It is ideal since it was created exclusively for electrolytes solutions, making it advantageous to other robust but less specialized approaches like Peng-Robinson. The steamNBS property approach was utilized to determine the pure water states [79]. When the simulated results are compared to experimental data, the model shows an excellent agreement of within 5% for water/lithium bromide and 7% for ammonia/water. Finally, among the three models, the best chiller design was chosen, and an annual performance analysis was performed to assess the predicted cooling performance and energy savings. A range of cycle choices were investigated when the model was developed in Aspen Plus. The exhaust from a gas turbine was used as the waste heat resource.

Several other researches have been conducted to model the absorption chiller in Aspen Plus [80,81]. Using the Aspen Plus simulator, Darwish et al. [81] investigated the absorption refrigeration system (water/ammonia). The findings were compared to data generated by manufacturers and published in the open literature. COP (coefficient of performance), heat duties of the evaporator, absorber, and condenser, concentration in the ammonia weak and ammonia strong solutions, and flow rates of the ammonia weak solution and refrigerant vapor exiting the evaporator were all used in the analysis. The model findings and the experimental data were found to be in good agreement.

The choice of Aspen Plus over other available programs to simulate the absorption chiller was principally motivated by two factors. First, Aspen chiller models might be immediately incorporated into the pyrolysis process. Second, Aspen Plus features an optimization capacity that will help in the development of a design that maximizes the energy savings.

1.9 Life cycle assessment (LCA)

LCA is a technique for evaluating a product's environmental performance across its whole life cycle, from raw material extraction to final disposal, including material recycling if necessary. The most common applications for an LCA are as follows:

- Identifying improvement possibilities in a product's life cycle by identifying environmental hot spots
- Assessment of the contribution of each step of the life cycle to the total environmental load, generally with the goal of prioritizing product or process upgradation.

- For internal or external communication, as well as a foundation for environmental product declarations, product comparisons are useful.
- The foundation for life cycle management and decision reporting in businesses is the use of standardized metrics and the identification of key performance indicators.

Unlike traditional environmental analysis tools, this method has the advantage of focusing on the elementary stages of the life cycle of the product studied. Main approaches are listed below:

- The 'cradle to grave' analysis includes all the basic steps from the extraction of raw materials and resources to the disposal or reuse of the product.
- The 'cradle to gate' approach deals with the extraction of raw materials to the finished product (ready to be shipped or transported at the factory gate). The use and disposal phase are not included in this study.
- The 'door to grave' analysis where only the use and disposal phases are taken into account.

Life cycle assessment (LCA) is a well-known technique that examines environmental implications over the whole life cycle of a product or service [82,83]. LCA is a complete monitoring of the energy and materials used in the product chain of items or systems, and is primarily used to compute the emission of each material and stage that finally forms the final product to the environment [84,85]. As a result, LCA assesses the aggregate possible environmental consequences [86]. The primary goal is to establish documentation and ameliorate the overall unfavourable environmental profile of the researched product or service [87].

1.9.1 Introduction

Life cycle assessment techniques were first developed as part of a research by Coca-Cola in 1969 to determine whether glass or plastic bottles were more environmentally friendly [88]. Over the next 20 years, more companies conducted their own studies aimed at environmentally friendly waste disposal. In the 1990s, the LCA framework was improved, leading to the establishment of ISO standards 14040 to 14044.

This standardization gathers the definitions of the vocabulary dedicated to the practice of LCA and establishes the phases of realization by describing the elements that compose them [89]. It also presents recommendations for communicating the conclusions and for carrying out the critical review of an LCA study. In accordance with the methodological framework defined by

SETAC and ISO 14044(2006), LCA is composed of four steps illustrated in the following figure.

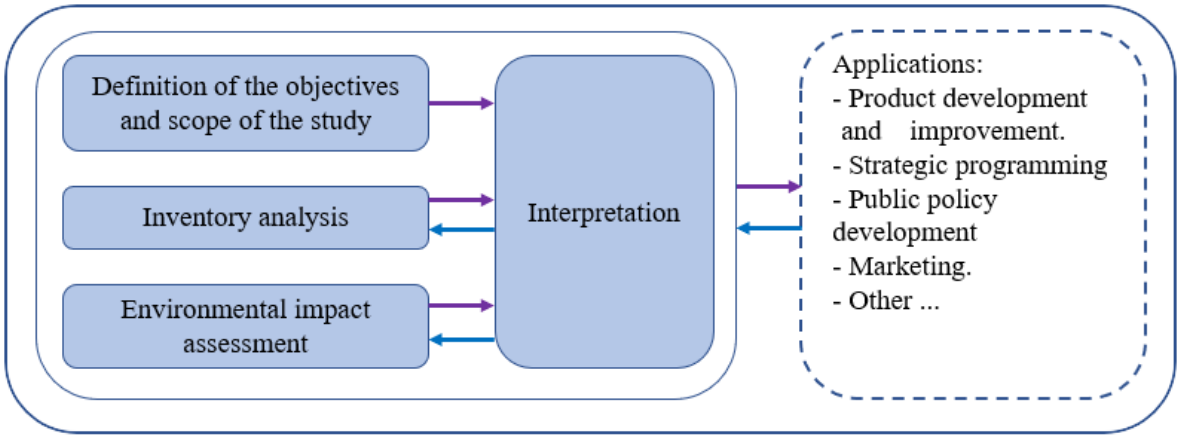

Figure 1.9. The phases of a life cycle assessment (ISO 14044, 2006)

1.9.2 LCA of biofuel production systems

The environmental issues related with the use of non-renewable feedstocks, as well as the uncertainty of the oil market, have sparked considerable interest in the use of readily accessible lignocellulosic materials as a source of energy and chemicals. This strategy is critical for developing nations as the substitution of petroleum and its derivatives creates a market for new biorefinery goods.

To minimize net greenhouse gas emissions and delay the depletion of fossil fuels, there has long been a pressing need to develop an alternative fuel that can replace rising fossil energy usage. Because of its substantial environmental benefits, biomass has garnered attention as a viable renewable fuel [92–94].

There is a broad consensus in the scientific community that life cycle assessment (LCA) is one of the best methods for evaluating the environmental burdens associated with the production and use of biofuels and fossil fuels. The most studied impact categories are Global Warming Potential (GWP) and non-renewable energy consumption. Their results can be very useful on a regional, national or global scale.

In general, LCA results can be used to suggest "greener" products or sustainable production methods by providing insights into raw material conservation and waste and emission reduction. They can also be used to identify potential improvements in the environmental performance of some of the systems studied.

In particular, comparing the emissions associated with bio-oil produced by different systems or those from a fossil fuel allows to determine the carbon benefit and mitigation performance of these emissions. The importance of such a study lies in proposing the most environmentally friendly biofuel production systems and demonstrating a reduction in greenhouse gas (GHG) emissions as a result of replacing fossil fuels with biofuels.

It should be noted that the environmental impacts of biomass recovery systems depend on the feedstock sources, conversion technologies and end use.

1.9.3 Previous studies

Given the variety of biomass-to-energy processes and the controversial discussion about their "net benefits", several studies have been conducted using the LCA approach. They are designed to analyze the processes to determine which biofuel involves the most negative environmental impacts. In this context, studies show that pyrolysis technologies are appealing in terms of sustainability and carbon footprint.

Along with the economic implications, the environmental impact of biorefinery technology is a concern. In this regard, studies demonstrate the desirability of pyrolysis technologies in terms of LCA and carbon footprint [95][96]. For example, Dang et. al. [97] conducted an LCA for biofuel production from corn stoves via pyrolysis and hydro processing, and discovered that global warming potential of bio-oil was reduced by 119% when compared to diesel. Similarly, Gebreslassie et al. [96] optimized the life cycle and economics of a hydrocarbon biorefinery via fast pyrolysis, hydrotreating and hydrocracking. They discovered a trade-off between the economic and environmental dimensions of biorefinery, which necessitates an integrated approach to investigate the technology.

In another research work, Steele et. al. [98] studied pine wood pyrolysis and estimated a 70% reduction in GHG emissions for bio-oil produced compared to diesel. Whereas, according to Peters et al. [99] this reduction is lower when we use poplar trees. They recorded a GHG reduction of about 54% of the biofuel blend produced compared to conventional gasoline and diesel.

Other authors have studied the impact of using bio-oil. As an example, Fan et al. [100] reported a GHG reduction of about 77-99% in the case of bio-oil combustion for electricity generation compared to electricity generated by fossil fuels. This is the result of accounting for the reintegration of carbon emitted as CO_2 when biomass is burned, by new plants in a time frame

of a few months to a few decades, which is small compared to the carbon cycle of fossil fuels that requires a few million years to reform.

Despite the available data on pyrolysis processes (primarily at the laboratory scale), no reports or series of papers have evaluated the environmental impacts associated with the pyrolysis of oil mill wastewater sludge. Therefore, we investigate for the first time:

- a comprehensive model of industrial-scale fast pyrolysis of OMWS.
- an environmental assessment of the pyrolysis of olive mill wastewater sludge for the production of bio-oil.

1.9.4 Methodology

The life cycle assessment has four phases, according to the ISO 14044 (2006) standards. These provide a framework for conducting an LCA and are detailed as follows:

Definition of objectives

Generally, LCA studies are conducted to answer specific questions, which determine the objectives of the study. The four classic objectives of an LCA are

- Determining the environmental impact of a product during its life cycle.
- Comparison of different systems to determine the most eco-efficient.
- Comparison of different components of a system's life cycle to determine which emissions contribute the most to the environment.
- Comparing a reference system to a product system.

Definition of the field of study

According to ISO14044 (2006), the main elements of the study scope are:

1.9.4.1 The system function and the functional unit

The function of the system must be well defined because it allows the determination of two important elements of the LCA; the system boundaries and the functional unit (FU). This FU must be quantifiable and additive. It provides a reference to which all flows are related. It is therefore the same in the different scenarios, thus allowing a comparison between them. In the study of bioenergy systems four types of functional unit are identified: the unit of input biomass (in mass or energy unit), the unit of production (unit of electricity, heat, or transport km), the unit of agricultural area used to produce biomass feedstock, and a year.

1.9.4.2 Description of the scenarios

The system is formed by a set of consecutive processes interacting with each other through flows of intermediate products and/or waste to be treated and with the environment through elementary flows (incoming and outgoing) of materials and energy. For the same function of the system, there can be different scenarios depending on the processes used and the existing interactions. In the case of a comparative LCA, a reference system is needed to provide a baseline against which other systems will be compared. In the case of biodiesel, the reference system is most often fossil diesel.

1.9.4.3 The limits and boundaries of the system

System boundaries define the elements that must be incorporated in the system under study. The question in LCA may start with "what should we include?" but can rapidly evolve to "what can we leave out?" while retaining system integrity and details.

1.9.4.4 Data and assumptions

It is important to avoid heterogeneity in the databases used in a single study and to try to use the same source as much as possible. Depending on the difficulty of this phase, it is possible to redefine the boundaries of the system under study and to add assumptions in order to avoid searching for too complicated data.

1.9.4.5 Life Cycle Inventory Analysis

This phase includes the steps of data collection, validation and processing according to the requirements established during the first phase of the LCA. It consists in establishing an inventory table summarizing the energy and material balances of the system's life cycle. Hence a list of inputs and outputs, linked to the functional unit, is elaborated and quantified on the system boundaries. For the data collection phase, the standard suggests these operational steps:

1. Preparation of data collection: life cycle diagram with list of associated data
2. Data collection (calculation, bibliography, measurement, database, expert opinion...)
3. Data validation: to remove all forms of ambiguity
4. Mapping of the data to the functional unit
5. Grouping of the balances of each elementary process on the global system.

1.9.4.6 Environmental impact assessment

The main purpose of the life cycle impact assessment is to convert the system input and output flows already established in the second phase of LCA into a limited number of impacts. This simplifies the understanding and analysis later on.

According to ISO 14044, the impact assessment consists of three steps. It starts with the classification of emissions and removals from the inventory into intermediate impact categories to which they contribute. Then each extraction/emission at the level of each intermediate category is weighted by an impact characterization factor according to its relative influence on the impact under consideration (intermediate characterization). Finally, the intermediate categories are grouped according to the type of damage they are associated with, weighted by damage factors (damage characterization). The impact categories typically addressed in LCA studies of bioenergy systems are Greenhouse Gases (GHG) or Global Warming Potential known as Global Warming Potential (GWP) and energy demands [101].

The following diagram is an example of impact category classification according to the Impact 2002+ method [102].

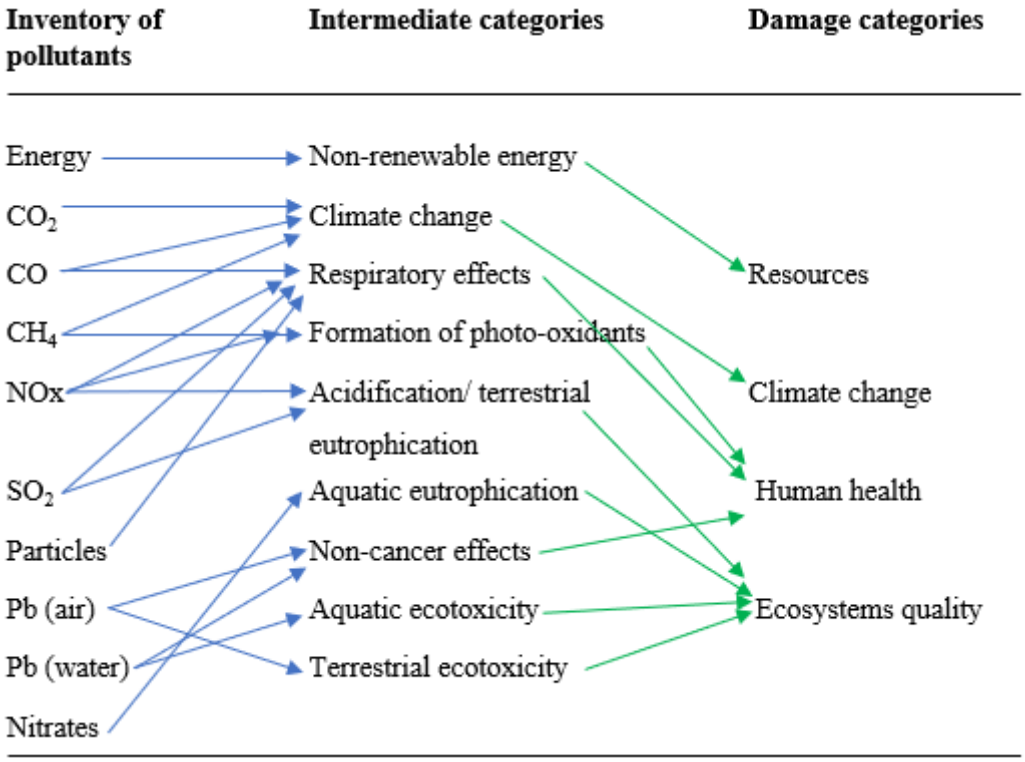

Figure 1.10. Classification of impact categories according to the Impact 2002+ method

To facilitate the analysis of the results obtained by the characterization of impacts, other optional and mathematical methods of multi-criteria analysis are proposed, namely normalization, aggregation and weighting.

It should be noted that this phase is often carried out using Life Cycle Assessment software such as OpenLCA, Gabi, Simapro, etc. The very large amount of data to consider and the need to vary some parameters in order to compare different life cycle scenarios have recently made these softwares very popular. Each software can integrate one (or more) database that allows to model all the information related to the life cycle of the studied system. Among the most used databases, we can mention EcoInvent, LCA Commons, Agri-footprint, Carbon Minds, etc.

1.9.4.7 Interpretation and recommendations

The final phase of the LCA involves interpreting the results of the inventory and impact assessment phases, focusing on the objectives set in the first phase. Interpretation puts the quantitative and qualitative results of the LCA into context, allowing for a better understanding of the impacts of the results. It allows to identify the life cycle phases on which it is necessary to intervene to reduce the environmental impact of the analyzed system. The results of this phase depend strongly on the assumptions, both explicit and implicit, contained in the first phase of defining the objective and the scope of the study.

1.9.4.8 Rules of allocation

The allocation problem arises when the system under analysis provides several products (main product plus co-products). A classical LCA is often only interested in the impacts of one product (or one service). It is then necessary to determine which part of the effect corresponds to it and which part will be attributed to the co-products.

In the scientific literature, many articles discuss this concept of allocation in LCA and describe various approaches (Ekvall et al., 2001 [103]; Bruijn et al 2004 [104]). This concept is very important for bioenergy systems, which are often characterized by multiple products (bio-oil, biogas and biochar). The work of Cherubini et. al. (2011) [101] shows that there is not the same distribution between the different possible allocation alternatives. Therefore, the question of the most appropriate allocation method still remains open.

The ISO 14040 standard proposes to avoid the use of allowances as much as possible. For this reason, the majority of studies use the extension of the system boundaries to an application of co-products. This method can be used when the co-products can substitute similar products

produced by external processes for which environmental impact data are available. In such cases, an additional impact is attributed to the main product of the overall extended system.

While other research allocates the environmental impacts of the system to the various co-products based on physical parameters between the products such as mass, volume, energy content etc. [102]. When no allocation based on physical object is feasible, an economic or functional relationship can be used. Mass-based allocation is one of the most commonly used methods, in contrast to economic allocation which is used when the product is intended for commercial purposes.

CHAPTER 2: METHODOLOGY

2.1 Experimental process overview

Experiments were performed by Agblevor et. al. [1] in Utah State University. Olive mill wastewater sludge (OMWS) is collected from a Tunisian evaporation pond. It is dried at room temperature and then it is passed through the grinder to make its size about 2 mm. The 160 grams of ground biomass is mixed with 40 grams biochar to make it less sticky. Nitrogen gas is used as carrier to blow it into the fluidizing bed reactor with red mud as heat carrier. The mixture of ground biomass, biochar and nitrogen is introduced into the pyrolysis reactor at ambient temperature. Nitrogen as fluidizing gas enters from bottom of pyrolysis reactor at 300°C, 1.02 bar. Red mud is heated at 550°C for five hours before using it in the reactor. The experiment is performed at three different temperatures i.e. 400, 450 and 500°C. At the exit of fluidized bed reactor, bio-oil, steam and NCG are gaseous products while biochar is the solid product. These are separated in a cyclone kept at 400°C so that bio-oil vapors may not condense at this stage. The gaseous products are then passed through two condensers (the first co-flow and the second counter-flow) to condense the maximum of bio-oil and water vapors. Water/ethylene glycol mixture at 8°C was used as cold fluid in the condensers (Figure. 2.2). Remaining bio-oil aerosols, NCG and nitrogen are passed through electrostatic precipitator (ESP) where bio-oil is collected at ambient temperature. The biogas and nitrogen are non-condensable at ambient temperature and pressure and can be used for other purposes.

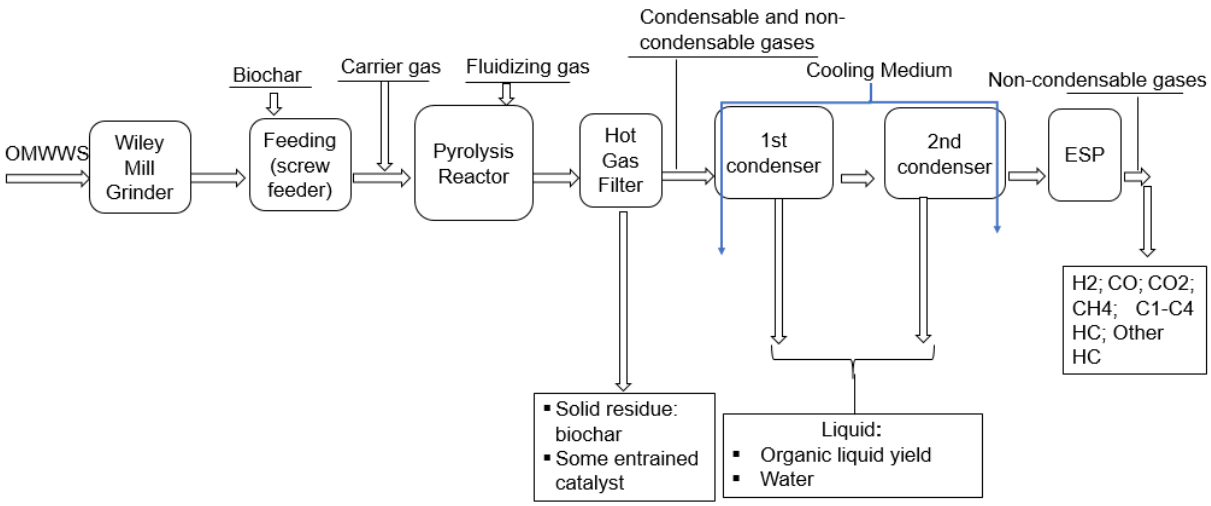

Figure 2.1. Schematic diagram of pyrolysis of OMWS

2.1.1 Feedstock handling and preparation

The handling and preparation of the biomass section aims to treat the OMWS so that it matches the pyrolysis conditions regarding moisture content and particle size. The initial moisture of the OMWS is 10% and particle size is 100 mm. The required particle size for pyrolysis is less than 2 mm with moisture content of 4%.

Proximate and ultimate analyses of OMWS is shown in the following table.

Table 2.1. OMWS attributes

Attribute	**OMWS Biomass**
Proximate analysis (wt. %)	
Moisture	4.08
Fixed Carbon	22.21
Volatile Matter	64.43
Ash	13.36
Ultimate analysis (wt.%)	
Carbon	52.89
Hydrogen	7.16
Nitrogen	1.96
Sulfur	0.6
Oxygen	24.03
HHV (MJ/kg)	25.64

2.1.2 Pyrolysis

The pyrolysis process is conducted in the fluidized bed reactor at 400°C, 450°C and 500°C in the presence of red mud. Fluidized bed reactor is 500 mm long and 50 mm in diameter with 100 μm orifice diameter of gas distributor. 160 grams of OMWS, 40 grams of biochar, 5 l/min of carrier gas (Nitrogen) and 13.3 l/min of fluidization gas (Nitrogen) are fed into the reactor. The residence time of the vapors is 2 seconds.

2.1.3 Solids preparation

After the pyrolysis, the biochar and catalyst particles are separated in a cyclone and hot gas filter (HGF). The larger particles are removed by cyclone while fine particles are eliminated in the hot gas filter. The cyclone operates at 400°C to avoid the pre-condensation of bio-oil vapors.

2.1.4 Vapor Condensation

Shell and tube heat exchangers were used in the experimental setup. The diameter of the shell is 60 mm and tube length is 500 mm with 20 mm diameter (Figure 2.2). Water/ethylene glycol mixture is used as cooling medium at 8°C with flow rate of 8 kg/hr in each heat exchanger.

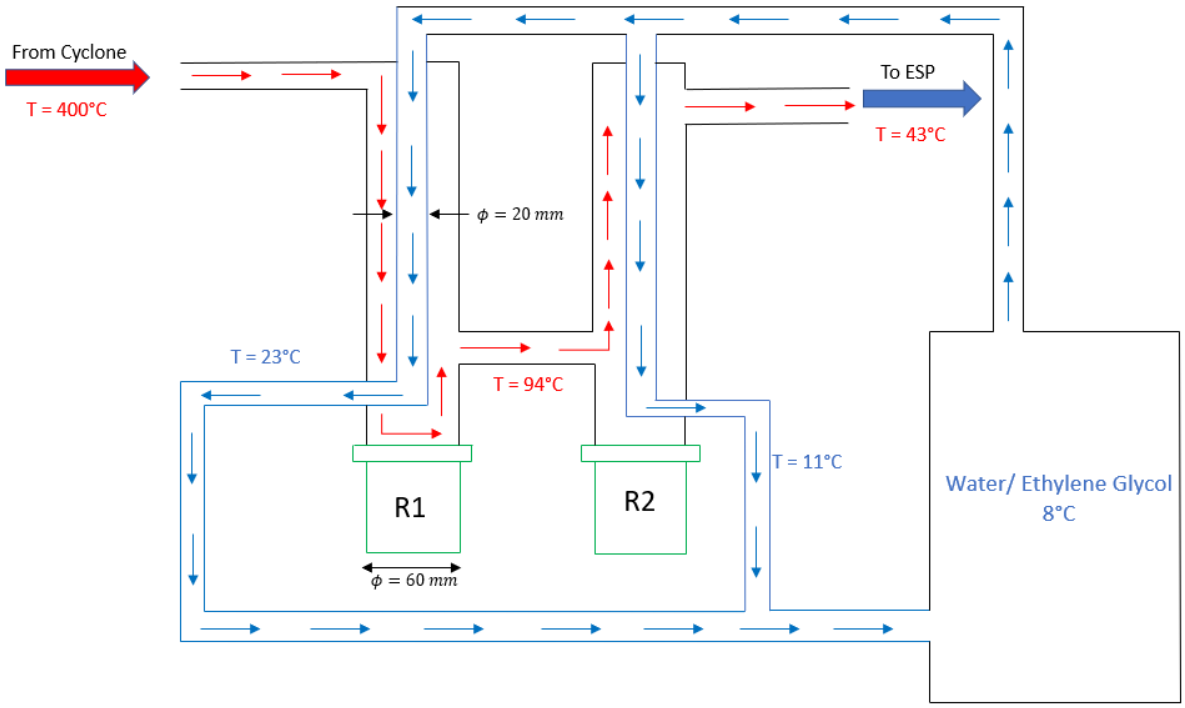

Figure 2.2. Schematic diagram of shell and tube type heat exchanger

2.1.5 Product Yields

Table 2.2 demonstrates the percentages of products in the experiments conducted at different temperatures [1].

Table 2.2. OMWS product yields

Temp. (°C)	400	450	500
Bio-oil (%)	34.6	29.8	29.5
Water (%)	11.3	17.6	11.8
Char (%)	29.1	22.7	20.4
Gas (%)	24.3	30.0	37.3

2.1.5.1 Bio-oil Composition

Bio-oil is a mixture of a number of compounds. The compounds with significant contribution for red mud are given in the following table [1].

Table 2.3. Bio-oil composition

No.	Chemical compound	Peak report (TIC Area %)
1	1-Decene	1.18
2	P-cresol	0.84
3	1-undecene	2.15
4	Undecane	1.47
5	5-undecene	1.51
6	5,6 undecadiene	1.37
7	4-ethyl phenol	0.94
8	2-dodecanone	1.34
9	1-tridecene	2.18
10	Dodecane	1.22
11	8-dodecene-1-ol	1.67
12	N-tridecan-1-ol	4.28
13	Hexadecane	2.82
14	1-tetredecene	4.28
15	N-pentadecanol	7.99
16	Heptadecane	4.47
17	9-octadecene-1-ol	8.0
18	3-heptadecene	6.0
19	n-nonadecanol-1	3.35
20	Heptadecane	2.02
21	Hexadecane nitrile	1.67
22	2-heptadecanone	3.98
23	Oleanitrile	4.80
25	Heptadecyl oxirane	5.48
26	9-octadecanoic acid ethyl ester	4.50
27	Oleic acid butyl ester	1.19
28	9- heptadecanon	1.72

2.1.5.2 Non-condensable gases (NCG)

Composition of NCG for pyrolysis of OMWS at different temperatures is given in the following table [1]. Carbon dioxide is the major component in the gas composition.

Table 2.4. NCG composition

Temp. (°C)	400	450	500
H_2 (%)	2.15	3.8	3.88
CO (%)	5.9	7.3	10.9
CO_2 (%)	78.5	72.5	65.2
CH_4 (%)	1.6	2.6	3.8
C_2-C_5	10.0	10.8	13.6
Other gases	1.9	2.9	2.6

2.2 Lab-scale model development

A steady state Aspen Plus simulation model is developed to investigate the mass and energy balance of the complete process. OMWS and biochar are characterized as non-conventional components as their properties are absent in Aspen Plus databanks. Instead, Aspen Plus calculates their enthalpy and density according to the ultimate analysis provided by the user. Thermal properties such as enthalpy, density and specific heat are determined from built-in models HCOALGEN and DCHARIGT in Aspen Plus. RK-SOAVE property method is employed as the global thermodynamic model because of presence of hydrocarbons and light gases [105]. RK SOAVE is comparable with PENG-ROB but it already contains a number of binary parameters for vapor-liquid and liquid-liquid equilibrium while PENG-ROB lacks these parameters. The Kirov correlation (1965) is used to compute the heat capacity of biomass, which takes into account the mass fraction of the proximate analysis (moisture, fixed carbon (FC), primary volatile matter (VM), secondary volatile matter (VM), and ash):

$$C_{p,i} = \sum_{j=1}^{ncn} w_j C_{p,ij} \qquad 2.1$$

Where C_p is the heat capacity, i is the component index, j is the constituent index and w_j is the mass fraction of the jth constituent on dry basis. The temperature dependent heat capacity of each proximate analysis is calculated according to the formula below:

$$C_{p,ij} = a_{ij1} + a_{ij2}T + a_{ij3}T^2 + a_{ij4}T^3 \qquad 2.2$$

Where a is a parameter or element, i is the component index, j is the constituent index (1 = moisture, 2 = FC, 3 = primary VM, 4 = secondary VM, 5 = ash).

The enthalpy of non-conventional component is calculated as

$$H^s = \Delta_f h^s + \int_{T^{ref}}^{T} C_p^s dT \quad 2.3$$

As non-conventional components are defined by their ultimate analysis so $\Delta_f h^s$ cannot be calculated directly. It is possible to calculate heat of formation from heat of combustion as combustion products and their molecular structures are well-known:

$\Delta_f h_{cp}^s$ is calculated by multiplying the mass fractions of elements with heats of formation in combustion products and summing them up. Coal enthalpy model HCOALGEN employs this approach to calculate the enthalpy of non-conventional components. DCHARIGT model is based on equations from IGT [106] and calculates the density of char or coke on dry basis using ultimate and sulfur analyses. As both conventional and non-conventional solids are involved in the simulation model, stream class MCINCPSD is a suitable choice. Molecular weights and other thermo-physical properties are retrieved from NIST database.

2.2.1 Feedstock pretreatment

The biomass is ground from 100 mm to less than 2 mm using a hammer mill in Aspen Plus. The drying process is simulated by a simple heater where OMWS is heated to dry the biomass to achieve 4% moisture content.

2.2.2 Pyrolysis

Pyrolysis is modeled by using fluidized bed reactor and *RCSTR* reactor. The fluidized bed reactor is used for modeling hydrodynamics of the bed and pyrolysis reaction is specified in *RCSTR* reactor. Pyrolysis reaction and temperature of reactor is specified in this reactor. The template for reaction kinetics is not able to deal with the kinetics of equations (2.5) and (2.7), so they are written in an external Fortran user-subroutine and then linked with *RCSTR* reactor (Figure 2.3). A general reaction is given by equation 2.4.

$$OMWWS = Bio\ oil + Biochar + NCG + Water \quad 2.4$$

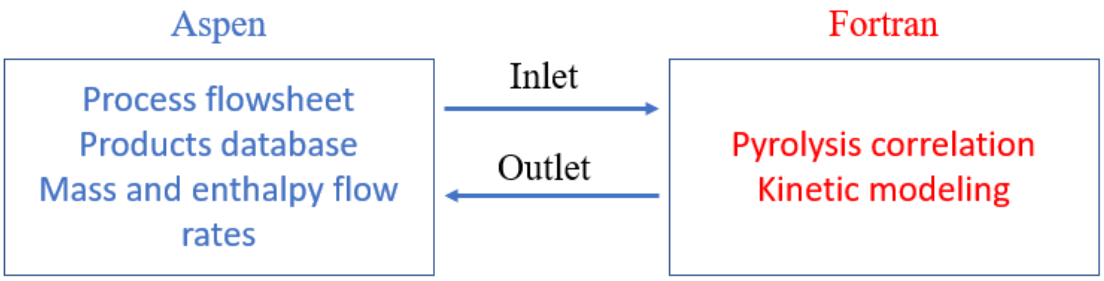

Figure 2.3. Coupling of external user sub-routine with Aspen Plus

The reaction rate of the pyrolysis of OMWS is determined from the analysis of experimental data of Agblevor et. al. [1] and formulated according to the modified Arrhenius law proposed by Diaz and Broun [107].

$$R = k.F_{ko}.(\frac{F_k}{F_{ko}})^n \quad \text{(kg/m}^3\text{.s)} \quad 2.4$$

Where R, k,, F_{ko}, F_k and n are reaction rate (kg/m^3.s), rate constant (1/s), original concentration of OMWS (kg/m^3), concentration of OMWS (kg/m^3) and Order of reaction (n=1) respectively [108].

The rate constant can be written by the following equation:

$$k = A\exp\left(\frac{-E_a}{RT}\right) \quad \text{(1/s)} \quad 2.5$$

Where: A is pre-exponentiel factor (A= 2.55×10^4 s^{-1}), E_a is Activation Energy ($E_a = 69.56\ \text{kJ/mol/K}$), T is temperature (K) and R is gas constant (J/mol. K). The decomposition curves are given in Annex I.

The subsequent production of bio oil, biochar, gases and water is calculated by the following relation [107,108] .

$$R_i = f_i \times R \quad \text{(kg/m}^3\text{.s)} \quad 2.6$$

where

R_i = reaction rate of i-th product, kg of i-th product/m^3.s

f_i = stoichiometric factor of i-th product, kg of i-th product/kg of OMMWS

f_i used in this model is based on the experimental data at 400°C, 450°C and 500°C and given in the following Table 2.5.

Table 2.5. f_i determined from experimental data of Agblevor et. al. [1]

Component	f_i (kg/kg of OMWS) 400°C	f_i (kg/kg of OMWS) 450°C	f_i (kg/kg of OMWS) 500°C
CHAR	0.291	0.227	0.204
H_2O	0.113	0.175	0.118
H_2	0.005375	0.0114	0.01486

CO	0.01485	0.02205	0.045003
CO_2	0.196	0.21765	0.252972
CH_4	0.004	0.0078	0.014554
C_2H_6	0.0125	0.0162	0.02267
C_3H_8	0.0125	0.0162	0.02298
C_4H_{10}	0.00475	0.0.0087	0.009958
Bio-oil	0.346	0.298	0.295

2.2.3 Condensers

Shell and tube heat exchangers were used to model the condensers in Aspen Plus. The diameter of the shell is 60 mm and tube length is 500 mm with 20 mm diameter (Figure 2.2). Water/ethylene glycol mixture is used as a cooling medium at 8°C with flow rate of 8 kg/hr in each heat exchanger.

The components used in the simulation model are summarized in Table 2.6.

Table 2.6. Components used in Aspen Plus

Component ID	Type	Component Name	Alias
OMWS	Nonconventional		
CHAR	Nonconventional		
Ash	Nonconventional		
N2	Conventional	NITROGEN	N2
O2	Conventional	OXYGEN	O2
H2	Conventional	HYDROGEN	H2
H2O	Conventional	WATER	H2O
CO	Conventional	CARBON-MONOXIDE	CO
CO2	Conventional	CARBON-DIOXIDE	CO2
CH4	Conventional	METHANE	CH4
C2H6	Conventional	ETHANE	C2H6
C3H8	Conventional	PROPANE	C3H8
C4H10	Conventional	ISOBUTANE	C4H10-2
ETHYL-01	Conventional	ETHYLENE-GLYCOL	C2H6O2
R22	Conventional	CHLORODIFLUOROMETHANE	CHCLF2
Catalytic Bio-oil			
1-DECENE	Conventional	1-DECENE	C10H20-5
P-CRESOL	Conventional	P-CRESOL	C7H8O-5

1-UNDECE	Conventional	1-UNDECENE	C11H22-2
N-UNDECA	Conventional	N-UNDECANE	C11H24
4-ETHPHE	Conventional	P-ETHYLPHENOL	C8H10O-3
2-DODECA	Conventional	DECYL-METHYL-KETONE	C12H24O-N9
1-TRIDEC	Conventional	1-TRIDECENE	C13H26-2
N-TRIDEC	Conventional	1-TRIDECANOL	C13H28O
HEXADECA	Conventional	N-HEXADECANE	C16H34
1-TETRAD	Conventional	1-TETRADECENE	C14H28-2
TETRADEC	Conventional	N-TETRADECANE	C14H30
N-PENTAD	Conventional	1-PENTADECANOL	C15H32O
HEPTADEC	Conventional	N-HEPTADECANE	C17H36
1-HEPTAD	Conventional	1-HEPTADECENE	C17H34-D1
1-NON-DE	Conventional	1-NONADECANOL	C19H40O
PALMI-01	Conventional	PALMITONITRILE	C16H31N
TRICY-01	Conventional	TRICYCLOHEXYLAMINE	C18H33N
ETHYL-01	Conventional	ETHYL-OLEATE	C20H38O2-N1
BUTYL-01	Conventional	BUTYL-OLEATE	C22H42O2-N5
9-HEP-01	Conventional	9-HEPTADECANONE	C17H34O

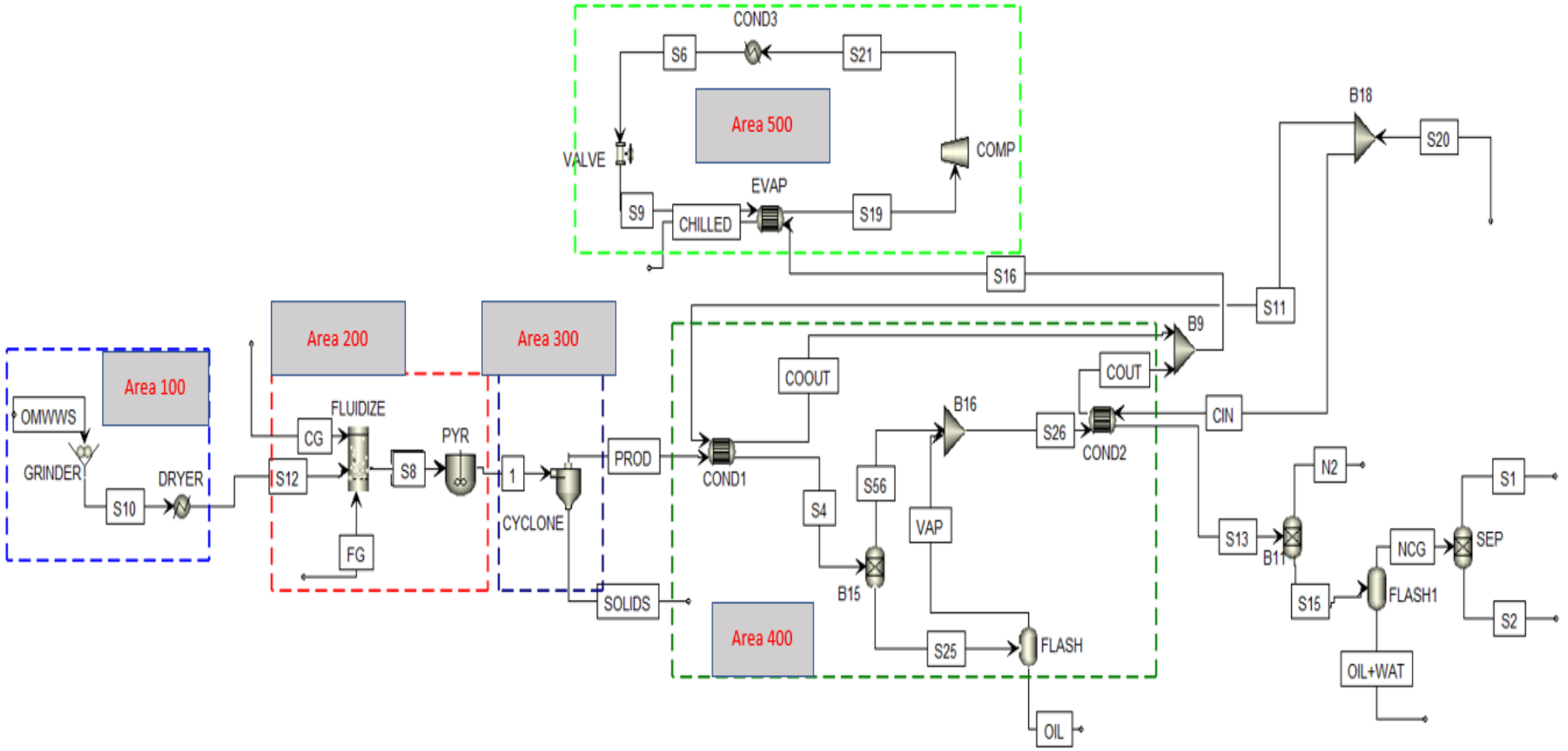

Figure 2.4. Aspen Plus flowsheet of catalytic fast pyrolysis process of OMWS

A list of Aspen Plus units and their description is given in Table 2.7.

Table 2.7. Aspen Plus unit models

Unit	Description
Fluidized bed reactor	Models the fluidization dynamics and calculates the minimum fluidization velocity and superficial velocity.
RCSTR	Stands for continuous stirred tank reactor. This unit is useful when kinetics of the chemical reaction are known.
Cyclone	Separates solids from gases
Cond	Models shell and tube heat exchanger to heat or cool down inlet streams
Comp	Compressor used in compression refrigeration system
Flash	Executes vapor-liquid equilibrium calculations
Sep	Separates inlet stream components into multiple outlet streams depending upon split fractions or specified flows

2.3 Scaling up from lab to industrial scale

The scale-up of any process to industrial scale is a complex and troublesome endeavor. The industrial scale is subjected to many eventualities and pitfalls which may drastically deteriorate the plant's performance and economy. The main challenge in the pyrolysis process is the proper scale up of hydrodynamics and chemical conversion inside the fluidized bed. A scale-up procedure established by Kelkar et. al [109,110] is shown in Figure 2.5.

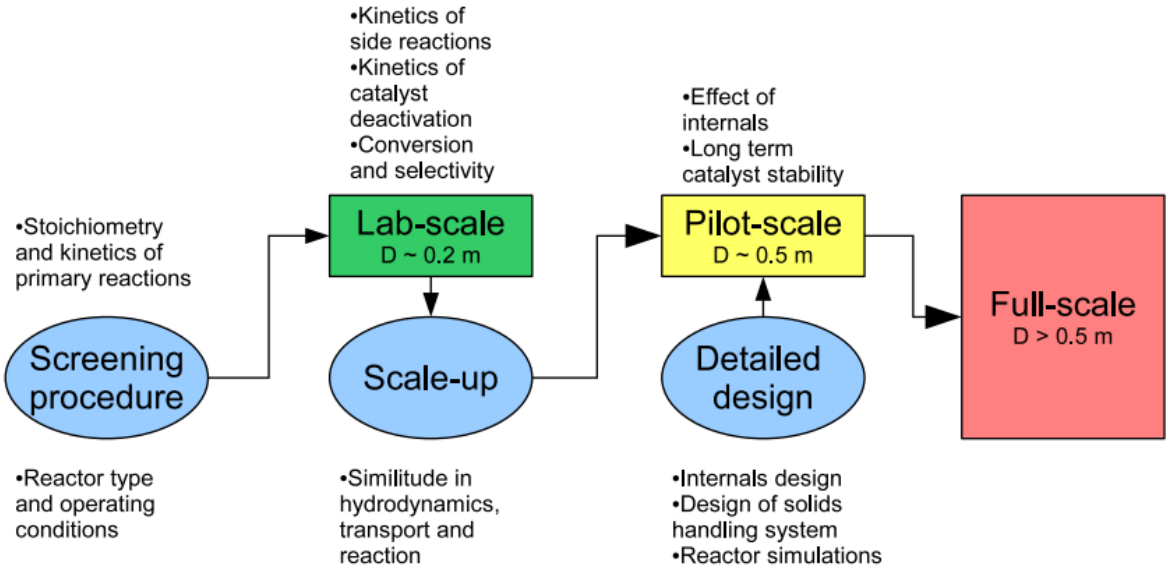

Figure 2.5. Upscaling from lab to industrial scale fluidized bed reactor

Scale up involves taking data obtained from smaller fluidized bed units and translating the data to larger fluidized beds. In our work, there is no data experimental data available for a pilot scale so in industrial scale we assume the same kinetic reactions and same kinetic rates as in lab scale. The important parameter is to calculate the minimum fluidization velocity and subsequent mass flow rate of fluidizing gas. The other equipment parameters are determined accordingly. For industrial scale product yields, same yields are used as obtained in the lab scale model.

2.3.1 Industrial Scale

Process overview can be seen in Figure 2.6. It is divided into seven major technical parts: (i) Pre-processing of feedstock (Area 100); (ii) Bio-oil production via catalytic fast pyrolysis (Area 200); (iii) Solids removal (Area 300); (iv) Bio-oil condensation (Area 400); (v) Compression/absorption machine (Area 500); (vi) Heat generation (Area 600); (vii) Electricity generation (Area 700).

In Area 100, wet biomass is ground to less than 2 mm and then dried to reduce the moisture from 10% to 4%. Drying is essential as water causes adverse effects on the properties of bio-oil. The dried biomass still contains 4% moisture but drying beyond this moisture content can lead to the loss of volatile matter and the risk of fire. Typically, drying is accomplished by subjecting the biomass to low humidity air at a high temperature [111]. The grinding of biomass is also important as it increases the heat transfer within the biomass. A smaller particle size helps to exploit the heat transfer [112]. Bio-oil is produced in Area 200 via a catalytic fast pyrolysis process. The Area 200 products are then fed into Area 300, which separates the solid

particles (red mud and biochar) from the hot vapors and gases. In the liquid recovery section (Area 400), bio-oil vapors are condensed using a compression refrigeration machine/ absorption refrigeration machine (Area 500). In Area 600, the red mud catalyst is regenerated by burning biochar. The catalyst is reactivated, and heat for the pyrolysis is provided in Area 200. Excess heat from the Area 600 is used to produce electricity in Area 700 and to dry the wet biomass in Area 100.

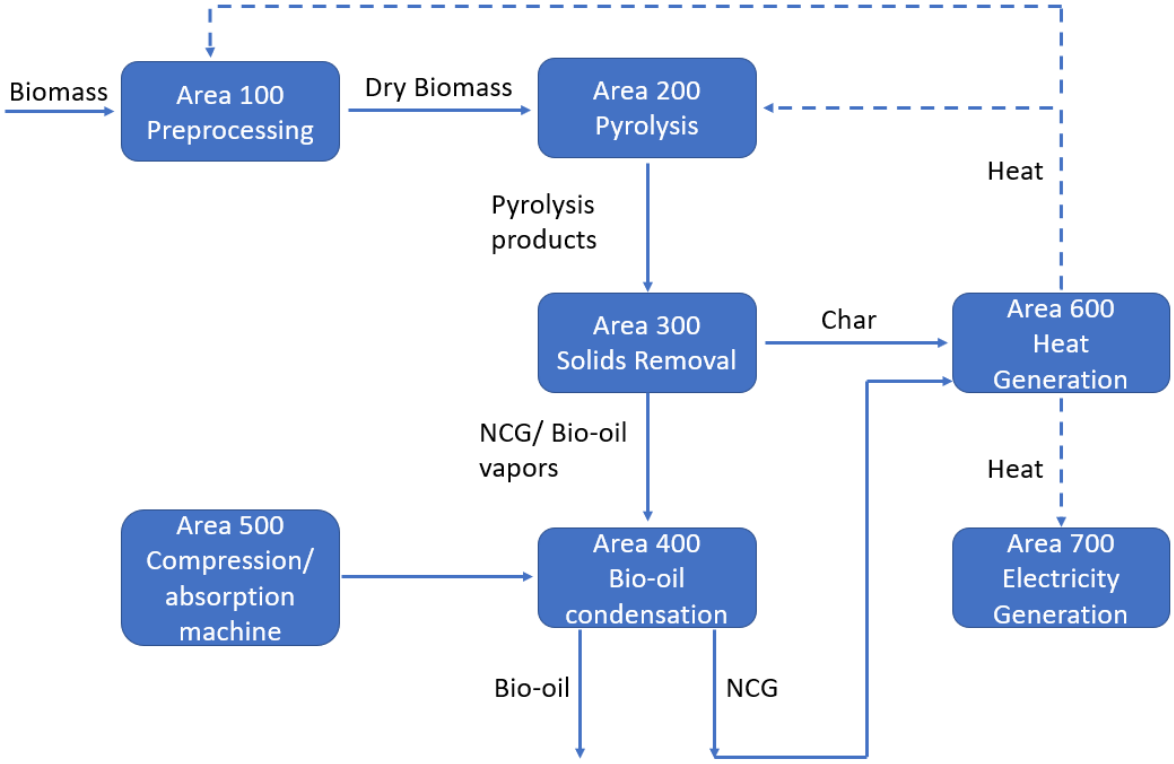

Figure 2.6. Process overview of industrial plant

2.3.2 Industrial scale model development

Model was developed in Aspen Plus and the two process schemes are shown in Figure 2.14 and Figure 2.15.

2.3.2.1 Feedstock preparation (Area 100)

Olive mill waste water sludge (OMWS) was collected from Sfax, Tunisia. The plant's capability is 100 tonnes of OMWS per day (wet basis), with a moisture content of 10% and a particle size of 100 mm. The biomass is ground and dried to meet the pyrolysis reactor's requirements, which are 2 mm particle size and 4% moisture content. 20% of biochar is mixed with OMWS to make

it less sticky and feed it into the pyrolysis reactor smoothly. Hot air is supplied at 120°C and exhausted at 60°C following the common practice of convective dryer. The characteristics of OMWS are shown in Table 2.1.

The pretreatment of biomass seeks to treat the OMWS to match the pyrolysis process conditions in terms of moisture content and particle size. Dryers evaporate volatile moisture from wet solids by applying energy supplied by hot inlet streams. The convective dryer model performs calculations based on drying rates of typical convective dryers where the wet solids come into contact with hot gases.

The overall mass balance in a continuous dryer is simply the moisture lost by the solids and gained by the gas.

$$W_g(Y_o - Y_i) = W_s(X_i - X_o) \qquad 2.7$$

where

W_g = Mass flow rate of the dry gas (kg/s)

W_s = Mass flow rate of dry solids (kg/s)

Y_i = Absolute humidity of inlet gas (kg/kg)

Y_o = Absolut humidity of exhaust gas (kg/kg)

X_i = Moisture content of entering solids, dry basis (kg/kg)

X_o = Moisture content of exhaust solids, dry basis (kg/kg)

The heat in the dryer can be supplied or lost from the system in many ways. The overall energy balance can be expressed by following relation.

$$W_g h_{ga} + Q_h + W_s h_{si} = W_g h_{go} + Q_{wl} + W_s h_{so} \qquad 2.8$$

where

h_{ga} = Enthalpy of inlet gas and associated vapor (kJ/kg)

h_{go} = Enthalpy of outlet gas and associated vapor (kJ/kg)

h_{si} = Enthalpy of inlet solids and associated vapor (kJ/kg)

h_{so} = Enthalpy of outlet solids and associated vapor (kJ/kg)

Q_h = Heat input from heater (kW)

Q_{wl} = Wall heat loss from dryer (kW)

The enthalpy of gas and solids is given by the following equations.

$$I_g = h_g + Yh_y = (C_{pg} + YC_{py})T_g + \lambda_o \quad \text{(kJ/kg)} \quad 2.9$$

$$I_s = h_s + Xh_l = (C_{ps} + XC_{pl})T_s \quad \text{(kJ/kg)} \quad 2.10$$

Where

h_g = Enthalpy of dry gas (kJ/kg)

h_y = Enthalpy of vapor in gas (kJ/kg)

h_s = Enthalpy of dry solids (kJ/kg)

h_l = Enthalpy of moisture in solids

C_{pg} = Heat capacity of dry gas (kJ/kg.K)

C_{py} = Heat capacity of vapor in gas (kJ/kg.K)

C_{ps} = Heat capacity of dry solids (kJ/kg.K)

C_{pl} = Heat capacity of moisture in solids (kJ/kg.K)

λ_o = Latent heat of vaporization (kJ/kg)

The heat supplied to the gas can be calculated from the following equation.

$$Q_h = W_g(h_{gi} - h_{ga}) \quad \text{(kW)} \quad 2.11$$

2.3.2.2 Crushing

Hammer mills belong to the group of mills that produce products with mean particle sizes of about 1 mm maximum. They are often used in the wide fields of chemicals, iron and steel, food, wood and recycling resources. In this type of mills, the size reduction is a result of the impact of the particles with the rotating hammers and the wall. A typical construction of a sieve hammer mill is shown in Figure 2.7.

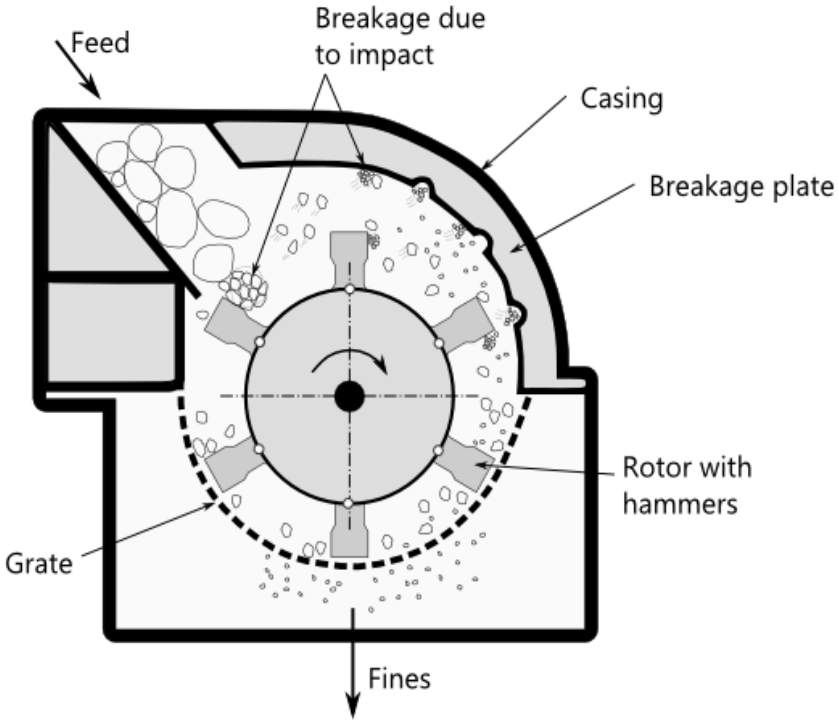

Figure 2.7. Hammer mill

The following equation determines the power requirement for crusher [105]:

$$P = \frac{0.01\left(\sqrt{X_F} - \sqrt{X_P}\right) \times BWI \times F_T}{\sqrt{X_F} \times \sqrt{X_P}} \quad \text{(Watt)} \quad 2.12$$

Where:

P = Required power (Watt)

X_F = Diameter larger than 80% of feed particle mass (m)

X_P = Diameter larger than 80% of product particle mass (m)

BWI = Bond work index

F_T = Total solids mass flow rate (kg/s)

Bond work index is a semi-empirical parameter that is determined by the characteristics of the material that is being treated. The following equation may be used to compute BWI. [113].

$$BWI = \frac{435}{HGI^{0.91}} \quad \text{(kWh/ton)} \quad 2.13$$

Where *HGI* is hardgrove grindability index. For olive cake, its value is 14 [113].

2.3.2.3 Pyrolysis (Area 200)

Fluidized bed reactor

As seen in Figure 2.8, fluidization occurs when tiny solid particles are suspended in an upward moving stream of fluid. The fluid velocity is adequate to suspend the particles but insufficient to transport them out of the vessel. The solid particles rapidly swirl around the bed, resulting in good mixing. The qualities and behavior of a fluidized bed are highly influenced by both solid and gas properties. The bubbling bed model of Kunii and Levenspiel is the most widely used fluidized bed reactor model [114].

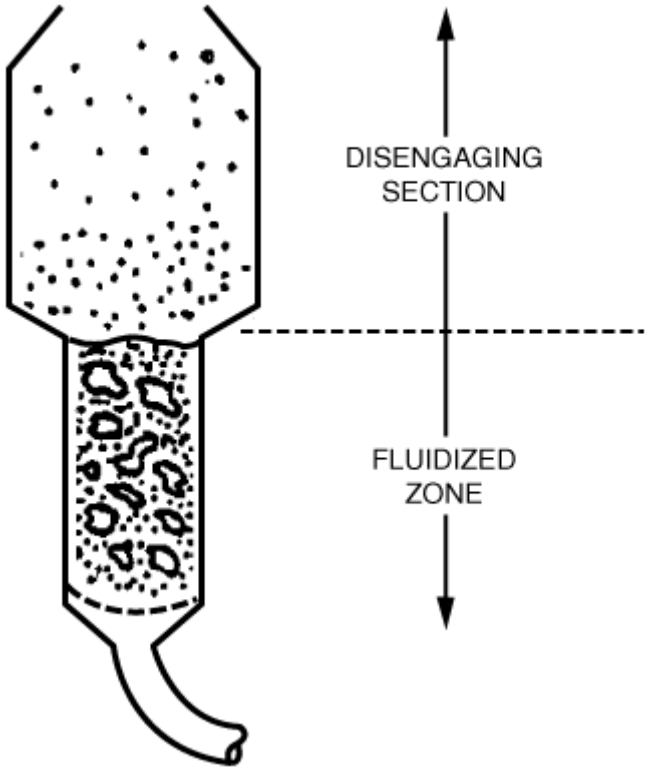

Figure 2.8. Fluidized bed reactor

Description of phenomenon

Figure 2.8 depicts a vertical bed of solid particles supported by a porous or perforated distributor plate. The movement of gas through this bed is upward. The moving gas drags on the solid particles, and for low gas velocities, the pressure loss caused by this drag follows the Ergun equation exactly like any other packed bed. When the gas velocity is raised to a certain point, the overall drag on the particles equals the weight of the bed, causing the particles to rise and barely fluidize. If ρ_c is the density of the solid catalyst particles, A_c the cross-sectional area, h_s the height of the bed settled before the particles start to lift, h the height of bed at any time, ε_s

and ε the corresponding porosities of the settled and expanded bed, respectively, the mass of solids in the bed, W_s , is

$$W_s = \rho_c A_c h_s (1 - \varepsilon_s) = \rho_c A_c h (1 - \varepsilon) \quad \text{(kg)} \quad 2.14$$

Once the drag force exerted on the particles equals the net gravitational force exerted on the particles, that is

$$\Delta P = g \left(\rho_c - \rho_g\right)(1 - \varepsilon)\, h \quad \text{(Pa)} \quad 2.15$$

Beyond this threshold, an increase in velocity will not enhance the pressure drop. From the point where bubbles first emerge in the bed, the gas velocity may be gradually raised across a wide range without affecting the pressure drop across the bed caused by the movement of particles out of the bed.

Minimum fluidization velocity

Fluidization will be regarded to commence at the gas velocity at which the weight of the solids equals the drag from the fluidizing gas. The gravitational force is given by equation 2.16 and the drag force by the Ergun equation. All parameters at the point where these two forces are equal will be characterized by the subscript mf (minimum fluidization). This is the value of a particular term when the bed is just beginning to become fluidized. The combination $g\left(\rho_c - \rho_g\right)$ occurs very frequently and this grouping is termed as η:

$$\frac{\Delta P}{h} = \eta\,(1 - \varepsilon_{mf}) \quad \text{(kg/m}^2\text{/s}^2\text{)} \quad 2.16$$

The Ergun equation can be written in the form

$$\frac{\Delta P}{h} = \rho_g U^2 \left[\frac{150\,(1-\varepsilon)}{Re_p \Psi} + \frac{7}{4}\right] \frac{1-\varepsilon}{\Psi d_p \varepsilon^3} \quad \text{(kg/m}^2\text{/s}^2\text{)} \quad 2.17$$

Where Ψ is the shape factor of catalyst particle, also called sphericity.

The weight of the bed simply equals the pressure drop across the bed at the point of minimum fluidization:

$$W_s . g = \Delta P A_c \quad \text{(N)} \quad 2.18$$

$$g(1-\varepsilon)\left(\rho_c - \rho_g\right) h A_c = \rho_g U^2 \left[\frac{150\,(1-\varepsilon)}{Re_p \Psi} + \frac{7}{4}\right] \frac{1-\varepsilon}{\Psi d_p \varepsilon^3} A_c h \quad 2.19$$

Reynolds number is given by

$$R_e = \frac{\rho_g d_p U}{\mu} \qquad 2.20$$

For Re < 10, equation 2.20 can be used to give minimum fluidization velocity

$$u_{mf} = \frac{(\Psi d_p)^2}{150\mu}\left[g(\rho_c - \rho_{g)}\right]\frac{\varepsilon_{mf}^3}{1-\varepsilon_{mf}} \qquad \text{(m/s)} \quad 2.21$$

Two dimensionless parameters in these two u_{mf} equations require special attention. The first is sphericity Ψ, which measures a particle's nonideality in form and roughness. Since the volume of the spherical particle is

$$V_p = \frac{\pi d_p^3}{6} \qquad (\text{m}^3) \quad 2.22$$

and its surface area is

$$A_s = \pi d_p^2 = \pi\left[\left(\frac{6V_p}{\pi}\right)^{1/3}\right]^2 \qquad (\text{m}^2) \quad 2.23$$

$$\Psi = \frac{A_s}{A_p} = \frac{\pi(6\,V_p/\pi)^{2/3}}{A_p} \qquad 2.24$$

Measured values of this parameter range from 0.5 to 1, with 0.6 being a normal value for a typical granular solid [115].

The void fraction ε_{mf} at the point of minimum fluidization is the second parameter of particular relevance. A correlation exists which apparently gives accurate predictions of measured values of ε_{mf} when the particles are fairly small [116].

$$\varepsilon_{mf} = 0.586\,\Psi^{-0.7}\left(\frac{\mu^2}{\rho_g \eta\, d_p^3}\right)^{0.029}\left(\frac{\rho_g}{\rho_c}\right)^{0.021} \qquad 2.25$$

Another correlation commonly used is that of Wen and Yu [117]:

$$\varepsilon_{mf} = \left(\frac{0.071}{\Psi}\right)^{1/3} \qquad 2.26$$

Typical value of ε_{mf} is around 0.5. When a particle size distribution is available, an equation for determining the mean diameter is given below.

$$d_p = \frac{1}{\sum f_i/d_{pi}} \qquad (\text{m}) \quad 2.27$$

Where f_i is the fraction of particles with diameter d_{pi}.

The superficial velocity can be from 2 to 4 times the minimum fluidization velocity. Thus the mass flow rate of fluidization gas is given by

$$\dot{M}_g = \rho_g S_b U_s \quad \text{(kg/s)} \quad 2.28$$

Heat of pyrolysis is calculated from energy balance across pyrolysis reactor [118].

$$Q_{pyro} = mH_{char}(T_{out}) + mH_{bio-oil}(T_{out}) + mH_{gas}(T_{out}) + mH_{water}(T_{out}) - mH_{OMWS}(T_{in}) \quad \text{(kW)} \quad 2.29$$

2.3.2.4 Solids removal (Area 300)

A high-performance cyclone in Area 300 separates the entrained catalyst and biochar particles from the gases and vapors, with a separation efficiency of 0.9. Another hot gas filter is used to thoroughly remove the biochar and catalyst particles from the products.

The overall separation efficiency of cyclone is given by

$$\eta_c = \frac{flowrate\ of\ solids\ removed\ from\ inlet}{total\ inlet\ flow\ rate\ of\ solids} \quad 2.30$$

$$\eta_c = \frac{C_i - C_o}{C_o} = \frac{Q_i C_i - E}{Q_i C_i} = 1 - \frac{E}{Q_i C_i} \quad 2.31$$

Where:

C_i = Concentration of solids in inlet gas

C_o = Concentration of solids in outlet cleaned gas

Q_i= Inlet gas flowrate

E = Outlet emission flow rate of solids in the cleaned gas

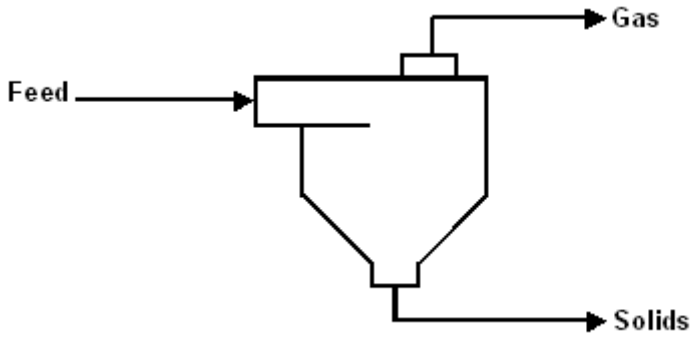

Figure 2.9. Cyclone

2.3.2.5 Bio-oil Condensation (Area 400)

The hot product gases flow through the first condenser at 400°C and exit at roughly 110°C, condensing the bulk of bio-oil vapors. The cooled products are sent to second condenser, which cools them to roughly 40°C and condenses part of the bio-oil vapors and water. To quench the residual bio-oil, the products pass through an electrostatic precipitator.

The cooling energy removed in the condensers for bio-oil and water is calculated from following equation.

$$Q_{removed} = \dot{m}C_p(T_{boil} - T_1) + \dot{m}\Delta h_{vap} + \dot{m}C_p(T_{pyro} - T_{boil}) \quad \text{(kW)} \quad 2.32$$

The first term of equation indicates the sensible heat below boiling point of fluid where T_{boil} is the boiling point of fluid and $T_1$is the temperature after condensation which is taken as 40°C. The second term points to the latent heat of vaporization of fluid and third term is the sensible heat above boiling point of fluid where T_{pyro} is the exit temperature of pyrolysis reactor which is 400°C.

For gases, only sensible heat is calculated.

$$Q_{removed} = \dot{m}C_p(T_{pyro} - T_1) \quad \text{(kW)} \quad 2.33$$

The heat capacity values, boiling points and heats of vaporization of bio-oil compounds are given in the Annex III.

2.3.2.6 Refrigeration machine (Area 500)

Two cooling machines were modelled in this study: (i) Vapor compression refrigeration machine (scheme-1) (ii) absorption refrigeration machine (LiBr-H_2O) (scheme-2).

Compression Refrigeration machine

A typical vapor compression refrigeration system is developed in Scheme-1. A compressor, condenser, valve, and heat exchanger (evaporator) are all modeled in the system. R134a is the refrigerant utilized in the simulation for refrigeration, while REFPROP is the base method.

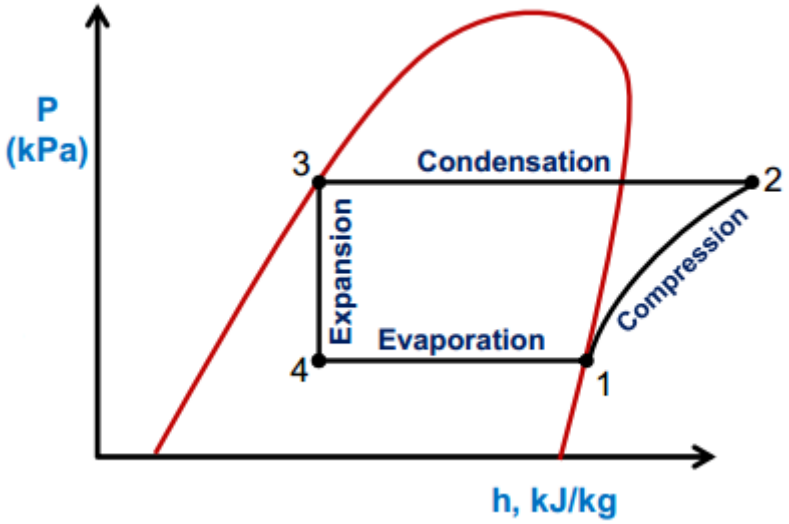

Figure 2.10. Standard vapor compression system

The work of compression can be written as

$$W_c = \dot{m}(h_2 - h_1) \quad \text{(kW)} \quad 2.34$$

The heat rejected by the condenser to the cooling fluid can be estimated from the following relation.

$$Q_c = \dot{m}(h_3 - h_2) \quad \text{(kW)} \quad 2.35$$

Condenser pressure corresponds to condenser temperature i.e.

$$P_c = P_{sat}(T_c)$$

The exit condition of refrigerant lies in the two-phase region:

$$h_4 = (1 - X_4)h_{f,e} + X_4 h_{g,e} = h_f + X_4 h_{fg} \quad \text{(kJ/kg)} \quad 2.36$$

Where X_4 is quality of refrigerant, $h_{f,e}$ is saturated liquid enthalpy, $h_{g,e}$ is saturated vapor enthalpy and h_{fg} is enthalpy of vaporization at evaporator pressure.

The refrigeration effect can be determined from the following equation.

$$Q_e = \dot{m}(h_1 - h_4) \quad \text{(kW)} \quad 2.37$$

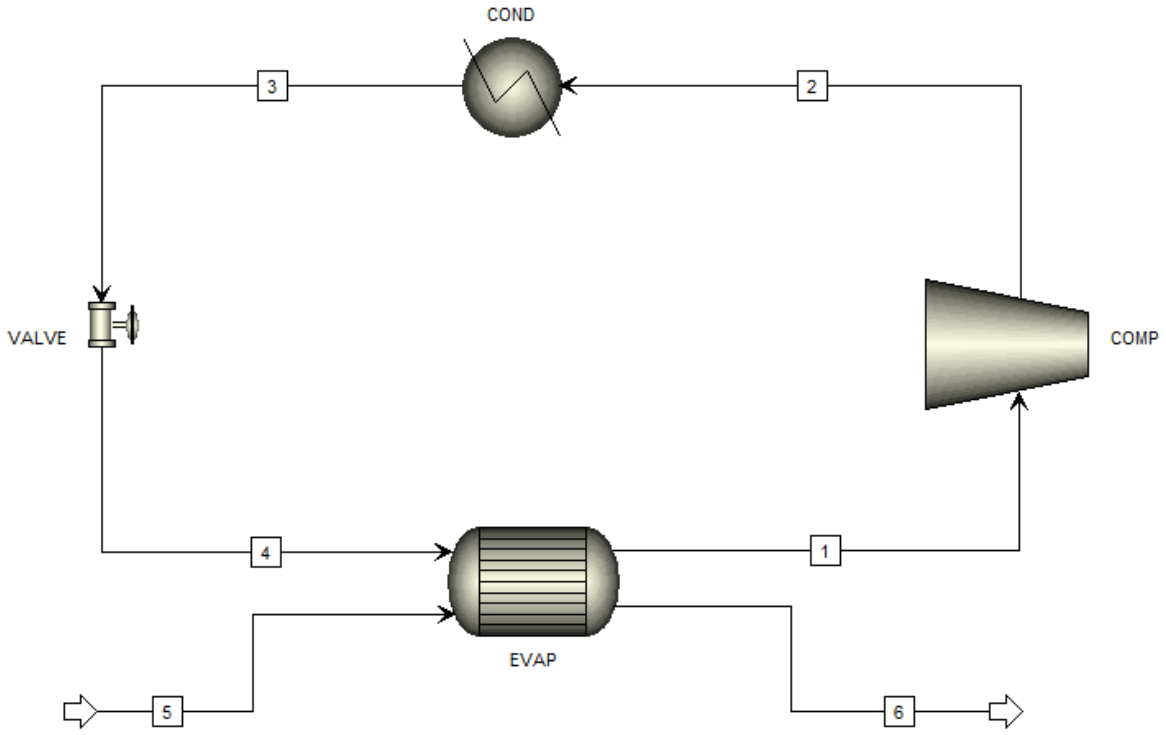

Figure 2.11. Compression refrigeration machine modelled in Aspen Plus

Absorption refrigeration machine

An absorption chiller is a closed loop cycle that utilizes waste heat to provide cooling. The coefficient of performance (COP) of an absorption chiller ranges between 0.5 and 1.5, whereas modern vapor compression cycles have COPs in excess of 3.0 [119,120]. However, absorption chillers are still frequently used since they can deliver cooling using low-temperature (<100°C) heat source. As a result, in operations where low temperature waste heat is accessible and cooling is needed, it is frequently advantageous to use an absorption chiller to improve the overall energy efficiency of the process [70,121].

As a working fluid, absorption chillers employ a refrigerant-absorbent pair. Water/lithium bromide (LiBr) and ammonia/water are the two most frequent working fluid combinations. The cooling required in the pyrolysis process is above 0°C so Li-Br/water solution is a suitable choice.

Assumptions

i. Steady state and steady flow is considered.

ii. Changes in potential and kinetic energies across each component are negligible.

iii. No pressure drops due to friction are considered.

$\dot{m}$ = mass flow rate of refrigerant (kg/s)

$\dot{m}_{ss}$ = mass flow rate of strong solution (rich in Li-Br) kg/s

$\dot{m}_{ws}$ = mass flow rate of strong solution (rich in LiBr) kg/s

Circulation ratio $\lambda = \frac{\dot{m}_{ss}}{\dot{m}_{ws}}$

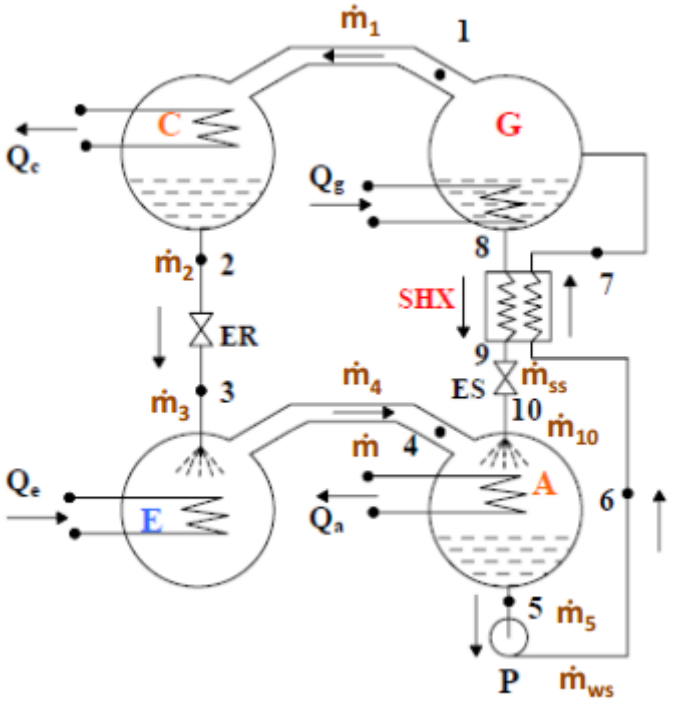

Figure 2.12. Single effect absorption cycle

Condenser

The mass balance and energy balance is given by following equations.

$$\dot{m}_1 = \dot{m}_2 = \dot{m} = mass\ flow\ rate\ of\ pure\ water \quad \text{(kg/s)}$$

$$Q_c = \dot{m}(h_2 - h_1) \quad \text{(kW)} \quad 2.38$$

$$P_c = P_{sat}(T_c) \quad \text{(kPa)}$$

Expansion valve

There is no change in mass and enthalpy across expansion valve.

$$\dot{m}_1 = \dot{m}_2 = \dot{m} \quad \text{(kg/s)}$$

$$h_2 = h_3 \quad \text{(kJ/kg)}$$

Evaporator

The mass flow rate remains the same and pressure is saturated pressure at evaporator temperature.

$$\dot{m}_3 = \dot{m}_4 = \dot{m} \quad \text{(kg/s)}$$

$$Q_e = \dot{m}(h_4 - h_3) \quad \text{(kW)} \quad 2.39$$

$$P_e = P_{sat}(T_e) \quad \text{(kPa)}$$

Absorber

The water vapors coming from the evaporator and strong solution of Li-Br coming from generator are mixed in the absorber.

$$\dot{m} + \dot{m}_{ss} = \dot{m}_{ws} \quad \text{(kg/s)} \quad 2.40$$

$$Circulation\ ratio = \lambda = \frac{\dot{m}_{ss}}{\dot{m}} \quad 2.41$$

$$\dot{m}_{ws} = (1 + \lambda)\dot{m} \quad \text{(kg/s)} \quad 2.42$$

$$Q_a = \dot{m}h_4 + \lambda\dot{m}h_{10} - (1 + \lambda)\dot{m}h_5 \quad \text{(kW)} \quad 2.43$$

$$Q_a = \dot{m}[(h_4 - h_5) + \lambda(h_{10} - h_5)] \quad \text{(kW)} \quad 2.44$$

Where:

$\dot{m}(h_{10} - h_1)$: Enthalpy change of water as it changes its state from vapor at state 4 to liquid at state 5.

$\dot{m}\lambda(h_6 - h_1)$: Sensible heat transferred as solution at state 10 is cooled to solution at state 5.

Solution pump

A solution pump is required between states 5 and 6. The work of pump can be determined from the following equation:

$$\dot{m}_1 = \dot{m}_2 = \dot{m}_{ws} \quad \text{(kg/s)} \quad 2.45$$

$$W_p = \dot{m}_{ws}(h_6 - h_5) = (1+\lambda)\dot{m}(h_6 - h_5) \quad \text{(kW)} \quad 2.46$$

$$W_p = (1+\lambda)\dot{m}v_{sol}(P_6 - P_5) = (1+\lambda)\dot{m}v_{sol}(P_c - P_e) \quad \text{(kW)} \quad 2.47$$

v_{sol} is the specific volume of the solution.

Solution heat exchanger

The strong solution of lithium bromide coming from the generator exchanges heat with the weak solution coming from the pump.

$$\dot{m}_6 = \dot{m}_7 = \dot{m}_{ws} \quad \text{(kg/s)} \quad 2.48$$

$$\dot{m}_8 = \dot{m}_9 = \dot{m}_{ss} \quad \text{(kg/s)} \quad 2.49$$

$$Q_{HX} = (1+\lambda)\dot{m}(h_7 - h_6) = \lambda\dot{m}(h_8 - h_9) \quad \text{(kW)} \quad 2.50$$

Effectiveness of solution heat exchanger can be defined as

$$\epsilon = \frac{T_8 - T_9}{T_8 - T_6} \quad 2.51$$

Generator

The weak solution of Li-Br and water is split into pure water and strong solution of Li-Br. The temperature of the heat input to the cycle determines the mass split between the two exit streams. From total mass balance:

$$\dot{m}_3 = \dot{m}_7 + \dot{m}_4 \quad \text{(kg/s)} \quad 2.52$$

From energy balance, heat input to generator is given by

$$Q_g = \dot{m}h_7 + \lambda\dot{m}h_4 - (1+\lambda)\dot{m}h_3 \quad \text{(kW)} \quad 2.53$$

$$Q_g = \dot{m}[(h_7 - h_3) + \lambda(h_4 - h_3)] \quad \text{(kW)} \quad 2.54$$

Where:

$\dot{m}(h_7 - h_3)$: Energy required to generate water vapor at state 7 from solution state at 3.

$\dot{m}(h_4 - h_3)$: Sensible heat required to heat the solution from state 3 to 4.

Solution expansion valve

$$\dot{m}_9 = \dot{m}_{10} = \dot{m}_{ss} \quad \text{(kg/s)}$$

$$h_9 = h_{10} \quad \text{(kJ/kg)}$$

System COP

The coefficient of performance (COP) of an absorption machine is defined by the ratio of heat absorbed at the evaporator and heat provided at the generator. The work of pump is negligible as compared with heat provided.

$$COP = \frac{Q_e}{Q_g + W_p} = \frac{Q_e}{Q_g} \qquad 2.55$$

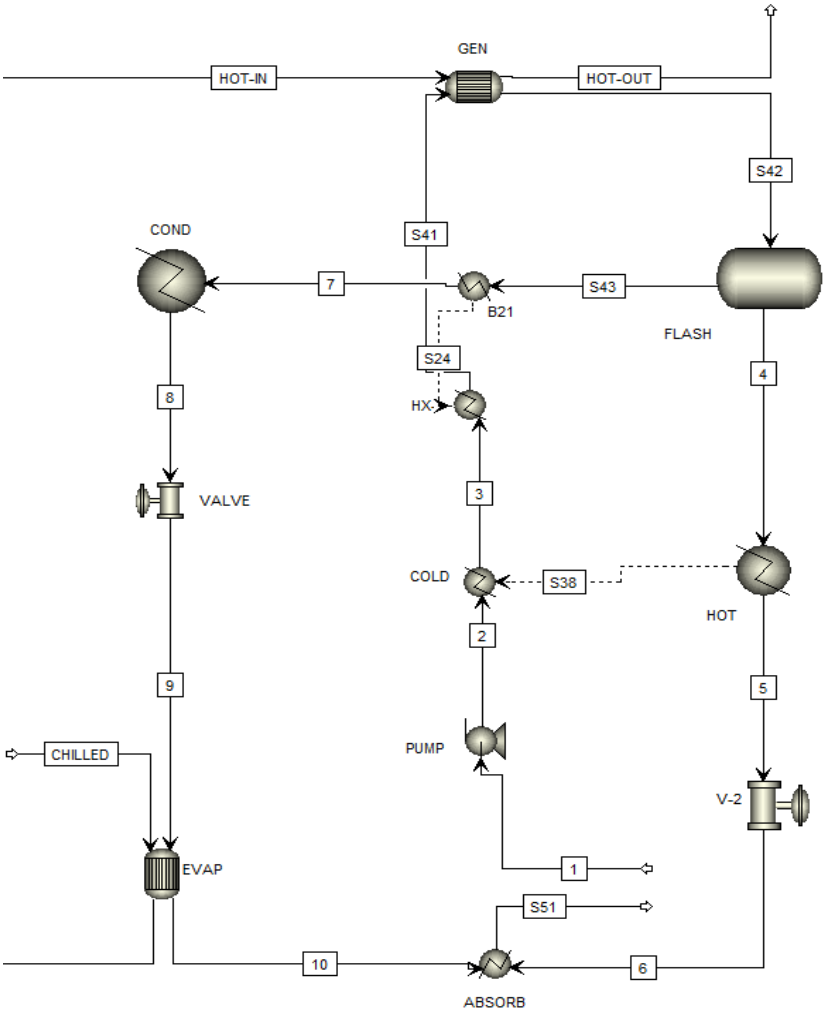

Figure 2.13. Absorption machine model implemented in Aspen Plus

Table 2.8. State point assumptions

State point	Assumption
1	Vapor fraction is 0
2	Pressure increase by solution pump

3	Temperature increase after SHX
4 and 7	Saturated liquid and saturated vapor respectively; the mass flow rate ratio between 4 and 7 is determined by the temperature of the waste heat source
5	Temperature reduction after SHX
6	Pressure reduction by valve
8	Vapor fraction is 0
9	Pressure reduction by valve
10	Vapor fraction of 1

Adaptation to desired inputs

Once the functioning model for the single effect cycle is developed, it is modified to require the inputs most relevant to an absorption cycle designer. Those inputs are:

- Quantity of available heat or required cooling load
- Evaporator temperature
- Condenser temperature (related to cooling medium temperature)
- Absorber temperature
- Generator temperature

Each of these parameters defines a pressure, concentration or mass flow rate. The mass flow rate via the bottom pump is determined by either the available waste heat or the cooling demand. The low pressure is defined by the evaporator exit temperature, and the solution concentration at the absorber exit is defined by the absorber exit temperature. The high pressure is defined by the condenser exit temperature. In the cycle, the concentration at the generator exit is defined by the temperature at the liquid exit of the generator (which is related to the temperature of the available heat).

Integration of absorption machine

The products in the first condenser are cooled down from 400°C to 110°C thus rejecting about 803 kW of heat. In the second condenser, the bio-oil vapors and water are condensed and non-condensable gases are cooled down from 110°C to 40°C and rejecting about 384 kW of heat. Therefore, there is a possibility of utilizing heat rejected in the first condenser to drive an

absorption cooling machine which only requires 632 kW of heat to produce 384 kW of cooling which can be used in the second condenser. Thus, there is a possibility of completely replacing a compression refrigeration machine by an absorption refrigeration machine which can reduce the electricity consumption significantly as absorption machine requires very little electricity for its operation.

2.3.2.7 Heat Generation (Area 600)

As biochar is handled as a non-conventional component in this model, therefore ultimate analysis of the biochar must also be calculated. The elemental balance in OMWS, gaseous components from OMWS pyrolysis, biochar, and bio-oil are used to compute the final analysis of biochar. The following is a general formula for calculating the percentage of carbon in biochar:

$$C_{biochar}\% = \frac{C_{OMWS}\% - \left(\frac{f_{CO}}{28} + \frac{f_{CO_2}}{44} + \frac{f_{CH_4}}{16} + \frac{f_{C_2H_6}}{30} \times 2 + \frac{f_{C_3H_8}}{44} \times 3 + \frac{f_{C_4H_{10}}}{58} \times 4 + \frac{f_{Biooil}}{MW_{biooil}} \times N_{Biooil}\right)}{f_{Biochar}} \quad 2.56$$

Lower heating value (LHV) of biochar (ash free) can be calculated as follows:

$$LHV = 32.88 * \%C + 120.5 * \left(\%H - \frac{\%O * 2}{18}\right) + 9.5 * \%S \quad \text{(MJ/kg)} \quad 2.57$$

The combustion of biochar is given by following reaction:

$$C_1H_{0.513}O_{0.084}N_{0.075}S_{0.011} + 1.17\ O_2 \rightarrow CO_2 + 0.256\ H_2O + 0.075\ NO_2 + 0.011\ SO_2 \quad 2.58$$

The combustion reactions for NCG are given below

$$H_2 + 0.5\ O_2 = H_2O \quad 2.59$$

$$CO_2 + 0.5\ O_2 = Co_2 \quad 2.60$$

$$CH_4 + 2\ O_2 = CO_2 + 2\ H_2O \quad 2.61$$

$$C_2H_6 + 3.5\ O_2 = 2\ CO_2 + 3\ H_2O \quad 2.62$$

$$C_3H_8 + 5\ O_2 = 3\ CO_2 + 4\ H_2O \quad 2.63$$

$$C_4H_{10} + 7.5\ O_2 = 4\ CO_2 + 5\ H_2O \quad 2.64$$

Biochar exiting cyclone is combusted in a combustor (*RStoic*). The biochar is combusted with 100% excess air and about 30% heat losses are considered. Similarly, non-condensable gases are also combusted and combined with the flue gases of combustion of biochar. These flue gases are used for heating the fluidizing gas and for generating steam to produce electricity in Area 700.

Finally, after drying the biomass in Area 100, the flue gases are still hot to preheat the air for combustion of biochar and NCG.

2.3.2.8 Electricity generation (Area 700)

In Area 600, the flue gases produced by the combustion of biochar and NCG are utilized to generate steam, which is subsequently used to generate electricity. A steam turbine, a heat exchanger, a condenser, and a feed water pump were used to represent the steam power cycle. The NBS/NRC steam table in Aspen Plus was used to simulate the thermodynamic parameters of the heat exchanger's water section. Superheated steam was created at 503°C and 40 bar and fed into the steam turbine to generate electricity. The steam turbine was designed to have a mechanical efficiency of 95% and an isentropic efficiency of 80% [58].

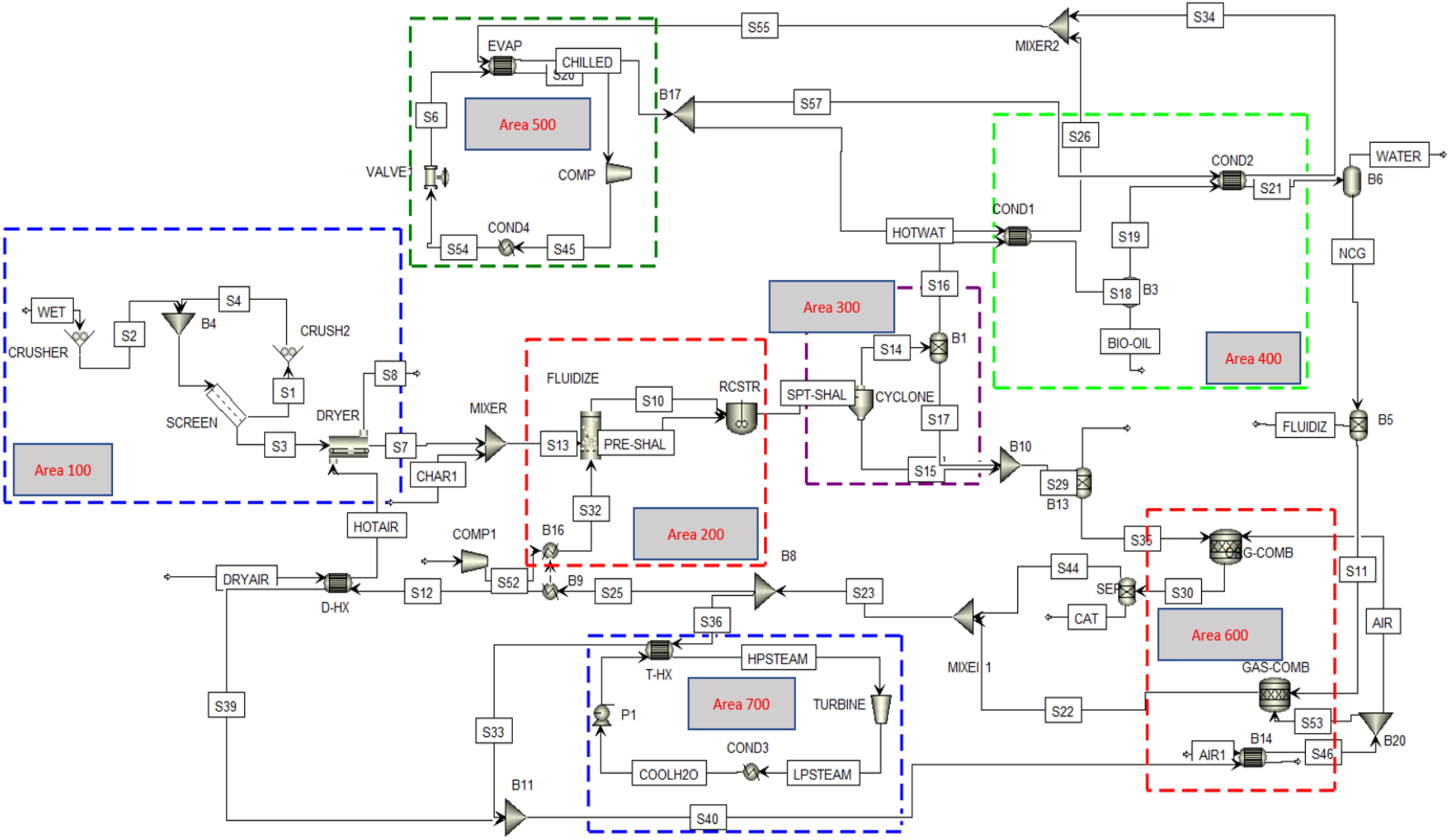

Figure 2.14. Process flow diagram with compression refrigeration machine

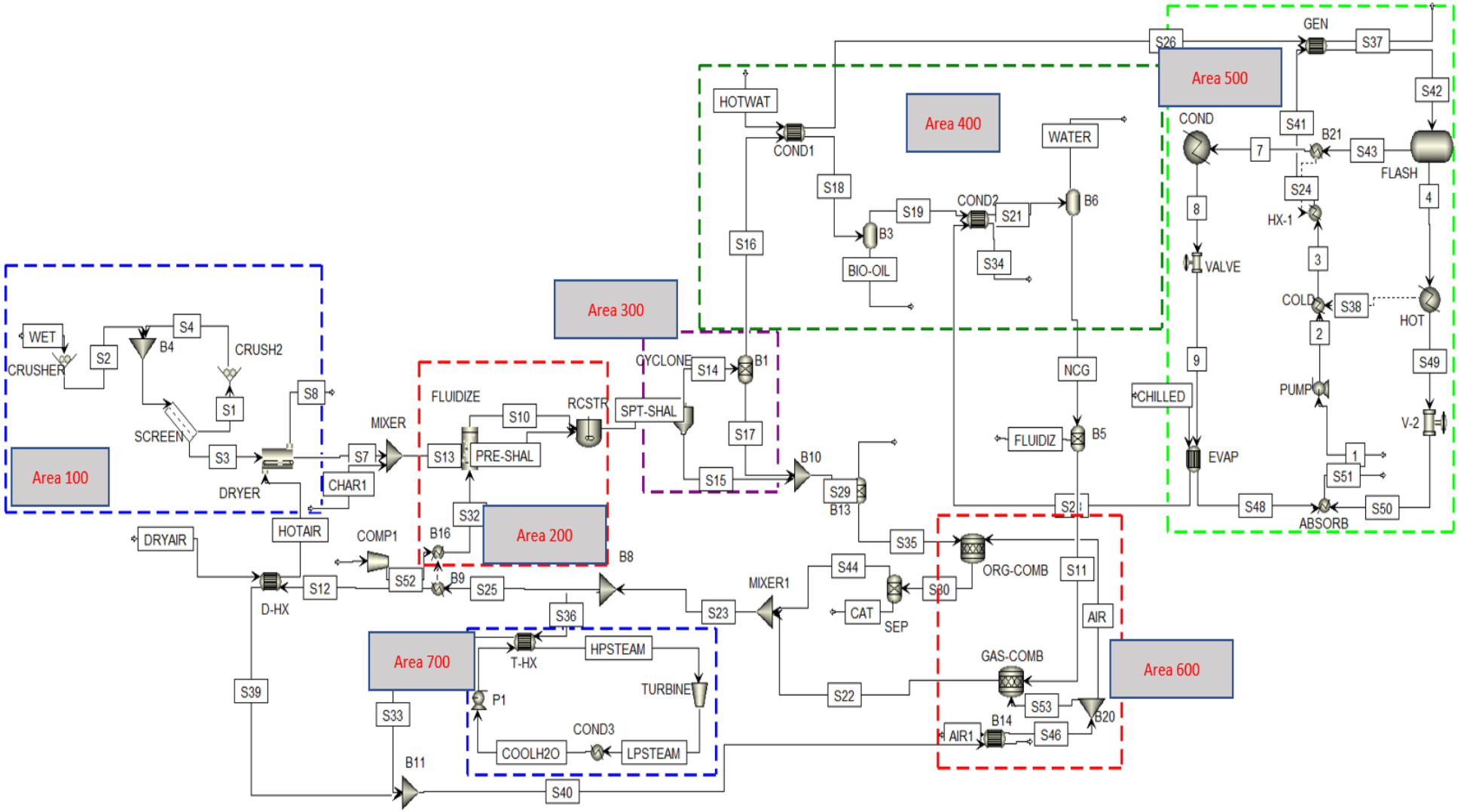

Figure 2.15. Process flow diagram with absorption refrigeration machine

2.4 Performance parameters

Energy efficiency of the complete process is calculated by dividing energy output from the system by the energy input to the system. The energy efficiency formula is shown in Eq. 2.66 [58].

$$\eta_{plant} = \frac{\dot{m}_o . HHV_o}{(\dot{m}_i . HHV_i) + (W_i - W_o)} \quad 2.65$$

where $\dot{m}_o$ represents the mass flow rate of bio-oil and gaseous products and HHV_o represents the corresponding higher heating value. The electricity generated by the turbine is denoted by W_o. Similarly, $\dot{m}_i$ and HHV_i are the biomass flow rate and higher heating value respectively. W_i is total power required to operate the complete system including pumps, fans, grinder and compressor.

Absolute average deviation e between simulated and experimental results is given by [122]:

$$e\ (\%) = 100 \times \left(\sum_{i}^{N} \frac{\left| Y_{i,sim} - Y_{i,exp} \right|}{Y_{i,exp}} \right) \Big/ N \quad 2.66$$

where $Y_{i,sim}$ is the quantity of a product calculated by simulation model and $Y_{i,exp}$ is the experimental quantity of a product.

2.5 Economic analysis

The overall technique used in this analysis is depicted in Figure 2.16. Modeling, equipment size and costing, profitability analysis using the discounted cash flow (DCF) approach and sensitivity analysis are all part of the methodology.

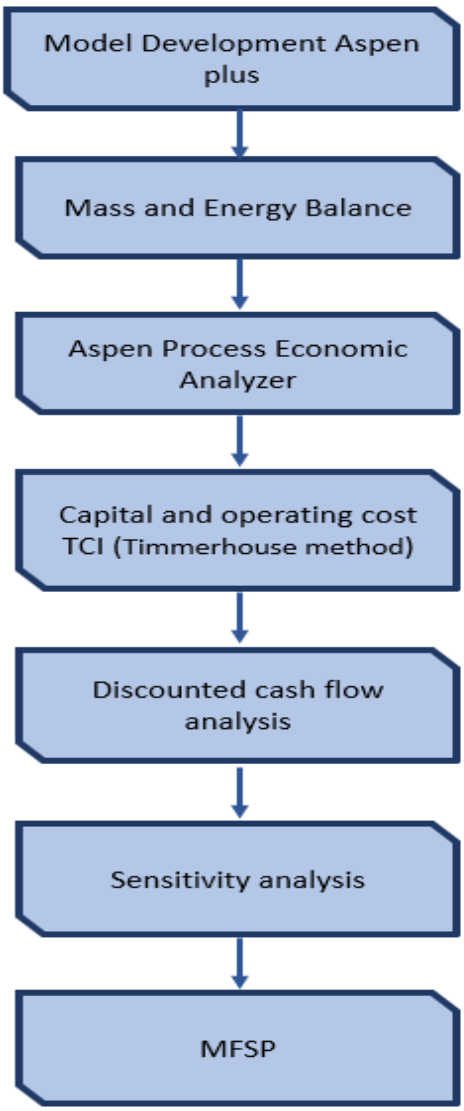

Figure 2.16. Methodology flow chart

To size the equipment and determine the purchasing costs, Aspen Process Economic Analyzer (APEA) was used. The unit processes modeled in Aspen Plus are transferred to APEA where they are mapped and scaled to the required equipment cost models to perform sizing measurements and approximate equipment procurement prices. The costs of the pyrolysis reactor and regenerator were computed using the scaling equation proposed by Wright et al. [59] as follows:

$$C_1 = C_o.\left(\frac{S_1}{S_o}\right)^{0.6} \quad (€) \quad 2.67$$

where C_1 is the new calculated cost with the size of S_1 and C_o is the base cost with the size of S_o. Table 2.9 shows the assumptions made during the calculation of total operating cost.

Table 2.9. Operating cost parameters

Material	**Cost**
Biomass cost [€/t]	30
Catalyst [€/kg]	3
Utilities	
Electricity [€/kWh] [123]	0.092
Cooling water [€/m^3]	0.032

Table 2.10. Inputs for DCF analysis

Economic Inputs	
Required rate of return	10%
Capital cost escalation	5%
Operating cost escalation	3%
Revenue escalation	5%
Income Tax	30%
Plant life	20 years

Table 2.11. Variation in different parameters

Parameter	**Range**
Discounted rate [%]	0% to 40%
Income tax [%]	10% to 60%
Capital cost [€]	± 30%
Operating cost [€]	± 30%
Fuel yield [liters/year]	± 30%

Total project investment was calculated using Peters and Timmerhaus's method [29] as shown in Table 2.12. The capital cost of the pyrolysis plant is made up of direct and indirect costs, as well as a contingency and position factor. Regional labor, supervisor, and service costs are included in the cost model. Total installed cost (TIC) is approximated by 3.02 times the purchased cost of equipment. Installation cost includes electrical wiring, plumbing, structures and other related costs. Indirect costs include contractor's fees, supervision and technical cost, legal fees and construction costs. It is calculated at a rate of 0.89 times the total purchased equipment cost.

Table 2.12. Total project investment estimation method

Parameter	**Value**
Total purchase equipment cost (TPEC)	100% TPEC
Total installed cost (TIC)	302% TPEC
Indirect cost (IC)	89% TPEC
Total direct and indirect cost (TDIC)	TIC + IC
Contingency	20% TDIC
Fixed capital investment (FCI)	TDIC + contingency
Location factor (LF)	10% FCI
Total project investment (TPI)	FCI + LF

The discounted cash flow approach is used to assess the profitability of all process schemes. Initially, eq. 2.68 was used to calculate the net present value (NPV).

$$NPV = -C_T + \sum_{n=1}^{N=t} \frac{\emptyset\, \dot{m}(1 - T_n) - O_n}{(1 + r)^n} \qquad 2.68$$

where C_T represents the initial capital investment, $\emptyset$ is the fuel price, annual fuel yield of plant is specified by $\dot{m}$, annual operating cost is represented by O_n, T_n is annual income tax and r is the required rate of return.

The plant was assumed to be operational for a 20-year period (t) in the DCF analysis. In addition, the DCF calculations were subjected to a 30% income tax. Following that, the minimum fuel selling price (MFSP) is calculated by setting the NPV to zero while keeping the other variables constant.

Sensitivity analysis

Sensitivity analysis is a technique for determining the profitability impact of changes in procedural and economic parameters. The impact of major parameters on the MFSP was explored, including bio-oil yield, capital investment, operating cost, discounted rate and income tax. These parameters were chosen because they have a direct impact on profitability; in other words, bio-oil's MFSP is strongly tied to these parameters.

The sensitivity analysis employs a 30% spectrum. Although the stated range of sensitivity analysis allows for individual evaluation of uncertainty in parameter estimations, it does so in a deterministic manner that ignores the researched parameters.

2.6 Life cycle assessment

2.6.1 Goal and scope definition

The current study focuses on the environmental impacts of liquid bio-oil production from fast pyrolysis of OMWS using two different cooling mechanisms using SimaPro 9.0 software. The method used in the analysis is Impact 2002+ and the database is EcoInvent 3. Non-renewable energy demand (NRE) and its associated global warming potential (GWP) are primarily evaluated in this LCA work. Depending upon the required heat and electricity, three different scenarios are investigated.

- In the 'basic scenario', heat and electricity are provided from the external sources.
- In the 'recycling heat' scenario, the heat is produced with the system by combustion of non-combustible gases (NCG) and biochar while electricity is provided from the external source.
- In the third scenario 'recycling heat and electricity', both heat and electricity are produced within the system and provided to the system.

2.6.2 Functional unit

To compare the environmental impact associated with the two cooling mechanisms. 1 kg of bio-oil is chosen as the functional unit.

2.6.3 System boundaries

The system boundaries for bio-oil production for all scenarios were considered including transport, electricity and fast pyrolysis stages. OMWS is transported from evaporation pond to pyrolysis plant. The system boundaries established for the LCA are presented in Figure 2.17.

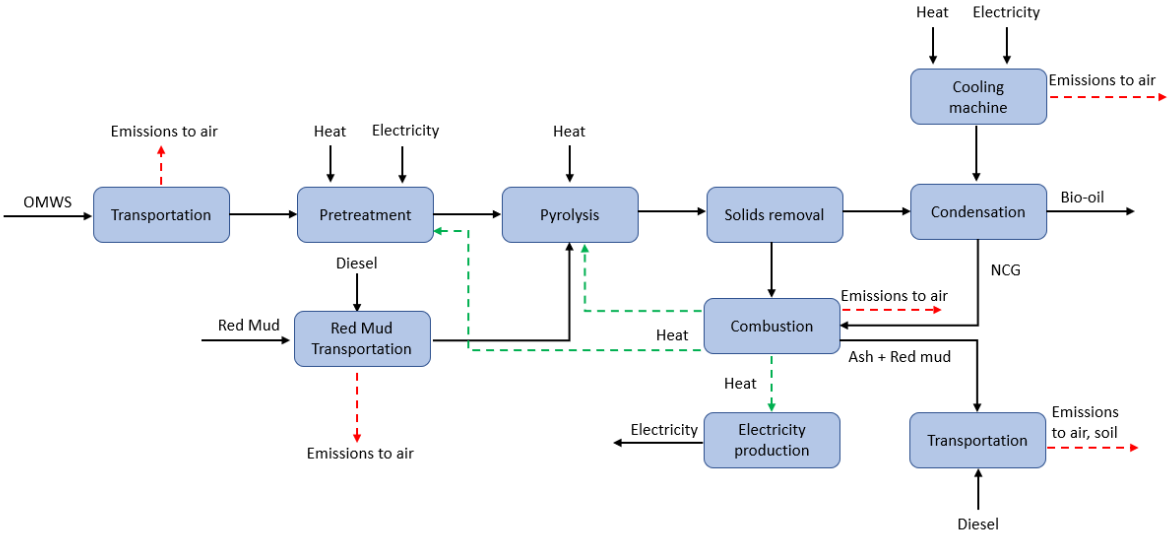

Figure 2.17. System boundaries for bio-oil production via fast pyrolysis

Biomass transportation stage considers the OMWS transport to pyrolysis plant. The OMWS is transported by trucks considering average distance 50 km. The distance traveled by the trucks is established based on the actual location of evaporation ponds in Sfax, Tunisia. The energy demand for pyrolysis has already been presented in the previous section. A summary of inventory data is given in Table 2.13.

Table 2.13. Inventory data for energy inputs associated with different processes for 100 tonnes/day of OMWS

Item	Unit	Value
OMWS transportation	Km	50
Red mud transportation	Km	50
Ash transport	Km	25
Electricity for grinding	kWh	55
Electricity for fan	kWh	0.7
Electricity for compressor	kWh	90
Electricity for compression machine	kWh	400
Heat for drying	MJ	1,749
Heat for pyrolysis	MJ	3,834

2.6.4 Inventory analysis

In this chapter we have produced models of the key processes involved in our analysis. In order to guarantee the quality of the data that will be used in this LCA, the inventories resulting from these models are the result of deterministic calculations where the mass and energy balances are respected.

Transport

Transport requires resources (diesel, ...) and generates polluting emissions. For the analyzed system, we will adopt road transport. The declaration of a road transport process in SimaPro requires the definition of the quantity of the material transported, the distance covered and the type of vehicle used. The software combines the first two parameters into a single indicator: the number of kilogram kilometers (kg.km). It is the product of the mass transported in (kg) and the distance covered in (km). Since the OMWS and the catalyst come from local sources, the distances travelled for transport are low (50 km).

Table 2.14 lists the transports used for each elementary stream and specifies the respective distance chosen.

Table 2.14 type and distance of transport

Transport vehicles	Material transported	Distance covered (km)	Number of tons kilometers (kg.km)
Truck, capacity > 32 metric tons, EURO3	OMWS	50	180
Truck, capacity 3.5-7.5 metric tons, EURO3	Catalyst	50	2.6
Truck, capacity 16 metric tons, EURO3	Ash	25	12.5

Summary

This chapter covers the methods for calculating heat and mass balance for an industrial scale pyrolysis process and elaborates data collection from experimental findings. The data for the lab scale is derived from the findings of Agblevor et al. [1] and the process is simulated in Aspen Plus. After the validation of simulation results with experimental data, the model is up-scaled to industrial scale and other processes; drying of biomass, combustion of biochar and steam production for electricity generation are modelled. The design parameters are derived from the literature, and the resulting mass flow rates and energy balances are computed. The reaction kinetics for industrial scale pyrolysis are the same as those used in the lab scale model. Modeling the absorption refrigeration machine to satisfy the needed cooling demand in the second condenser is the most essential portion. In the last section, an economic analysis of production of bio-oil is performed. The total capital investment is computed from Timmerhous's method by considering all the necessary equipment used in the simulation model. The equipment cost is derived from different sources including vendors, literature and Aspen Process Economic Analyzer (APEA). Finally, a discounted cash flow analysis is used to determine the minimum bio-oil fuel selling price. The last section is about the life cycle assessment of bio-oil production via fast pyrolysis. SimaPro 9.0 is used for this assessment and the electricity and heat required are already have been calculated.

CHAPTER 3: RESULTS AND DISCUSSION

This section comprises of four vital sections: (i) model validation with experimental data, (ii) mass and energy balance for industrial scale, (iii) exergy analysis of whole process and (iv) economic analysis of production of bio-oil.

3.1 Model validation

The pyrolysis of olive mill wastewater sludge is modeled in Aspen Plus. 160 g of OMWS and 40 g of biochar are used for simulation purpose. The grinding of OMWS is accomplished using a crusher and drying is modelled using a simple heater. The dried OMWS is introduced into the fluidized bed reactor and then RCSTR reactor where pyrolysis of OMWS takes place. After pyrolysis, the products pass through a cyclone where biochar is separated from gaseous products. The bio-oil and water vapors are condensed in two heat exchangers cooled by a compression refrigeration machine. Bio-oil in Aspen Plus is represented by 21 different compounds. The compression refrigeration machine is modelled by a compressor, two heat exchangers and one valve.

Simulations are performed at different temperatures and product yields are tabulated in Table 3.1 and compared with experimental yields. The variation in yields is computed by absolute average deviation (AAD).

Table 3.1. Comparison of simulation and experimental results

	Yields (wt.%)					
	400°C		450°C		500°C	
	Experimental	Simulated	Experimental	Simulated	Experimental	Simulated
Bio-oil	34.6	35.5	29.8	28.6	29.5	28.4
Biochar	29.1	29.8	22.7	22.1	20.4	19.9
Gas	25.0	23.5	30.0	31.1	38.3	39.7
Water	11.3	11.4	17.5	18.0	11.8	11.7

Table 3.2. Absolute average deviation for different temperatures

Product	AAD (%) 400°C	AAD (%) 450°C	AAD (%) 500°C
Bio-oil	2.60	4.17	2.79

Biochar	2.41	2.66	2.64
Gas	6.01	3.64	3.70
Water	0.88	2.64	0.14
Overall	2.97	3.27	2.56
Global		2.36%	

The model is validated against the experiments of Agblevor et. al. [1] conducted in a fluidized bed pyrolyzer. The simulation results with experimental data of the products yield distribution are shown in Figure 3.1 and the absolute average deviation values are depicted in Table 3.2. It can be seen that the simulation model of the biochar and water yield distribution correlates better with experimental data of Agblevor et. al. [1] particularly at temperatures 400 and 500°C (AAD < 3%). At temperature 400 °C, water yield in the simulation is 11.4% while in the experiment is 11.3% resulting the AAD about 0.88%. Correlation between the model and experimental data reported by Agblevor et. al. [1] was found to be satisfactory for bio-oil and gas yield results at different pyrolysis temperatures in the range of 400 – 500°C showing that the AAD is lower than 4.2%. However, the overall AAD values of products yields at temperatures 400, 450 and 500°C are 2.97%, 3.27% and 2.56%, respectively and the global AAD value comes out to be 2.36%.

As shown in Fig. 3.1, bio-oil yield decreases when the temperature increases from 400 to 500°C while the gas yield increases with the temperature and the biochar yield decreases. This result can be explained by the triggering of the secondary bio-oil vapor cracking reactions to produce non-condensable gases in the presence of red mud. It implies that high yields of bio-oil can be achieved if cracking of primary bio-oil vapors can be avoided. At higher temperatures, the decrease in biochar yield is due to thermal decomposition effect. The water content in the liquid product is maximum at 450°C while it is low for other temperatures.

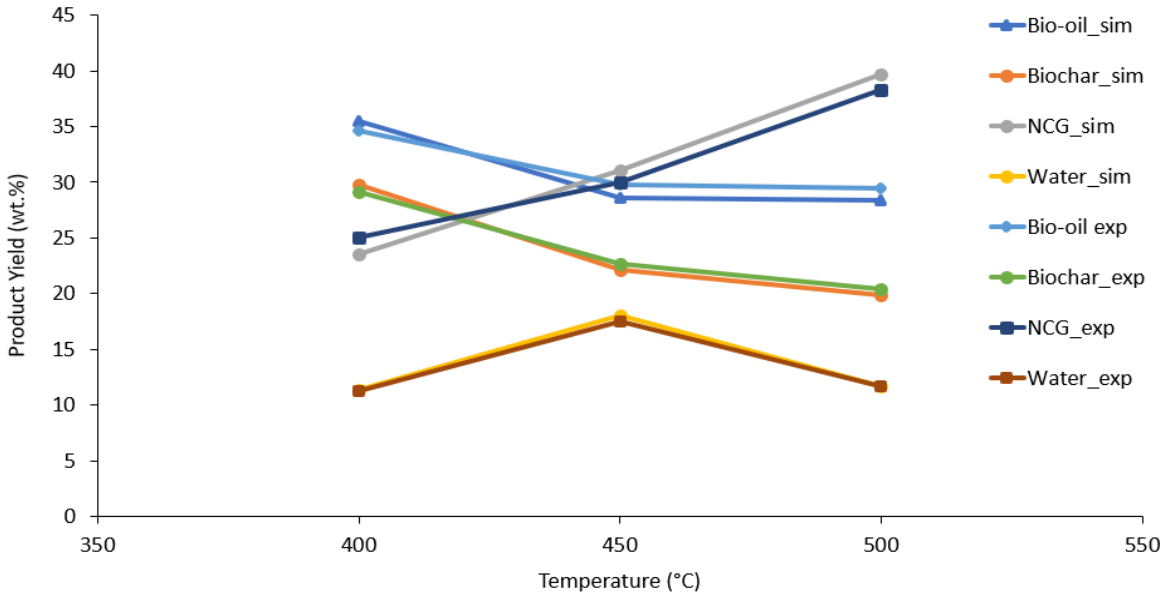

Figure 3.1. Comparison between simulation and experimental yields at different temperatures

The composition of fast catalytic pyrolysis product gases predicted from Aspen plus-based simulation is also investigated and compared with the experimental data. The distribution of the gas composition with different pyrolysis temperatures is shown in Figure 3.2. The yield of CO_2 decreased from 78% at 400 °C to 66.1% at 500°C whereas the CO, H_2, and CH_4 increased from 6.45%, 2.1%, and 1.6% at 400 °C to 11.8% 3.9% and 3.8% at 500°C, respectively.

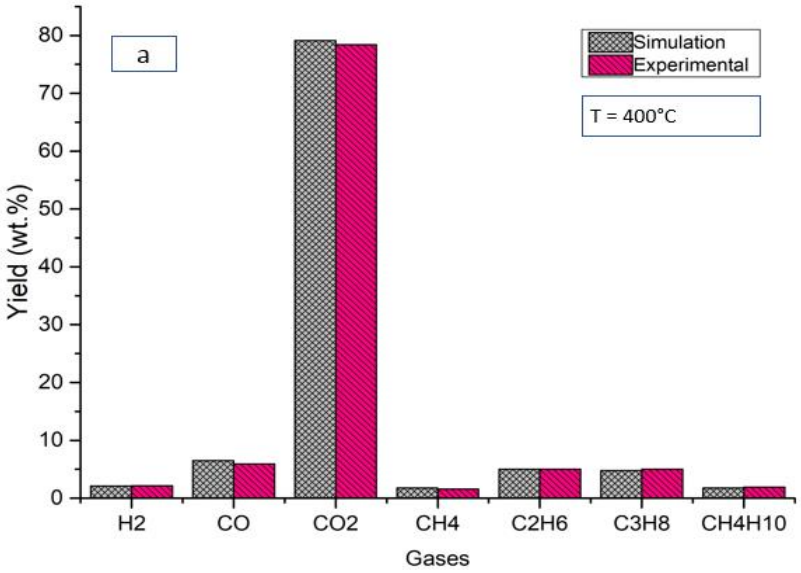

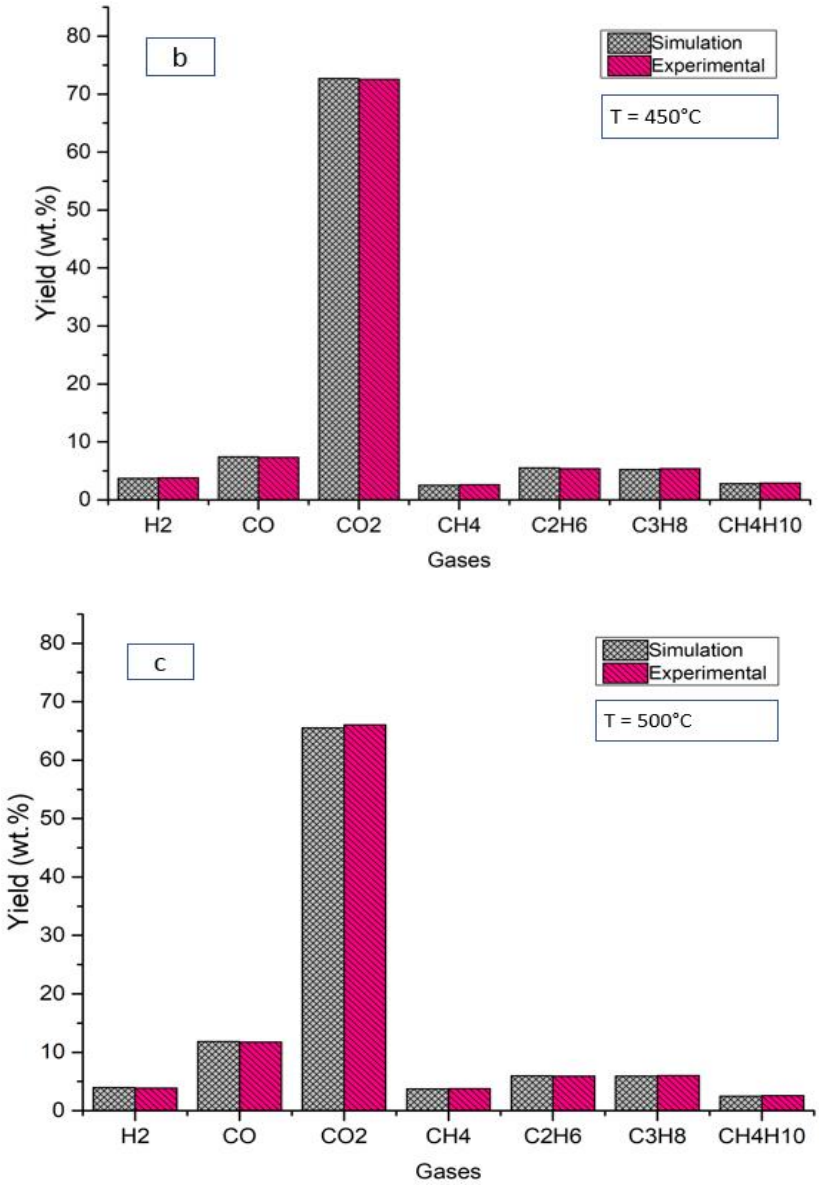

Figure 3.2. Gas composition of OMMWS at different temperatures

The composition distribution of catalytic bio-oil produced at 450°C is depicted in Figure 3.3. The differences between the model predictions and the experimental results are noticeable for all bio-oil components. These differences owe to the fact that, in addition to a high number of chemicals found, about 30% of bio-oil composition could not be determined experimentally.

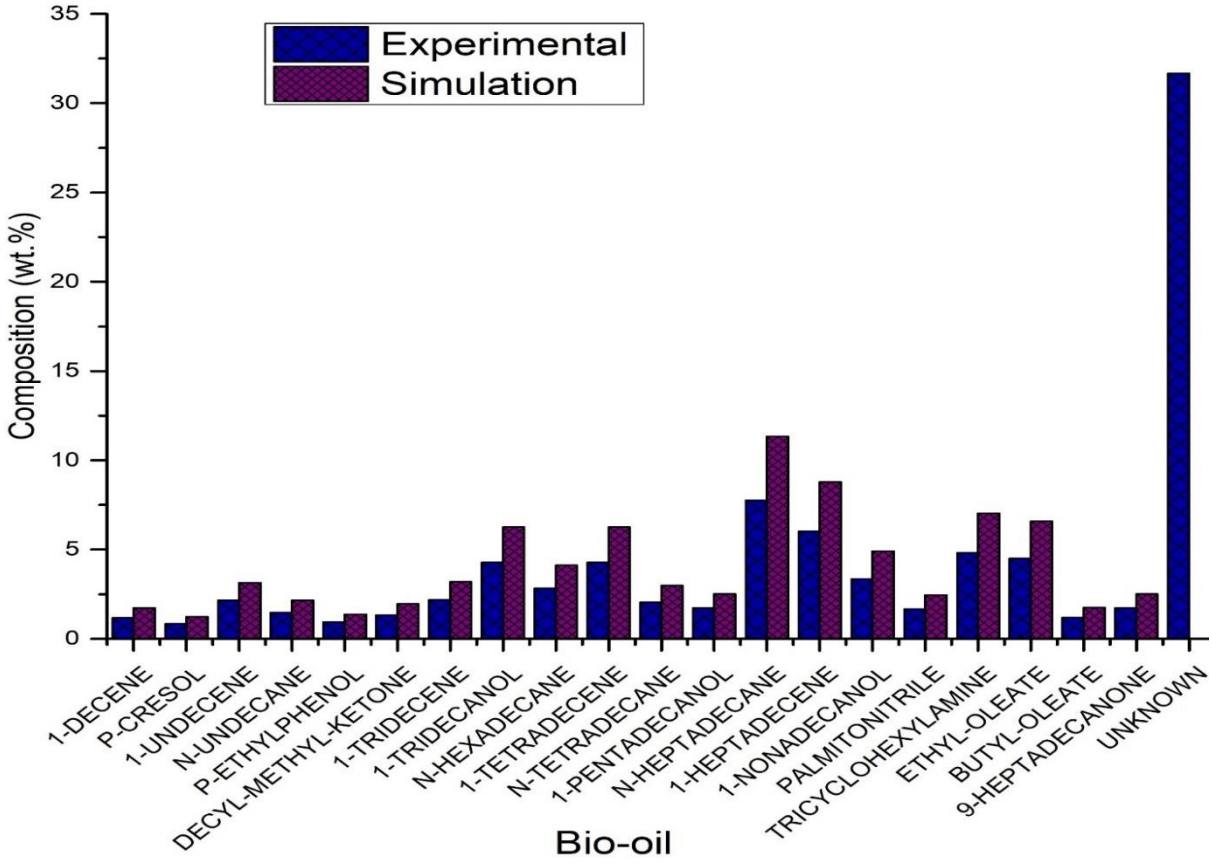

Figure 3.3. Composition of bio-oil for catalytic fast pyrolysis at 450°C.

3.2 Industrial scale

Overall mass balance

The following Figure 3.4 presents an overview of the mass balance of the whole process. About 17,000 kg/hr of air at 120°C is required to dry 4,166 kg/hr of OMWS. The hot air carries away 260 kg/hr of water from the OMWS reducing the moisture content from 10% to 4%. In the pyrolysis section, about 1,150 kg/hr of bio-oil, 1,472 kg/hr of biochar, 770 kg/hr NCG and 514 kg/hr of water is produced. The pyrolysis takes place at 400°C as bio-oil yield is maximum at this temperature. The biochar is separated in the cyclone and rest of products pass through the two condensers. About 749 kg/hr of bio-oil is condensed in the first condenser and 401 kg/hr of bio-oil in the second condenser along with 514 kg/hr of water. Non-condensable gases are combusted with 2,600 kg/hr of air to produce flue gases (3,370 kg/hr). Similarly, biochar is combusted with 1,472 kg/hr of air and flue gases are produced at high temperature (21,086 kg/hr). Theses flue gases are utilized for drying of OWMS, fluidized bed reactor heating and electricity generation. Detailed mass and energy balances are given in the following sections.

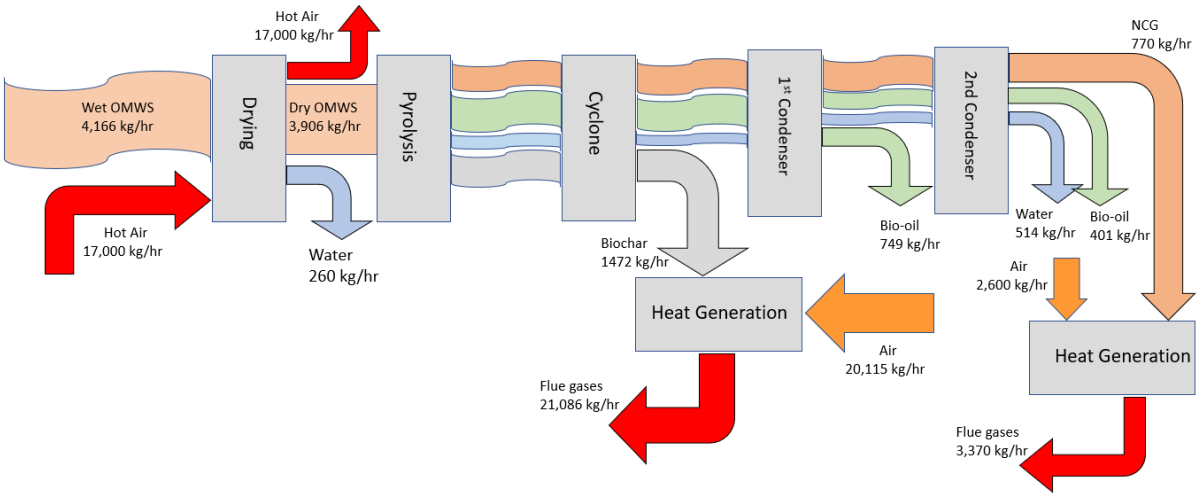

Figure 3.4. Overall mass balance

3.2.1.1 Feedstock drying

Flue gases from the combustion of biochar and NCG are used to heat the air for drying the OMWS. The feedstock is dried in a convective dryer by hot air at 120°C. Process demands 17,000 kg/hr of hot air to dry about 4 tons of feedstock from 10% wt. moisture to 4% wt. moisture content. The exit temperature of the gases is 60°C. The direct contact during drying transfers 260 kg of water from wet biomass to the hot air thus increasing the moisture content

of hot air from 10 inlet (10 g/kg dry solid) to 25.5 outlet (25.5 g/kg dry solid). Heat required to heat the air from 20 to 120°C is 486 kW.

3.2.1.2 Grinding

The biomass is ground from 10 mm to 2 mm using a hammer mill. The product particles are filtered and if size is greater than 2 mm they are sent back to the crusher to be ground again. From eq. 2.14, the power required for the crusher is calculated to be 53.55 kW.

3.2.1.3 Fluidized bed reactor

The minimum fluidization velocity is one of the most important parameters associated with a fluidized bed reactor. From eq. 2.28, void fraction at minimum fluidization velocity is given below.

$$\varepsilon_{mf} = 0.48$$

From equation 2.24, minimum fluidization velocity is determined.

$$u_{mf} = 0.20\ m/s$$

Reynolds number at minimum fluidization is calculated from eq. 2.23.

$$R_e = 4.37$$

The superficial velocity can be from 2 to 4 times the minimum fluidization velocity. So, in our case we take is as 2 times.

$$U_s = 0.40\ m/s$$

Hence the mass flow rate of fluidization gas is given by

$$\dot{M}_g = 2{,}029 \text{ kg/hr}$$

For a bed mass of 2,000 kg and diameter 1.5 m, the pressure drop in the reactor is calculated to be 0.11 bar and void fraction is 0.48. The minimum fluidization velocity is determined to be 0.20 m/s. The mass flow rate of fluidization gas is 2,029 kg/hr.

The heat required by pyrolysis reactor comes out to be 1,065 kW (1.18 MJ/kg) from equation 2.30. Hua Yang et. al. [124] reported that pyrolysis at 600°C consumes 1.1-1.6 MJ energy per kilogram dry biomass and lower number is expected for lower temperature.

3.2.1.4 Condensation

The heat removed in the first condenser from vapors is determined from equations 2.33 and 2.34 and is found to be 803 kW and in the second condenser 384 kW. With a COP of 3.0, the electricity needed to operate a compression refrigeration machine is 395 kW. For absorption machine with a COP of 0.61 (calculated), the heat required at generator is 632 kW to cool down the products in the second condenser. The operating conditions of the absorption machine are taken from the equipment manufacturer's data and given in the following table.

Table 3.3. Absorption refrigeration machine operating parameters

Generator Temperature (T_g)	=	90	°C
Condenser Temperature (T_c)	=	35	°C
Absorber Temperature (T_a)	=	30	°C
Evaporator Temperature (T_a)	=	5	°C
Saturation pressure at 35°C	=	7.46	kPa
Saturation pressure at 5°C	=	0.874	kPa
Mass flow rate of weak solution	=	0.84	kg/s
Concentration of LiBr in weak solution	=	54	%
Concentration of LiBr in weak solution	=	67	%
Mass flow rate of water	=	0.16	kg/s
Heat provided at generator	=	632	kW
Heat rejected at condenser	=	410	kW
Heat released in absorber	=	606	kW
Heat absorbed in evaporator	=	384	kW
COP	=	0.61	

3.2.1.5 Heat Generation

From eq. 2.59, the ultimate analysis of ash free biochar is given in the following table.

Table 3.4. Ultimate analysis of biochar (ash free)

Ultimate analysis (wt.%)	
Carbon	78.61
Hydrogen	3.36
Nitrogen	6.91
Sulfur	2.32
Oxygen	8.8
LHV (MJ/kg)	29

NCG and biochar are combusted to provide heat for pyrolysis, drying of biomass and steam generation for electricity production. The combustion air is preheated by recovering heat from flue gases after steam generation and biomass drying. The air required for combustion of biochar is calculated to be 20,115 kg/hr and for NCG is 2,600 kg/hr.

Based on the ultimate analysis of biochar, lower heating value is calculated to be 29 MJ/kg.

Energy balance for the whole system is given in the following table.

Table 3.5. Energy balance

Process	*Energy (kW)*
Drying	486
Fan for drying	0.7
Grinding	53.5
Pyrolysis	1,065
Compression refrigeration machine	395
Compressor for fluidizing gas	90
Electricity produced	303

Table 3.6 Mass flows for different streams in Aspen Plus model

Stream		WET	S3	S7	CHAR1	S32	SPT-SHAL	S15	S14	BIO-OIL	S19	WATER	NCG
Temperature	C	25	25	50	25	900	400	400	400	105	105	43.17	43.17
Mass Flows													
N2	kg/hr	0	0	0	0	0	0	0	0	0	0	0	0
H2	kg/hr	0	0	0	0	49.45	66.03	0	66.03	0	66.03	66.03	66.03
H2O	kg/hr	0	0	0	0	0	513.8	0	513.8	19.93	493.89	490.21	3.68
CO	kg/hr	0	0	0	0	136.62	182.3	0	182.3	0	182.3	0	182.3
CO2	kg/hr	0	0	0	0	1803.43	2407.8	0	2407.8	0	2407.8	0	2407.8
CH4	kg/hr	0	0	0	0	36.8	49.12	0	49.12	0	49.12	0	49.12
C2H6	kg/hr	0	0	0	0	115.01	153.6	0	153.6	0	153.6	0	153.6
C3H8	kg/hr	0	0	0	0	115.02	153.69	0	153.69	0	153.69	0	153.69
C4H10	kg/hr	0	0	0	0	43.70	58.44	0	58.44	0	58.44	0	58.44
1-DECENE	kg/hr	0	0	0	0	0	25.35	0	0	16.51	8.83	8.79	0.04
P-CRESOL	kg/hr	0	0	0	0	0	19.18	0	0	12.49	6.68	6.65	0.03
1-UNDECENE	kg/hr	0	0	0	0	0	68.58	0	0	44.68	23.90	23.79	0.11
N-UNDECANE	kg/hr	0	0	0	0	0	27.63	0	0	18.01	9.63	9.58	0.04
P-ETH-PHENOL	kg/hr	0	0	0	0		18.20	0	0	11.85	6.34	6.31	0.03
1-TRIDECENE	kg/hr	0	0	0	0	0	71.18	0	0	46.37	24.80	24.69	0.11
1-TRIDECANOL	kg/hr	0	0	0	0	0	104.66	0	0	68.18	36.47	36.30	0.16
N-HEXADECANE	kg/hr	0	0	0	0	0	60.45	0	0	39.38	21.07	20.97	0.09
1-TETREDECENE	kg/hr	0	0	0	0	0	72.16	0	0	47.01	25.14	25.03	0.11
N-TET-DECANE	kg/hr	0	0	0	0	0	57.20	0	0	37.27	19.93	19.84	0.09
1-PEN-DECANOL	kg/hr	0	0	0	0	0	28.93	0	0	18.84	10.08	10.03	0.05
N-HEPTADECANE	kg/hr	0	0	0	0	0	147.24	0	0	95.93	51.30	51.07	0.23
1-HEPTADECENE	kg/hr	0	0	0	0	0	125.78	0	0	81.95	43.83	43.63	0.20
1-NONADECANOL	kg/hr	0	0	0	0	0	57.85	0	0	37.69	20.16	20.07	0.09

PALMITONOTRILE	kg/hr	0	0	0	0	0	32.83	0	0	21.38	11.44	11.39	0.05
TRICYCLO-HEXYLAMINE	kg/hr	0	0	0	0	0	82.88	0	0	54.01	28.88	28.75	0.13
ETHYL-OLEATE	kg/hr	0	0	0	0	0	95.23	0	0	62.04	33.18	33.03	0.15
BUTYL-OLEATE	kg/hr	0	0	0	0	0	23.40	0	0	15.24	8.15	8.12	0.04
9-HEPTA-DECANONE	kg/hr	0	0	0	0	0	31.85	0	0	20.75	11.10	11.05	0.05
OMWS	kg/hr	4166	4166	3909	0	0	0	0	0	0	0	0	0
CHAR	kg/hr	0	0	0	0	0	1472.5	1472.5	0	0	0	0	0
FE2O3	kg/hr	0	0	0	1079.6	0	1079.6	1079.6	0	0	0	0	0
AL2O3	kg/hr	0	0	0	270.6	0	270.6	270.6	0	0	0	0	0
SIO2	kg/hr	0	0	0	178.2	0	178.2	178.2	0	0	0	0	0
TIO2	kg/hr	0	0	0	123.6	0	123.6	123.6	0	0	0	0	0
NA2O	kg/hr	0	0	0	170.6	0	170.6	170.6	0	0	0	0	0
CAO	kg/hr	0	0	0	177.4	0	177.4	177.4	0	0	0	0	0
CHAR1	kg/hr	0	0	0	977	0	977	977	0	0	0	0	0

3.3 Exergy analysis

Chemical and physical exergies for all the substances across all the components were calculated and tabulated. β for biomass, biochar and bio-oil is calculated from equations 1.6-1.8.

$$\beta_{biomass} = 1.097$$

$$\beta_{biochar} = 1.062$$

$$\beta_{bio-oil} = 1.067$$

The chemical exergy for OMWS is found to be 26,256 kW, for biochar 8,400 kW and for bio-oil 14,839 kW from equation 1.5. Equation 1.19 is used to calculate the chemical exergy of a gas mixture and is found to be 2,162 kW. The exergy associated with electrical power is equivalent to electrical energy and is calculated to be 545 kW for scheme-1 and 145 kW for scheme-2. [53]. Table 3.8 lists the standard chemical exergies of various gases [53].

Table 3.7. Standard chemical exergy of some gases at 25°C, 0.1 MPa

Gas	E_x^{ch} (kJ/mol)
H_2	236.1
CO	275.1
CO_2	19.8
CH_4	831.6
C_2H_6	1,495
C_3H_8	2,152.8
C_4H_{10}	2,804
SO_2	313.4

Table 3.9 presents the result of exergetic analysis on the fast pyrolysis plant. The overall exergetic efficiency for scheme-1 (compression machine) is 55.9% and for scheme-2 (absorption machine) 57% when only bio-oil is considered the desired product. The difference in the exergetic efficiencies of two schemes is due to the excessive electricity used for compression refrigeration machine. The two sources of exergy input in the drying process are the chemical exergy of biomass and the heat required by the drying process. About 88% of

physical exergy in dryer is destroyed while chemical exergy destruction is negligible as water has negligible chemical exergy.

Table 3.8. Exergy analysis

Operating units		Ex_{in}/kW	Ex_{out}/kW	Ex_D/kW	Ψ%
Dryer	E_x^{Phy}	59	7	52	11.8
	E_x^{ch}	26,262	26,258	4	99.9
Hot air for dryer	E_x^{Phy}	3,736	3,032	704	81.7
Pyrolysis	E_x^{Phy}	407	374	33	95.8
	E_x^{ch}	26,258	25,402	856	96.7
Hot Fluidizing gas	E_x^{Phy}	3,859	2,636	1,223	68.3
Condensation	E_x^{Phy}	374	2	372	0.5
	E_x^{ch}	14,839	14,836	3	99.9
Combustion	Biochar $(E_x^{Phy} + E_x^{ch})$	8,729	4,359	4,369	49.9
	NCG $(E_x^{Phy} + E_x^{ch})$	2,204	1,097	1,107	49.7
Hot air for combustion	E_x^{Phy}	3,847	1,716	2,131	44.6
Steam generation	E_x^{Phy}	1,977	1,408	569	71.2
Net Electricity	E_x^{Elec}	545	303	242	55.5
Total	Compression	26504	14836	11665	55.9
Total	Absorption	26262	14993	11269	57

The maximum exergy destruction (65%) takes place in the combustion of biochar and non-condensable gases. The exergy destruction in this process is caused by the combustion of the char and NCG to produce CO_2 with the low standard chemical exergy. Pyrolysis accounts for only 18% exergy destruction as shown in Figure 3.5. The main part of exergy destruction is lost in the heat exchanger to heat the fluidizing gas to a higher temperature. Total physical exergy destruction accounts for 43.6% in the whole system while 54.3% consists of chemical exergy

destruction. Electrical exergy only constitutes 2.1% of exergy destruction. To conclude, physical exergy destruction can be minimized by improving the effectiveness of heat exchangers. The exergetic efficiency of plant indicates that pyrolysis is a viable energy conversion process.

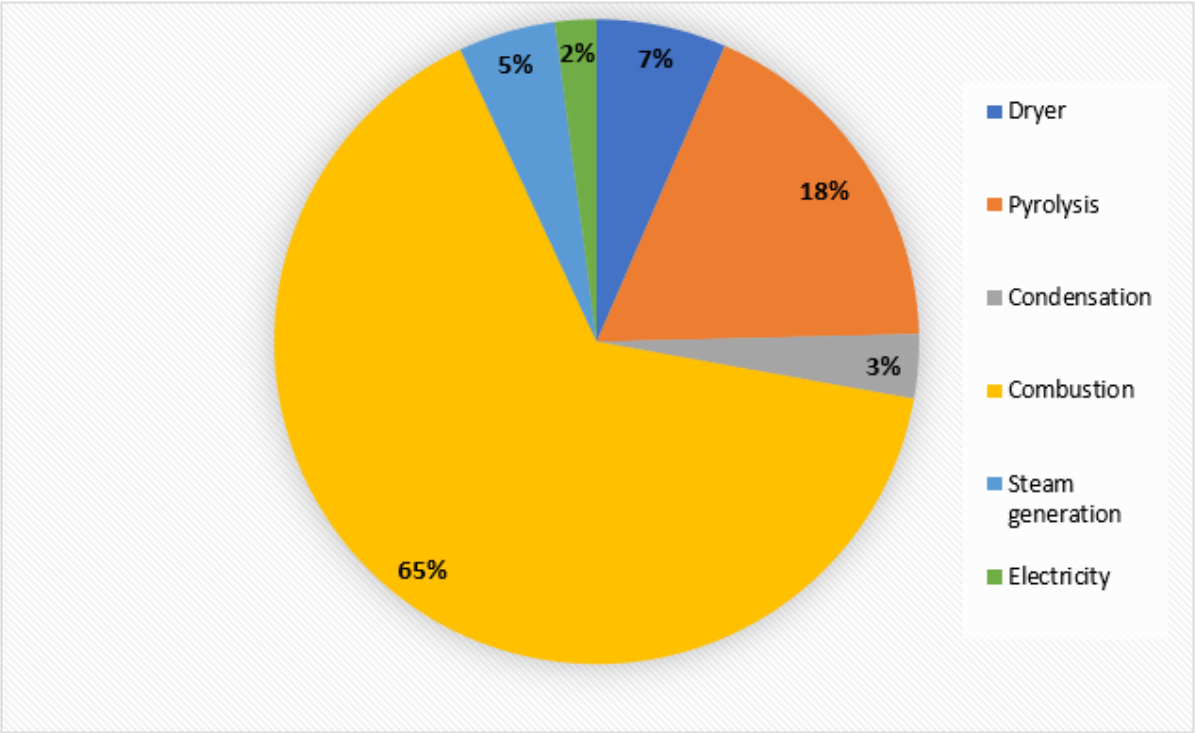

Figure 3.5. Exergy destruction in different processes

3.4 Process performance

The model processed 4,166 kg/h of dry OMWWS and produced bio-oil at a rate of 1,150 kg/h. Biochar and NCG were combusted to supply heat for the pyrolysis, biomass drying and electricity production in an integrated steam cycle. In addition, Area 700 produced 303 kW of power. Since the reactor temperature for both process schemes was set to 400°C, there is no difference in fuel yields between the two process schemes. According to experimental results published Agblevor et. al. [1], the same reactor yields were presumed for both schemes. Nonetheless, the two models vary in terms of electric power usage and capital costs. The electricity needed to run the compression refrigeration system was liable for the disparity in electric power consumption. The energy efficiency of the process is calculated to be 57.5% for scheme-1 and 58.7% for scheme-2. The discrepancy in energy efficiencies can be explained by the fact that the two systems used different amounts of electricity. The mass and energy balances derived from the Aspen Plus simulation of the process are shown in the following table.

Table 3.9. Mass and energy flowrates

Process inputs	
Wet OMWS (kg/h)	4,166
Electricity (kWh)	545
Process outputs	
Bio-oil (kg/h)	1,150
Biochar (kg/h)	1,472
NCG (kg/h)	770
Water vapors	514
Electricity (kWh)	303

3.5 Economic assessment

The economic analysis was performed using Aspen Process Economic Analyzer (APEA). The total project investment was calculated by Peters and Timmerhaus Method. The equipment purchase costs were taken from manufacturer's data (absorption machine), published data (fluidized bed reactor and combustor) and Aspen Process Economic Analyzer (compression machine, heat exchangers, dryer, grinder etc.). In the following section, the total project investment and operating costs for two schemes are given.

3.5.1 Total project investment and operating cost

Figures 3.6 and 3.7 show the proportions of total capital investment for the industrial scale pyrolysis plant for both schemes in ascending order. The pyrolysis unit accounted for the maximum cost (about €5.67 million) while solids separation section constitutes the minimum capital cost (about €0.11 million). Overall, the total capital costs of the process is estimated to be €17.9 million for scheme-1 and €14.9 million for scheme-2. The higher capital cost observed in scheme-1 compared to scheme-2 is attributable to cost of vapor compression refrigeration machine which is significantly bigger than the absorption refrigeration machine.

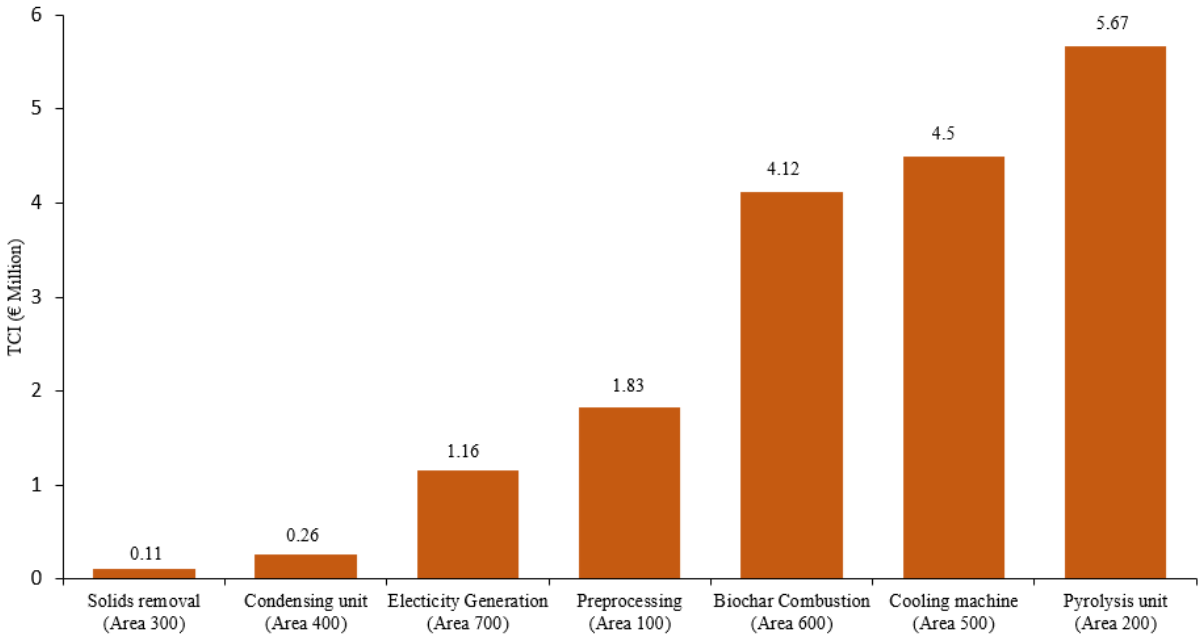

Figure 3.6. Total capital cost investment proportions for scheme-1

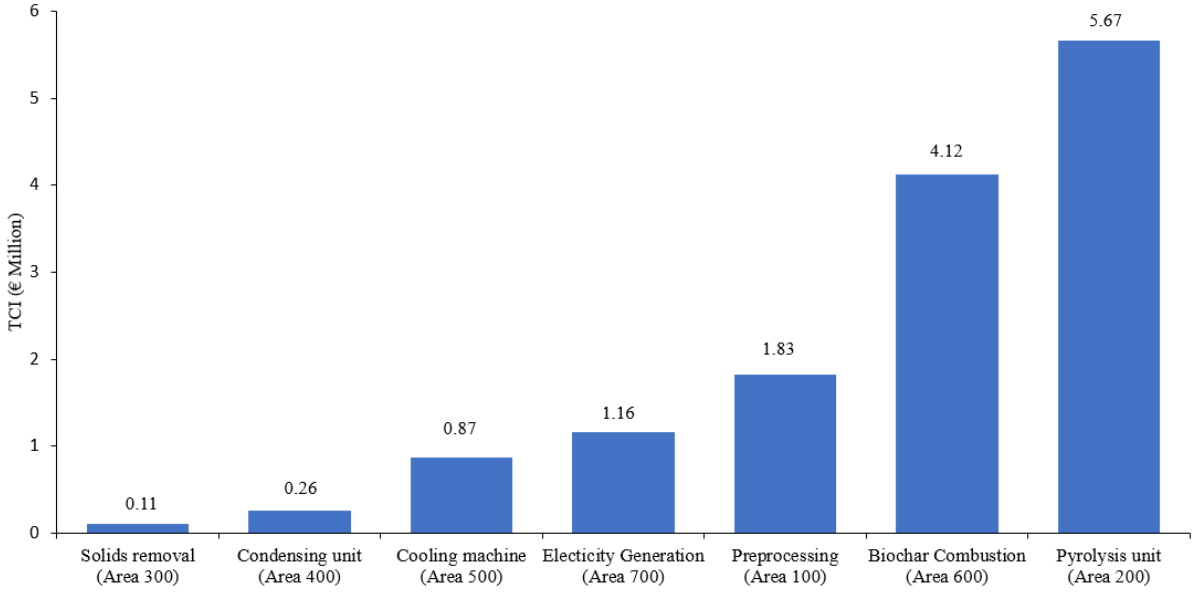

Figure 3.7. Total capital cost investment proportions for scheme-2

The overall operating costs for scheme-1 and scheme-2 are estimated to be €4.9 million and €3.6 million respectively. The allocation of the constituent operating costs of the two schemes is depicted in Figure 3.8. The increased operational cost in scheme-1 compared to scheme-2 is due to the compression refrigeration machine's higher power consumption. The minimum fuel selling price (MFSP) for scheme-1 is determined to be €3.63/GGE, whereas the MFSP for scheme-2 is calculated to be €2.99/GGE.

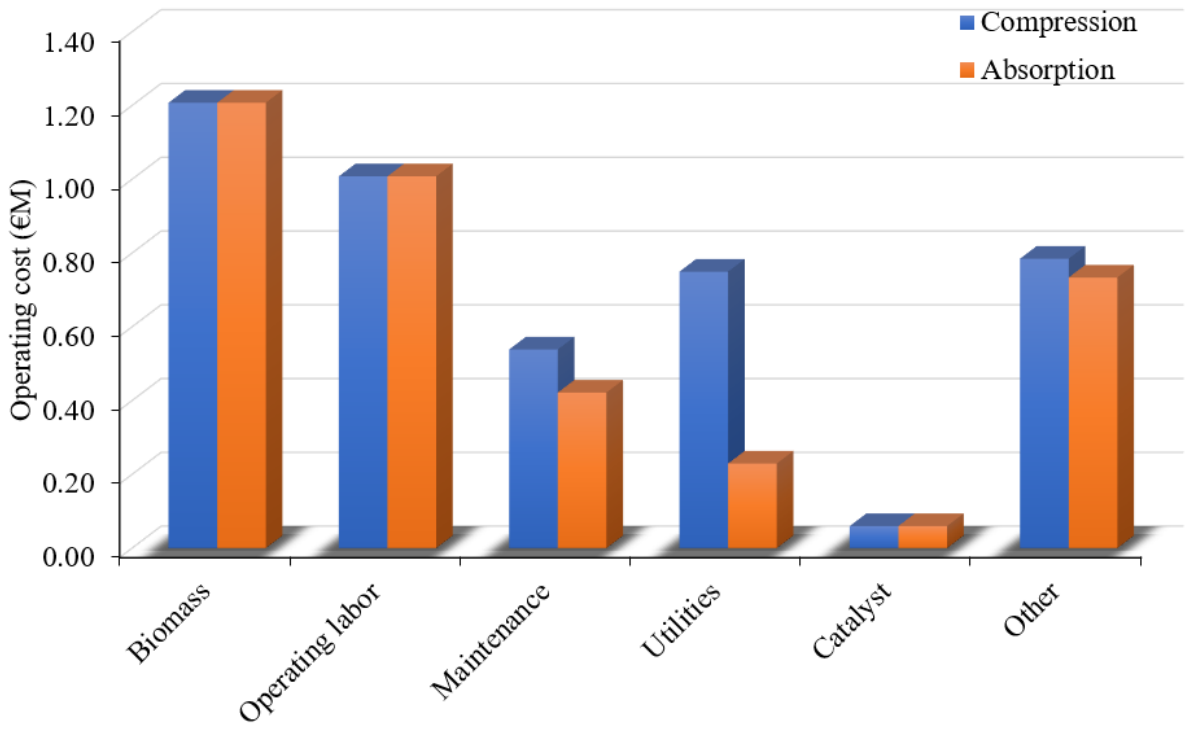

Figure 3.8. Operating cost proportions

3.5.2 Sensitivity analysis

The impact of 30% difference in parameters listed in Table 2.12 was analyzed on the MFSPs of the two process schemes. The effect of variations in these parameters on the MFSP of scheme-1 and scheme-2 can be seen in the sensitivity charts in Figs. 3.9 and 3.10. The grey bars depict how sensitive base MFSPs are sensitive to a 30% rise in the parameters, while the blue bars portray how sensitive the base MFSPs are to a 30% decrease in the parameters. In general, the longer the bars, the more sensitive the base MFSPs are to parameter changes, and vice versa. Due to the marginal disparity in their capital and operational costs, and similarly in fuel yields, the MFSPs of both process schemes display equal sensitivities to parameter variations, as seen in Figs. 3.9 and 3.10.

A 30% reduction in fuel yield resulted in a 44% increase in MFSP for scheme-1 and scheme-2 (scheme-1: €5.24; scheme-2: €4.31). In contrast, a 30% rise in fuel yield resulted in a 22% decrease in MFSP for scheme-1 and a 26% decrease in MFSP for scheme-2 (scheme-1: €2.34; scheme-2: €2.31). This means that yield losses, which can occur as a result of events like operating and servicing issues, will hurt the profitability of both process schemes.

Scaling up the plant capacity, on the other hand, would be more commercially profitable for both process schemes. Increased plant capacity is one way to increase fuel yield, but it will give rise to capital and operating costs. Both designs' MFSPs were also highly sensitive to changes in their

operating costs. A 30% rise in operating costs resulted in 21% increase in the MFSP for scheme-1 and scheme-2 (scheme-1: €4.39; scheme-2: €3.61). In contrast, a 30% reduction in operating costs resulted in MFSP reductions of 19% for scheme-1 and 26% for scheme-2 (scheme-1: €2.93; scheme-2: €2.21). Since biomass feed costs account for a large portion of the operating expense, as seen in Fig. 3.8, finding a less expensive option would be a safer economic decision. Variations in income tax had a major impact on the profitability of both method schemes.

A 20% rise in income tax resulted in a 50% increase in MFSPs (scheme-1: €5.45; scheme-2: €4.50), while a 30% decline in income tax resulted in an 33% decrease in MFSPs (scheme-1: €2.43; scheme-2: €2.01). This means that income tax reductions or deductions would be beneficial to the both operation schemes' profitability. As compared to the parameters discussed above, the MFSPs demonstrated less exposure to capital cost, with a 30% rise in capital cost triggering a 10% increase in scheme-1 and a 9% increase in scheme-2 (scheme-1: €4.01; scheme-2: €2.71), and vice versa (scheme-1: €3.29; scheme-2: €2.71). The small impact of higher capital investment on MFSPs, compared to the strong impact of higher bio-oil yield, indicates that the profitability could be scaled up by increasing plant capacity.

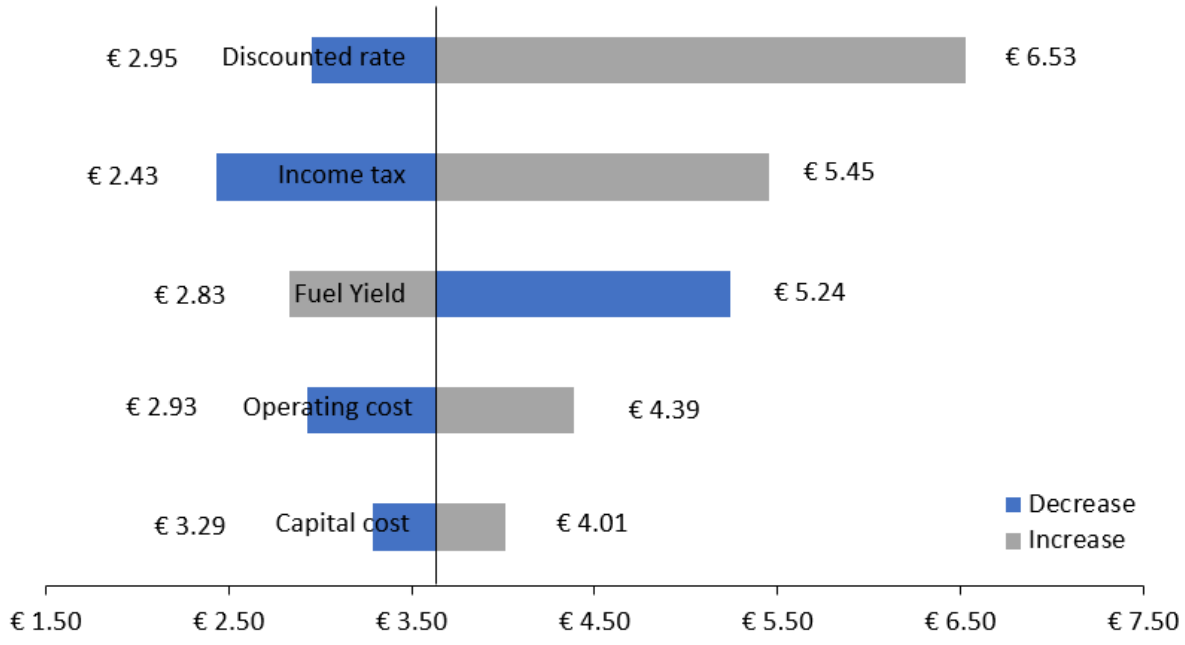

Figure 3.9. Scheme-1: Sensitivity of MFSP

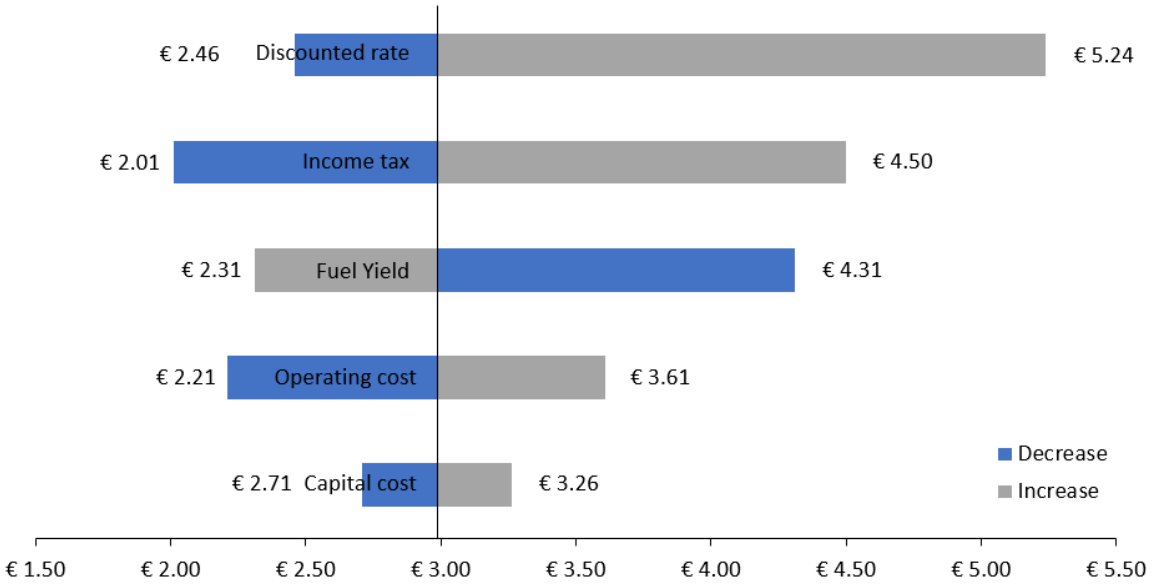

Figure 3.10. Scheme-2: Sensitivity of MFSP

3.5.3 Monte Carlo sensitivity analysis

The above sensitivity analysis considered only single point variation of a parameters on MFSP while other parameters were kept constant. To understand the variation of more than one parameter at a time, a Monte Carlo sensitivity analysis was performed using ModelRisk software [54]. In the 3.11 and 3.12, a spider chart has been created to analyze the sensitivity of the mean of the MFSP. Spider plots describe how sensitive the value of an output variable is to the input variable of the model. The horizontal axis shows the cumulative percentile of the economic parameters and the vertical axis shows the mean for the MFSP if the studied economic parameter value was around the percentile value of the horizontal axis. The horizontal line in the middle marks the mean MFSP. The precision of the percentile depends upon the number of tranches; in this case it is 10. This plot is generated using 10,000 samples so each mean MFSP is calculated from 1,000 samples. Spider plot gives more information about the nature of the relationship between economic variables and MFSP. From the charts, it can be observed that capital cost and operating cost remain close to the mean MFSP line so they are least sensitive to MFSP. On the other hand, discounted rate and income tax cover the largest vertical range indicating that they are the most crucial parameters to be observed. Fuel yield has the similar relationship with MSFP but has slightly less influence. The mean MFSP is calculated to be €4.18/GGE for scheme-1 and €3.48/GGE for scheme-2. As discounted rate and

income tax are more likely to remain constant during the life of the plant, so increasing the fuel yield can bring down the MFSP of bio-oil significantly.

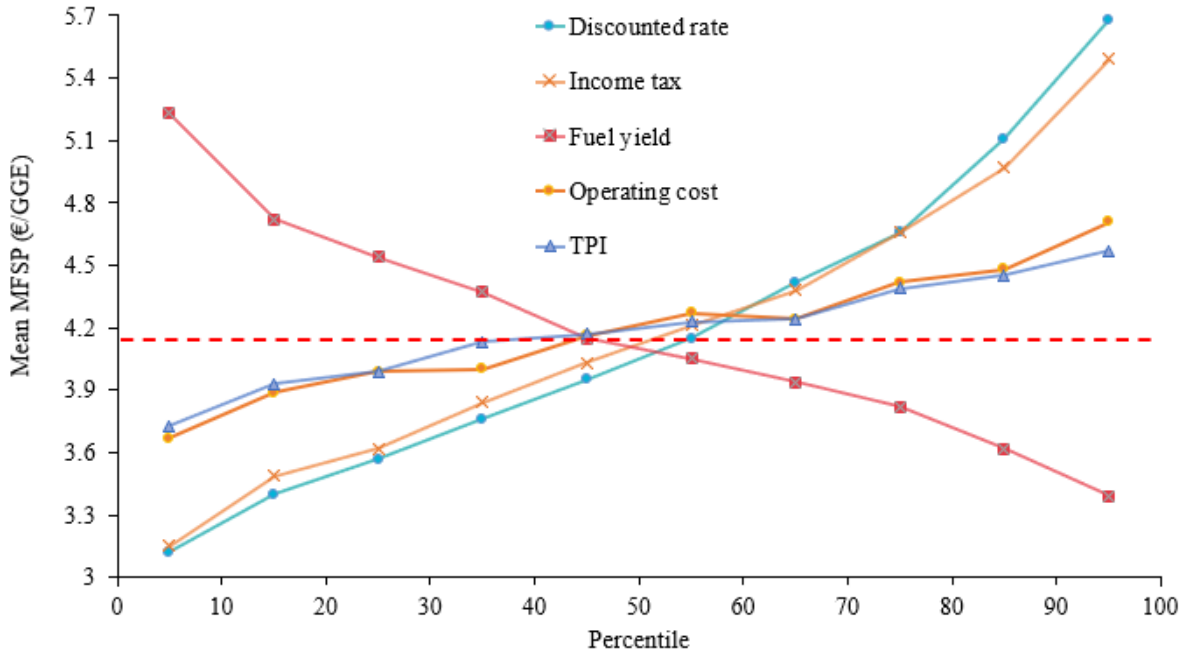

Figure 3.11. Monte Carlo sensitivity analysis for scheme-1

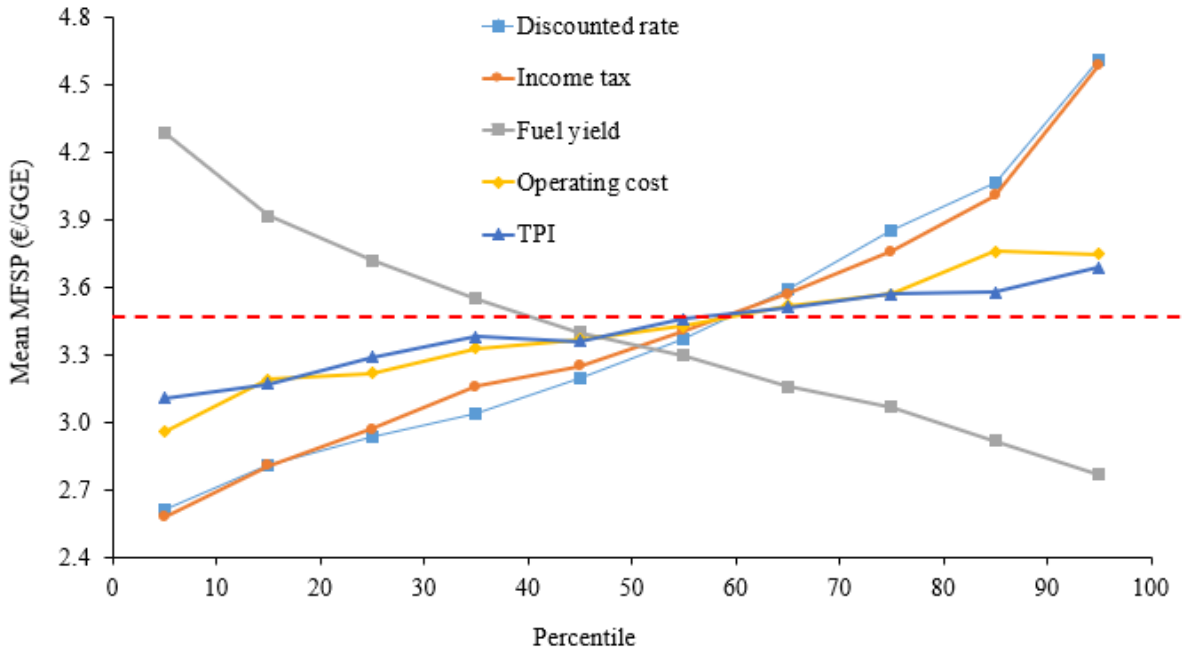

Figure 3.12. Monte Carlo sensitivity analysis for scheme-2

3.6 Life cycle assessment

The life cycle assessment of three scenarios is performed in SimaPro 9.0. The scenarios differ in the fact if the heat and electricity provided to the system are produced in the process or

provided from external sources. The baseline scenario is based on the Tunisian electricity which is produced mainly from natural gas. Another scenario is proposed depending upon the geographic location of the plant. Therefore, France and Greece are considered which are collaborative partners in this research project.

In the baseline scenario, just by replacing compression refrigeration machine by absorption refrigeration machine, NRE and GWP are reduced by 43% and 4% respectively. By introducing thermal energy recycling scenario for absorption machine, the environmental impacts are further reduced by 82% for NRE and 76% for GWP (NRE: 1.72MJ, GWP: 1.26 kg CO2 eq.). The production of electricity in scheme-2 allows to produce more electricity than what is consumed by the process, thus GWP is reduced by 94% and NRE by 116%. Figures 3.13 and 3.14 show the non-renewable energy demand and global warming potential for baseline scenario for compression refrigeration machine. The red color shows the evolution of NRE through different product stages of bio-oil production. Almost all non-renewable energy demand is because of the Tunisian electricity production and heat generation from gas. The transport sector does not have a significant effect on the investigated environmental impacts. Figures 3.13 and 3.14 represent the NRE and GWP for scenario 'recycling heat and electricity' for absorption refrigeration machine. In this case, the green color is dominant for NRE indicating negative NRE as more electricity is produced by the process than what is consumed in the process. The GWP is due to the combustion of biochar and non-condensable gases.

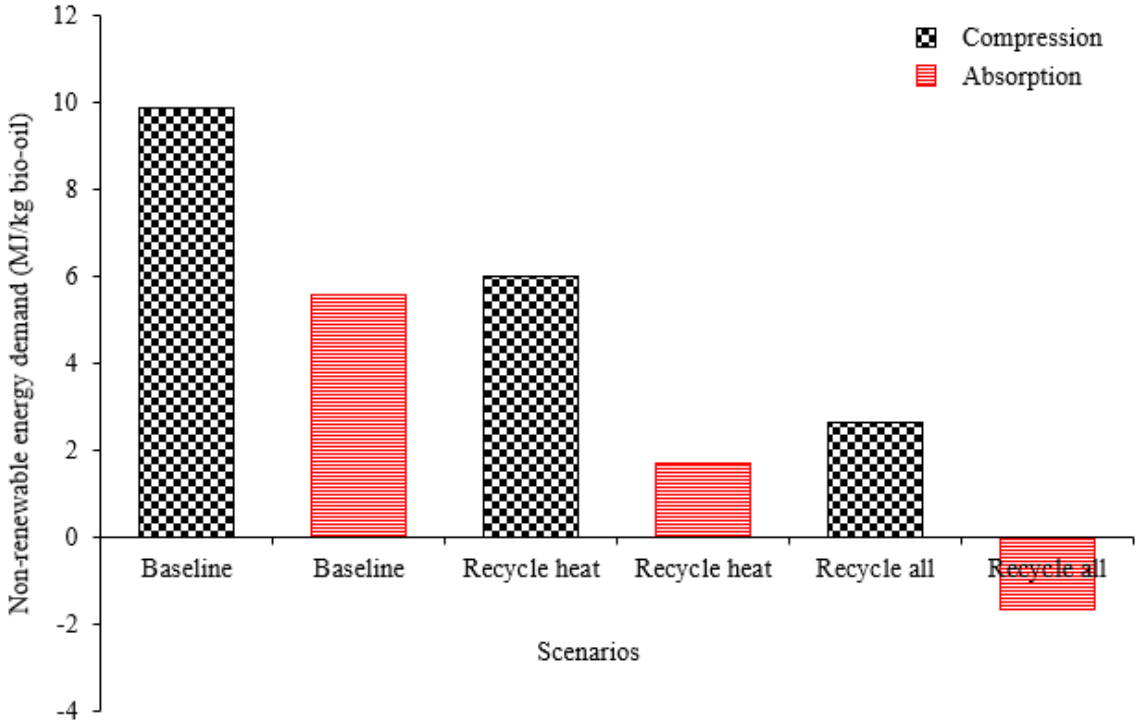

Figure 3.13. Non-renewable energy demand for three scenarios

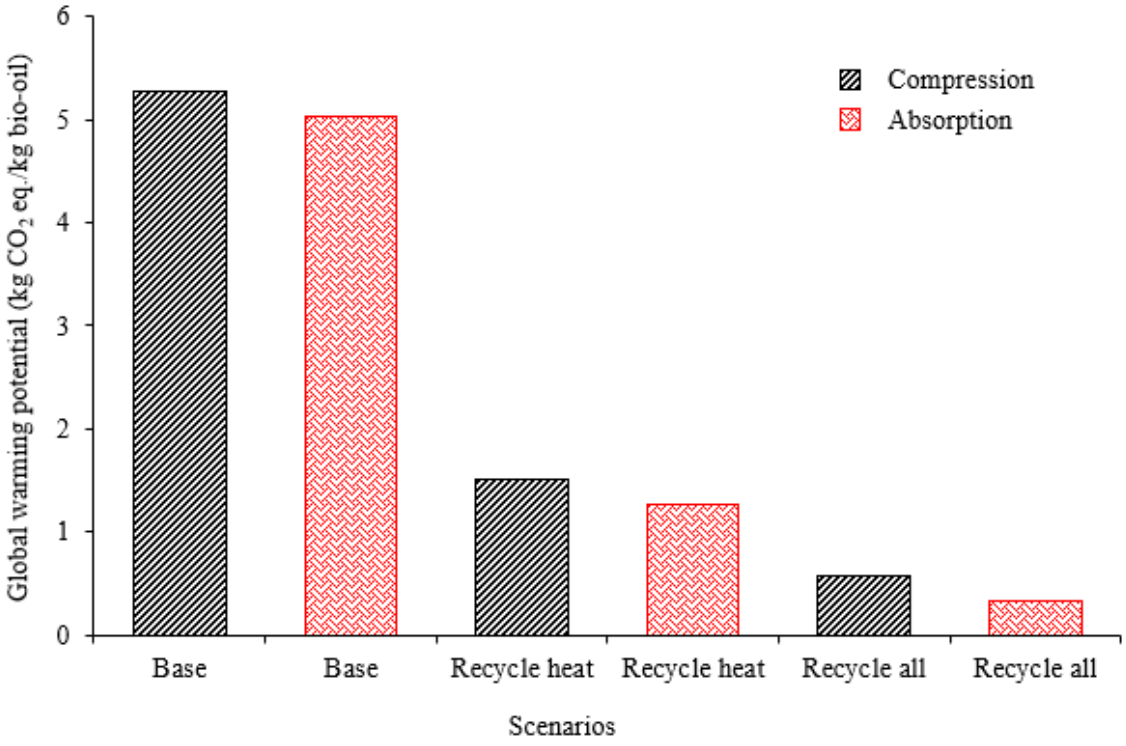

Figure 3.14. Global warming potential for three scenarios

The analysis of the geographical impact on the production of bio-oil on the basis of electricity generation sources by a country shows that the process is more interesting for France whose main source of electricity production is nuclear power. Greece has slightly higher environmental impacts than France as its major sources of electricity are fossil fuels i.e. natural gas (30%), lignite (29.3%), oil (9%) and renewable energy resources (31.7%) while for Tunisia, electricity is produced mainly from natural gas (95%). The distribution of non-renewable energy demand (NRE) and global warming potential (GWP) for different scenarios for 1 kg bio-oil production is presented in Table 3.11.

Table 3.10. Non-renewable energy demand (NRE) and global warming potential (GWP) for 1-kg bio-oil produced in different scenarios

Sr. No.	Scenario		NRE (MJ)	GWP (kg CO_2 eq)
1	Baseline (Tunisia)	Compression	9.85	5.27
		Absorption	5.55	5.03
2	Recycling heat (Tunisia)	Compression	6.01	1.5
		Absorption	1.72	1.26
3	Recycling heat and electricity (Tunisia)	Compression	2.62	0.566
		Absorption	-1.67	0.321
4	Recycling heat and electricity (France)	Compression	2.24	0.466
	Recycling heat and electricity (France)	Absorption	-1.22	0.438
5	Recycling heat and electricity (Greece)	Compression	4.7	0.724
	Recycling heat and electricity (Greece)	Absorption	-4.12	0.134

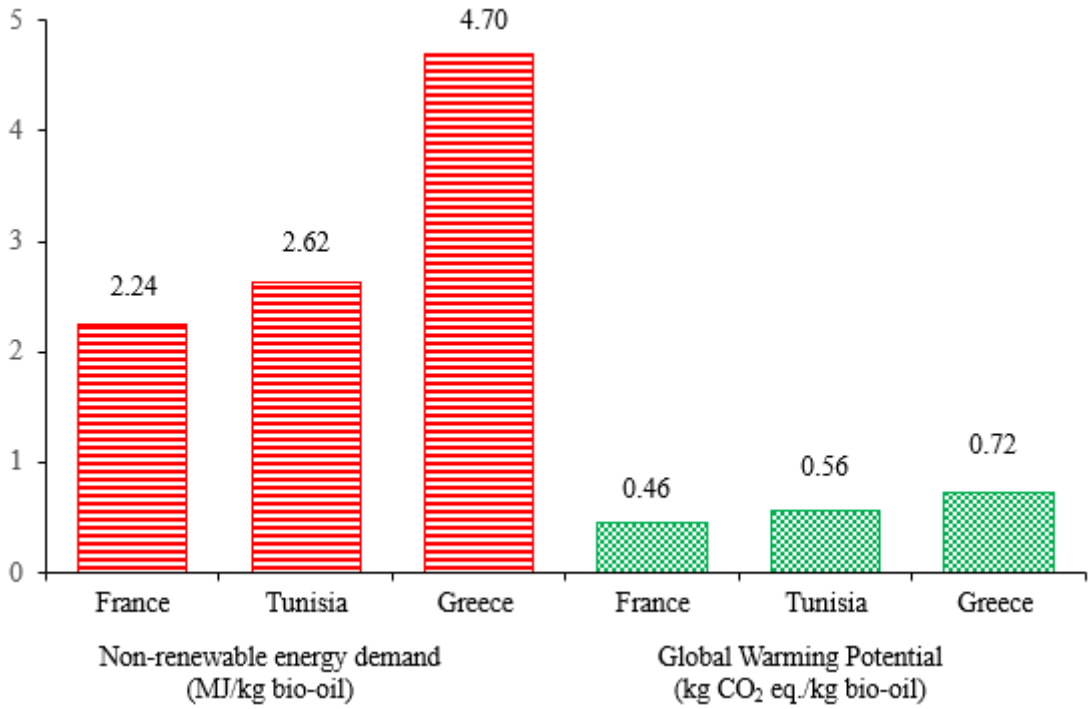

Figure 3.15. Non-renewable energy demand and global warming potential for different countries for scheme-1

A comparison of non-renewable energy demand and global warming potential has been carried out France, Tunisia and Greece for scenario recycling heat and electricity for scheme-2 also. In this case, NRE and GWP is minimum for Greece as opposite to scheme-1. We are producing more electricity in the process than it is required by the process so we export it to external sources reducing the environmental impacts. On the other hand, France has the maximum NRE and GWP for scheme-2 as exporting the electricity from process to external sources does not have much environmental impacts because it is already low in case of scheme-1.

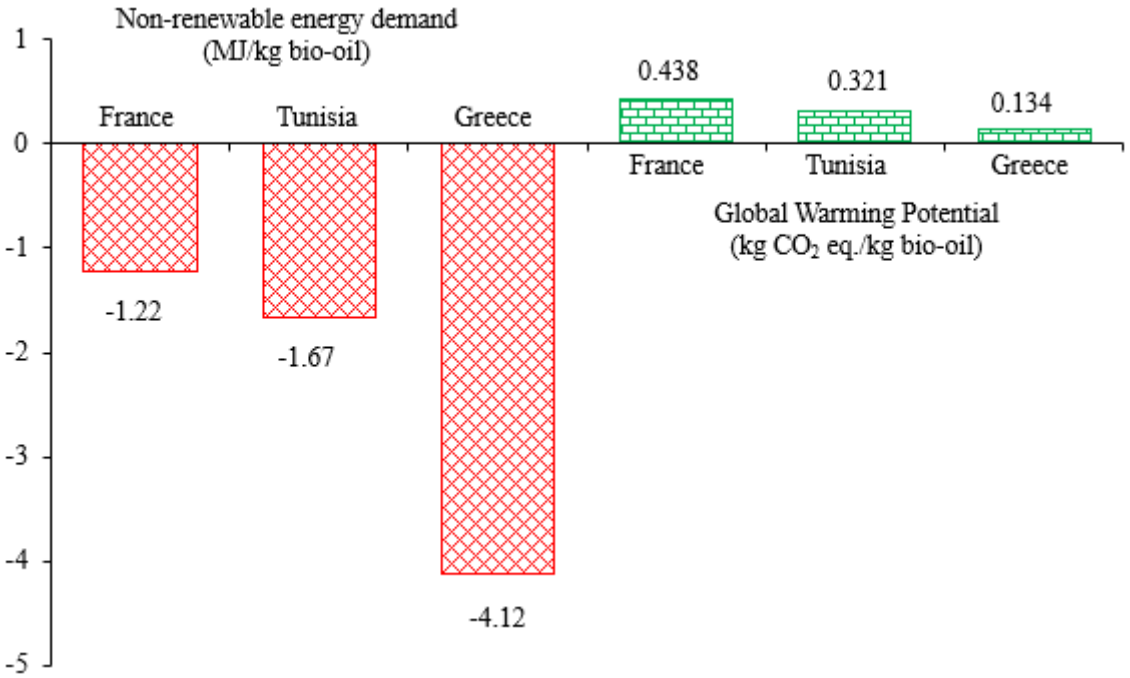

Figure 3.16. Non-renewable energy demand and global warming potential for different countries for scheme-2

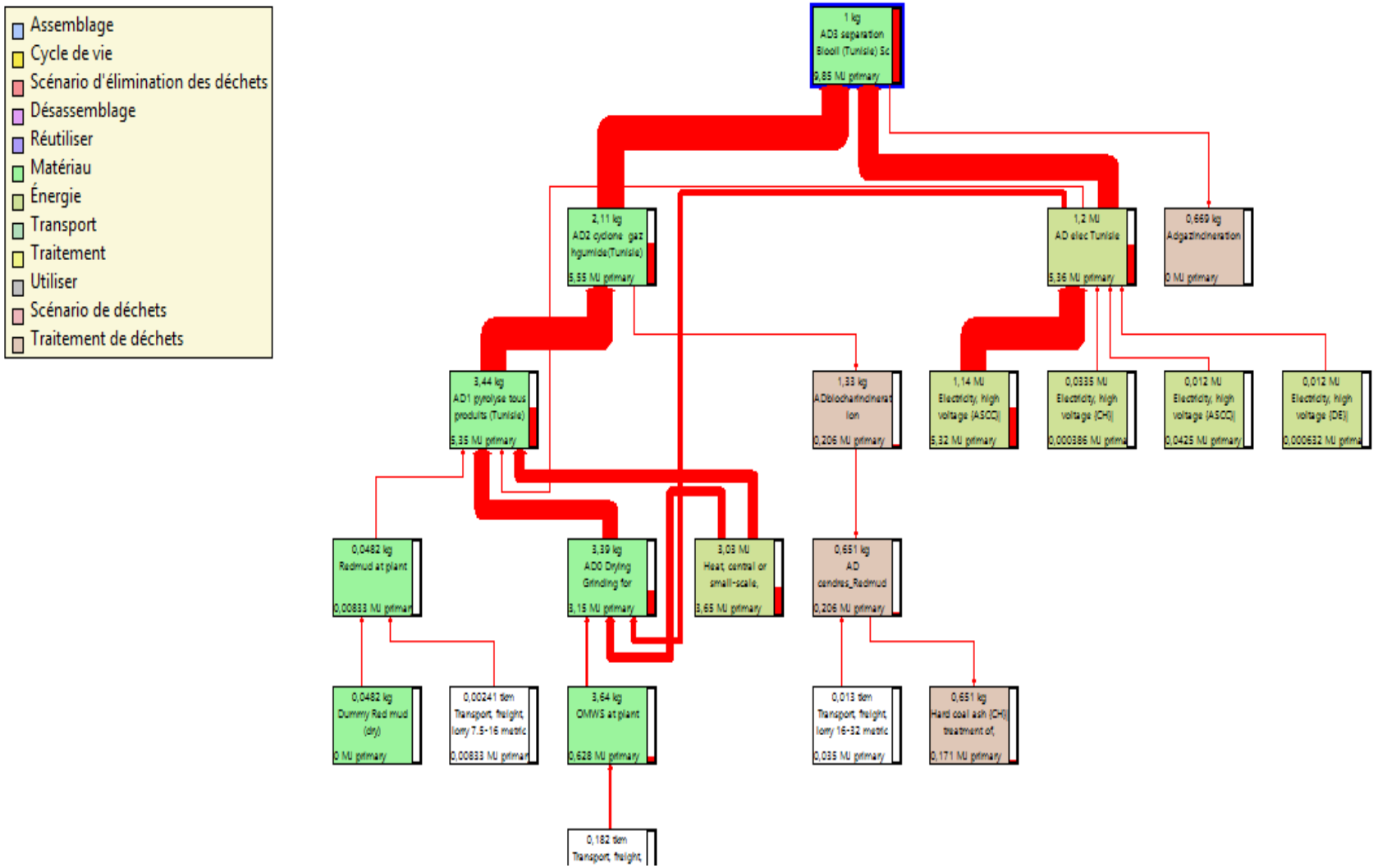

Figure 3.17. Non-renewable energy demand (NRE) for baseline scenario for compression machine

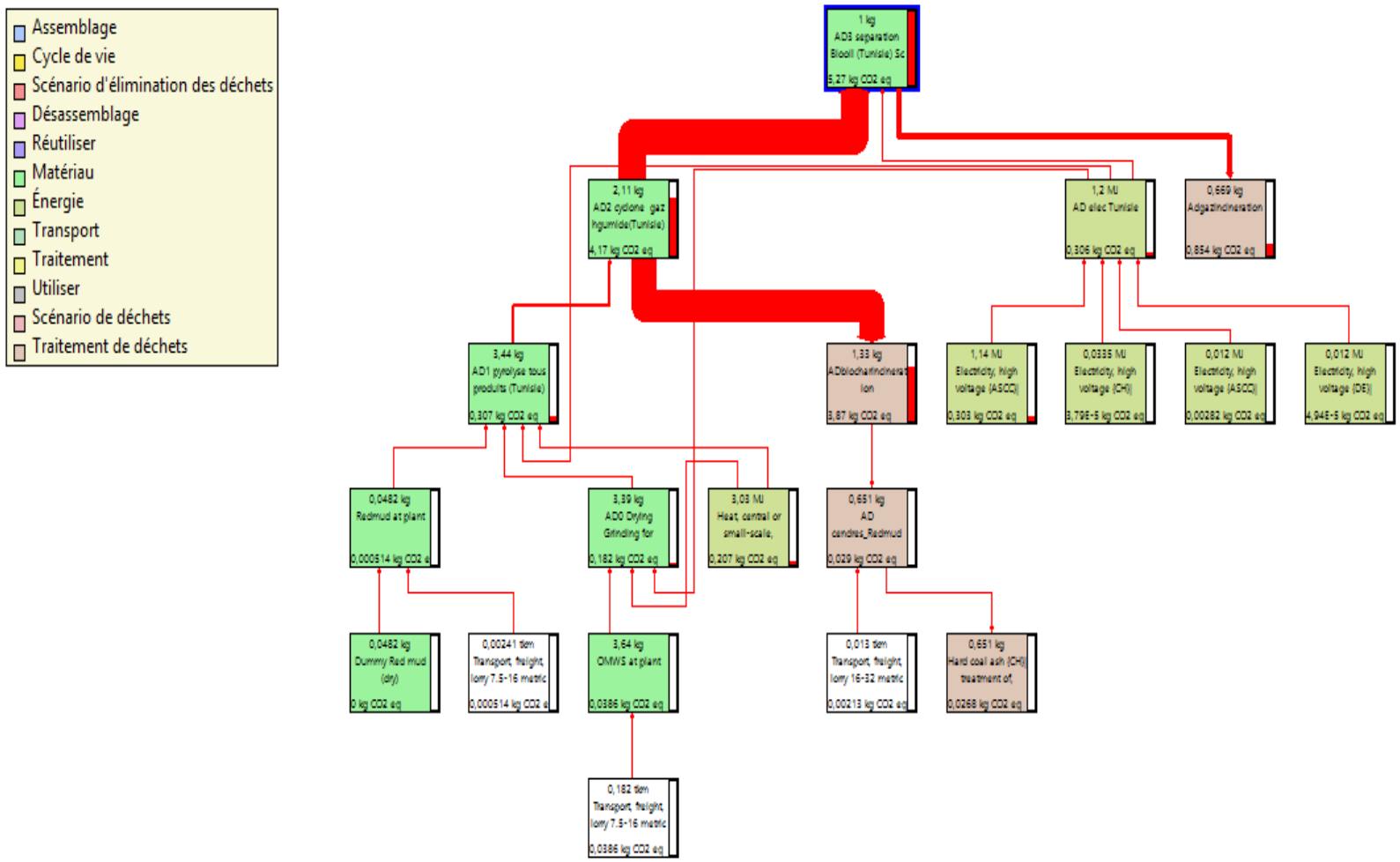

Figure 3.18. Global warming potential (GWP) for baseline scenario for compression machine

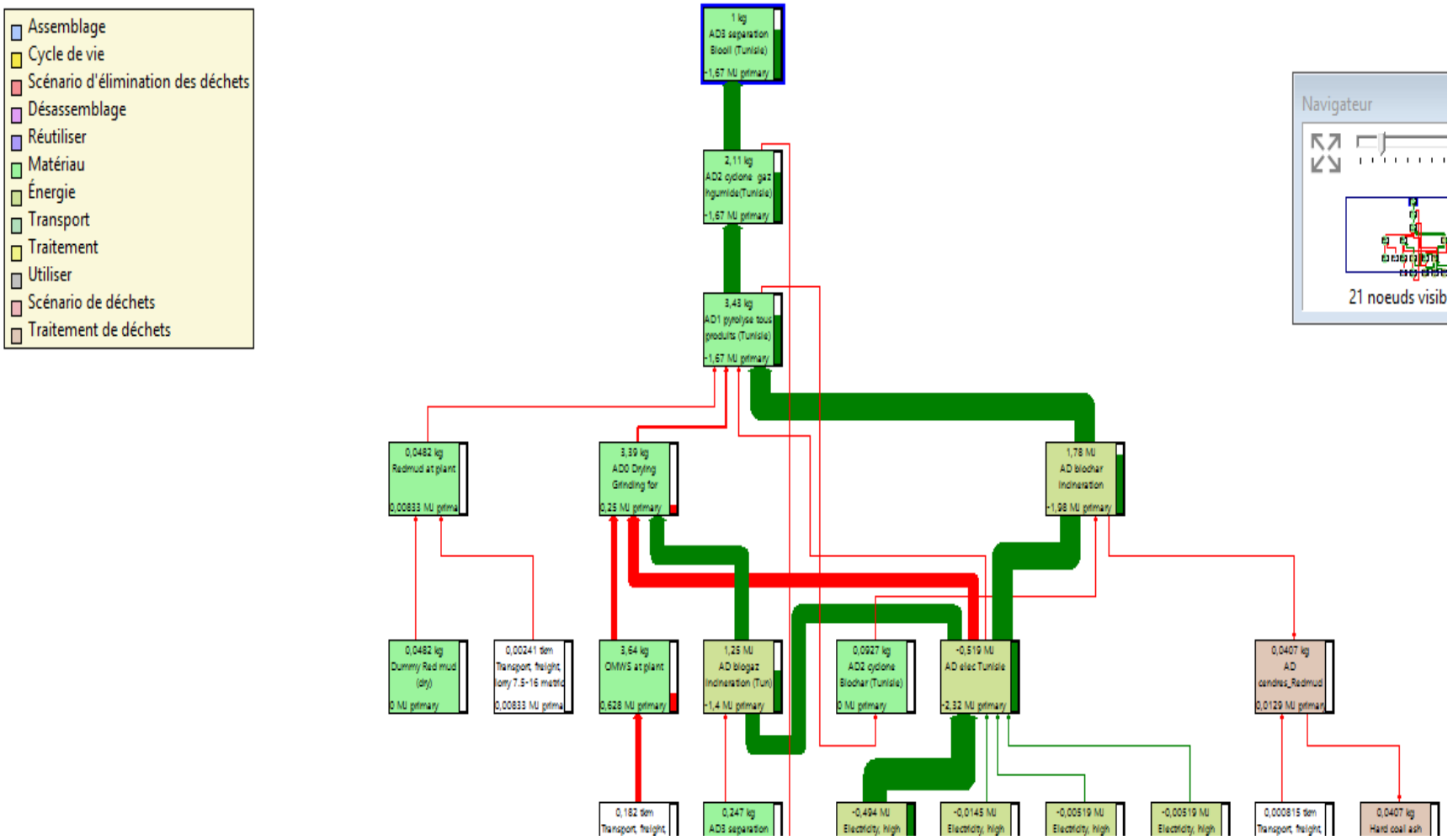

Figure 3.19. Non-renewable energy demand for ‘recycling heat and electricity’ scenario for absorption machine

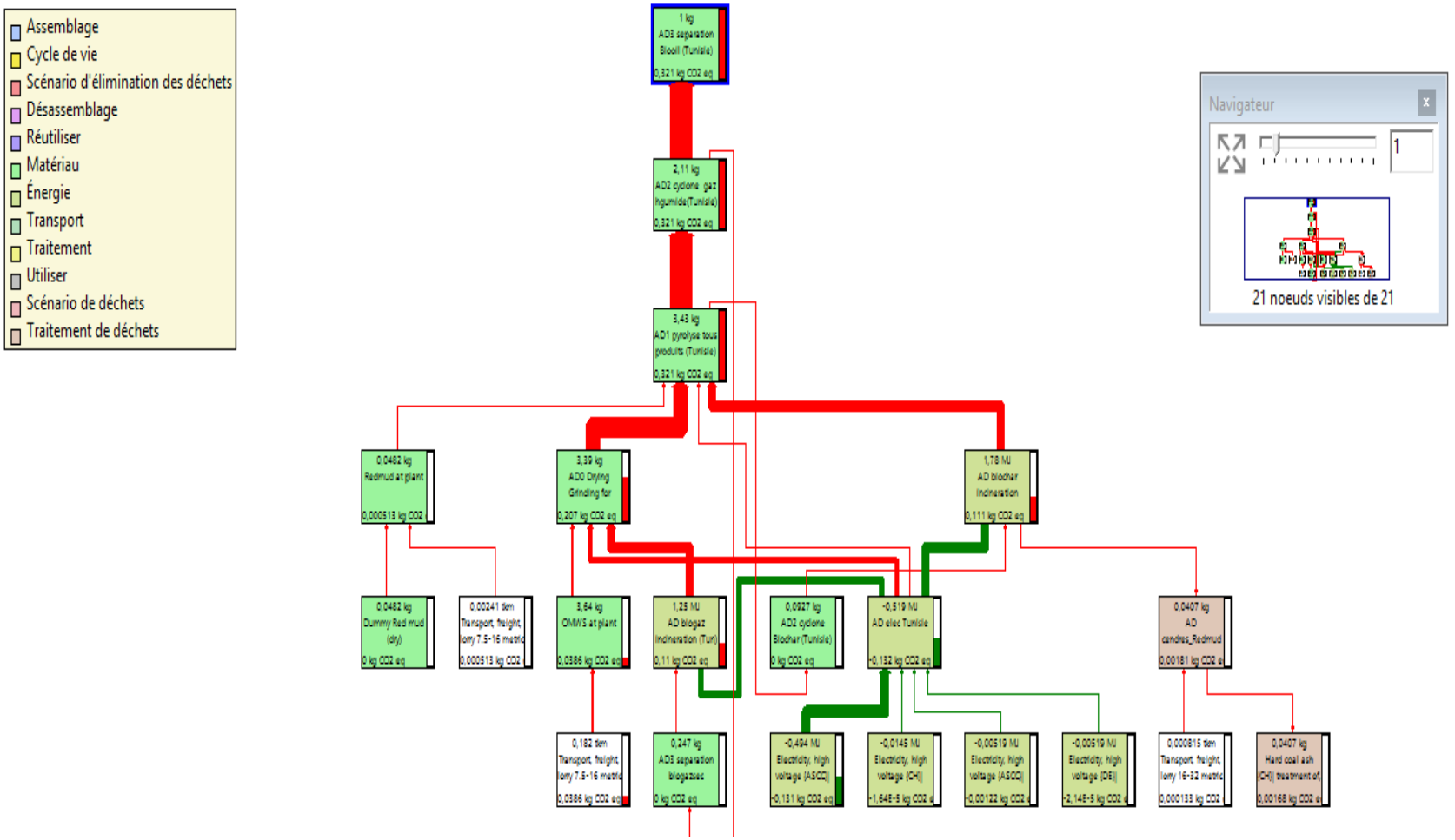

Figure 3.20. Global warming potential (GWP) for scenario ‘recycling heat and electricity’ for absorption machine

Conclusion

A steady state model of pyrolysis of OMWS is developed in Aspen Plus under standard pyrolysis conditions. A global reaction with kinetic parameters is employed in an external Fortran user-subroutine and coupled with *RCSTR* reactor. The model is validated against the experimental results of Agblevor et. al. A good agreement between simulation and experimental yields can be observed.

After validation, the model is extrapolated to industrial scale to process 100 tonnes of OMWS per day. Mass and energy balances are established for each component in the process. The plant produces 1,150 kg/hr (35.4 wt%) bio-oil, 971 kg/hr (29.9 wt%) biochar and 770 kg/hr (23.6 wt.%) NCG. The yields are based on moisture free and ash free OMWS which is 3,249 kg/hr. For scheme-1 with compression refrigeration machine, the plant requires 242 kW of electricity from external sources while for scheme-2 with absorption refrigeration machine, the plant is self-sufficient.

An exergy analysis of the plant is also conducted which indicates that maximum exergy destruction takes place in combustion of biochar and NCG (65%) followed by pyrolysis (18%). Chemical exergy destruction constitutes 54.3% of total exergy destruction while physical exergy destruction is 43.6%. The analysis shows the heat losses in the heat exchangers are major part of the exergy destruction. The exergy efficiency of the whole system for scheme-1 is 55.9% while for scheme-2 is 57%. The difference in the exergetic efficiency can be attributed to the large amount of electricity usage in the compression refrigeration machine as compared with absorption refrigeration machine.

From an economic standpoint, the production of bio-oil from fast pyrolysis of olive mill waste water sludge has been investigated. In terms of energy consumption and MFSP/GGE, two process schemes (scheme-1 and scheme-2) were examined and compared. The MFSP for scheme-1 is €3.63/GGE, based on a capital investment of €17.9 million and operational expenses of €4.6 million. Scheme-2, on the other hand, had a capital cost of €14.9 million and an operating cost of €3.6 million. Changes in bio-oil yield, operational expenses, and income tax were all equally sensitive to the MFSPs of scheme-1 and scheme-2. According to Monte Carlo sensitivity analysis, the mean MFSP is calculated to be €4.18/GGE for scheme-1 and €3.48/GGE for scheme-2. In both sensitivity analyses, increase in plant capacity capital cost does not have significant effect on MFSP so increasing the plant capacity will increase bio-oil

production, which could be more profitable and reduce the MFSP/GGE. The profitabilities can be improved considerably with reduction in income tax or exemptions.

A comparative life cycle study of 1 kg bio-oil production from OMWS fast pyrolysis is performed. Based on heat and electricity provision to the process, three scenarios have been proposed. The objective of these three scenarios is to compare the environmental impacts of heat and electricity sources on the production of 1 kg bio-oil. For external sources, heat and electricity are generated by combustion of natural gas for Tunisia. For France, the main source of electricity production is nuclear power and for Greece it is natural gas and lignite. From the results it can be observed that the NRE and GWP are maximum for baseline scenario i.e. 9.85 MJ/kg bio-oil and 5.27 kg CO_2 eq./ kg-bio-oil for compression refrigeration machine. For the same scenario, both NRE and GWP are reduced by 43% and 4% respectively for absorption machine. For Tunisia, in the case of 'recycling heat and electricity' for absorption machine, a reduction of 116% non-renewable energy demand and 94% global warming potential is observed. Among countries, France has the minimum non-renewable energy demand (2.24 MJ) and global warming potential (0.466 kg CO_2 eq.) for compression refrigeration machine.

References

[1] F. Aryi Agblevor, H. Abdellaoui, K. Halouani, S. Hakis Beis, Pyrolytic Conversion of Olive Mill Wastewater Sludge to Biofuels Using Red Mud as Catalyst, Int. J. Energy Power Eng. 6 (2017) 108. https://doi.org/10.11648/j.ijepe.20170606.14.

[2] D. Hernández, L. Astudillo, M. Gutiérrez, C. Tenreiro, C. Retamal, C. Rojas, Biodiesel production from an industrial residue: Alperujo, Ind. Crops Prod. 52 (2014) 495–498. https://doi.org/10.1016/j.indcrop.2013.10.051.

[3] R. Sekret, M. Turski, Research on an adsorption cooling system supplied by solar energy, Energy Build. 51 (2012) 15–20. https://doi.org/10.1016/j.enbuild.2012.04.008.

[4] D. Mohan, C.U. Pittman, P.H. Steele, Pyrolysis of wood/biomass for bio-oil: A critical review, Energy and Fuels. 20 (2006) 848–889. https://doi.org/10.1021/ef0502397.

[5] M.M. Hasan, X.S. Wang, D. Mourant, R. Gunawan, C. Yu, X. Hu, S. Kadarwati, M. Gholizadeh, H. Wu, B. Li, L. Zhang, C.Z. Li, Grinding pyrolysis of Mallee wood: Effects of pyrolysis conditions on the yields of bio-oil and biochar, Fuel Process. Technol. 167 (2017) 215–220. https://doi.org/10.1016/j.fuproc.2017.07.004.

[6] T. Kan, V. Strezov, T.J. Evans, Lignocellulosic biomass pyrolysis: A review of product properties and effects of pyrolysis parameters, Renew. Sustain. Energy Rev. 57 (2016) 1126–1140. https://doi.org/10.1016/j.rser.2015.12.185.

[7] A. Demirbaş, G. Arin, An overview of biomass pyrolysis, Energy Sources. 24 (2002) 471–482. https://doi.org/10.1080/00908310252889979.

[8] M. Amutio, G. Lopez, R. Aguado, J. Bilbao, M. Olazar, Biomass oxidative flash pyrolysis: Autothermal operation, yields and product properties, Energy and Fuels. 26 (2012) 1353–1362. https://doi.org/10.1021/ef201662x.

[9] M.I. Jahirul, M.G. Rasul, A.A. Chowdhury, N. Ashwath, Biofuels production through biomass pyrolysis- A technological review, Energies. 5 (2012) 4952–5001. https://doi.org/10.3390/en5124952.

[10] P. Gable, R.B.- Fuel, U. 2016, Effect of biomass heating time on bio-oil yields in a free fall fast pyrolysis reactor, Fuel. 166 (2016) 361–366. https://doi.org/10.1016/j.fuel.2015.10.073.

[11] J. Jeong, U. Lee, W. Chang, S.J.-B. Technology, U. 2016, Production of bio-oil rich in acetic acid and phenol from fast pyrolysis of palm residues using a fluidized bed reactor: Influence of activated carbons, Bioresour. Technol. 219 (2016) 357–364. https://doi.org/10.1016/j.biortech.2016.07.107.

[12] T. Kan, V. Strezov, T.E.-R. and S.E. Reviews, U. 2016, Lignocellulosic biomass pyrolysis: A review of product properties and effects of pyrolysis parameters, Renew. Sustain. Energy Rev. 57 (2016) 1126–1140. https://doi.org/10.1016/j.rser.2015.12.185.

[13] I. Torri, V. Paasikallio, C. Faccini, … R.H.-B., U. 2016, Bio-oil production of softwood and hardwood forest industry residues through fast and intermediate pyrolysis and its chromatographic characterization, Bioresour. Technol. 200 (2016) 680–690. https://doi.org/10.1016/j.biortech.2015.10.086.

[14] A. V. Bridgwater, D. Meier, D. Radlein, An overview of fast pyrolysis of biomass, Org. Geochem. 30 (1999) 1479–1493. https://doi.org/10.1016/S0146-6380(99)00120-5.

[15] M. Patel, X. Zhang, A. Kumar, Techno-economic and life cycle assessment on lignocellulosic biomass thermochemical conversion technologies: A review, Renew. Sustain. Energy Rev. 53 (2016) 1486–1499. https://doi.org/10.1016/j.rser.2015.09.070.

[16] A. V. Bridgwater, Review of fast pyrolysis of biomass and product upgrading, Biomass and Bioenergy. 38 (2012) 68–94. https://doi.org/10.1016/j.biombioe.2011.01.048.

[17] X. Deglise, A. Donnot, Bois énergie - Propriétés et voies de valorisation, Ref TIP202WEB - "Ressources Énergétiques Stock. (2017). https://www-techniques-ingenieur-fr.bases-doc.univ-lorraine.fr/base-documentaire/tiabeb-archives-ressources-energetiques-et-stockage/download/be8535/2/bois-energie.html (accessed October 20, 2021).

[18] D. Mohan, C.U. Pittman, P.H. Steele, Pyrolysis of wood/biomass for bio-oil: A critical review, Energy and Fuels. 20 (2006) 848–889. https://doi.org/10.1021/ef0502397.

[19] Phyllis2 - diesel oil (#1468), (n.d.). https://phyllis.nl/Biomass/View/1468 (accessed April 2, 2021).

[20] D. Mohan, C.U. Pittman, P.H. Steele, Pyrolysis of wood/biomass for bio-oil: A critical review, Energy and Fuels. 20 (2006) 848–889. https://doi.org/10.1021/ef0502397.

[21] J.A. Garcia-Nunez, M.R. Pelaez-Samaniego, M.E. Garcia-Perez, I. Fonts, J. Abrego, R.J.M. Westerhof, M. Garcia-Perez, Historical Developments of Pyrolysis Reactors: A Review, Energy and Fuels. 31 (2017) 5751–5775. https://doi.org/10.1021/acs.energyfuels.7b00641.

[22] A. AlNouss, G. Mckay, T. Al-Ansari, Optimum Utilization of Biomass for the Production of Power and Fuels using Gasification, in: Comput. Aided Chem. Eng., Elsevier B.V., 2018: pp. 1481–1486. https://doi.org/10.1016/B978-0-444-64235-6.50258-8.

[23] S. Elkhalifa, A. AlNouss, T. Al-Ansari, H.R. Mackey, P. Parthasarathy, G. Mckay, Simulation of Food Waste Pyrolysis for the Production of Biochar: A Qatar Case Study, in: Comput. Aided Chem. Eng., Elsevier B.V., 2019: pp. 901–906. https://doi.org/10.1016/B978-0-12-818634-3.50151-X.

[24] E. Ranzi, A. Cuoci, T. Faravelli, A. Frassoldati, G. Migliavacca, S. Pierucci, S. Sommariva, Chemical kinetics of biomass pyrolysis, Energy and Fuels. 22 (2008) 4292–4300. https://doi.org/10.1021/ef800551t.

[25] J.F. Peters, S.W. Banks, A. V. Bridgwater, J. Dufour, A kinetic reaction model for biomass pyrolysis processes in Aspen Plus, Appl. Energy. 188 (2017) 595–603. https://doi.org/10.1016/j.apenergy.2016.12.030.

[26] J.Y. Park, J.K. Kim, C.H. Oh, J.W. Park, E.E. Kwon, Production of bio-oil from fast pyrolysis of biomass using a pilot-scale circulating fluidized bed reactor and its characterization, J. Environ. Manage. 234 (2019) 138–144. https://doi.org/10.1016/j.jenvman.2018.12.104.

[27] I.Y. Mohammed, Y.A. Abakr, R. Mokaya, Integrated biomass thermochemical conversion for clean energy production: Process design and economic analysis, J. Environ. Chem. Eng. 7 (2019). https://doi.org/10.1016/j.jece.2019.103093.

[28] I.A. Vasalos, A.A. Lappas, E.P. Kopalidou, K.G. Kalogiannis, Biomass catalytic pyrolysis: process design and economic analysis, Wiley Interdiscip. Rev. Energy Environ. 5 (2016) 370–383. https://doi.org/10.1002/wene.192.

[29] M. Patel, A.O. Oyedun, A. Kumar, R. Gupta, What is the production cost of renewable diesel from woody biomass and agricultural residue based on experimentation? A comparative assessment, Fuel Process. Technol. 191 (2019) 79–92.

https://doi.org/10.1016/j.fuproc.2019.03.026.

[30] K. Onarheim, Y. Solantausta, J. Lehto, Process simulation development of fast pyrolysis of wood using aspen plus, Energy and Fuels. 29 (2015) 205–217. https://doi.org/10.1021/ef502023y.

[31] J.F. Peters, D. Iribarren, J. Dufour, Predictive pyrolysis process modelling in Aspen Plus ®, in: Researchgate.Net, Copenhagen, 2014. https://doi.org/10.5071/21stEUBCE2013-2CV.4.8.

[32] M.B. Shemfe, S. Gu, P. Ranganathan, Techno-economic performance analysis of biofuel production and miniature electric power generation from biomass fast pyrolysis and bio-oil upgrading, Fuel. 143 (2015) 361–372. https://doi.org/10.1016/j.fuel.2014.11.078.

[33] H. Zhang, R. Xiao, H. Huang, G. Xiao, Comparison of non-catalytic and catalytic fast pyrolysis of corncob in a fluidized bed reactor, Bioresour. Technol. 100 (2009) 1428–1434. https://doi.org/10.1016/j.biortech.2008.08.031.

[34] T.R. Carlson, Y.T. Cheng, J. Jae, G.W. Huber, Production of green aromatics and olefins by catalytic fast pyrolysis of wood sawdust, Energy Environ. Sci. 4 (2011) 145–161. https://doi.org/10.1039/c0ee00341g.

[35] A. Dutta, A. Sahir, E. Tan, D. Humbird, L.J. Snowden-Swan, P. Meyer, J. Ross, D. Sexton, R. Yap, J.L. Lukas, Process Design and Economics for the Conversion of Lignocellulosic Biomass to Hydrocarbon Fuels. Thermochemical Research Pathways with In Situ and Ex Situ Upgrading of Fast Pyrolysis Vapors, Golden, CO (United States), 2015. https://doi.org/10.2172/1215007.

[36] M. Corbetta, S. Pierucci, E. Ranzi, H. Bennadji, E.M. Fisher, Multistep Kinetic Model of Biomass Pyrolysis, XXXVI Meeting of the Italian Section of the Combustion Institute Procida, Italy, 2013.

[37] M. Calonaci, R. Grana, E. Barker Hemings, G. Bozzano, M. Dente, E. Ranzi, Comprehensive kinetic modeling study of bio-oil formation from fast pyrolysis of biomass, Energy and Fuels. 24 (2010) 5727–5734. https://doi.org/10.1021/ef1008902.

[38] A.A. Boateng, C.A. Mullen, L. Osgood-Jacobs, P. Carlson, N. Macken, Mass Balance, Energy, and Exergy Analysis of Bio-Oil Production by Fast Pyrolysis, J. Energy

Resour. Technol. 134 (2012). https://doi.org/10.1115/1.4007659.

[39] K.J. Ptasinski, Thermodynamic efficiency of biomass gasification and biofuels conversion, Biofuels, Bioprod. Biorefining. 2 (2008) 239–253. https://doi.org/10.1002/bbb.65.

[40] M.A. Rosen, I. Dincer, M. Kanoglu, Role of exergy in increasing efficiency and sustainability and reducing environmental impact, Energy Policy. 36 (2008) 128–137. https://doi.org/10.1016/j.enpol.2007.09.006.

[41] D. Iribarren, F. Petrakopoulou, J. Dufour, Environmental and thermodynamic evaluation of CO2 capture, transport and storage with and without enhanced resource recovery, Energy. 50 (2013) 477–485. https://doi.org/10.1016/j.energy.2012.12.021.

[42] F. Petrakopoulou, G. Tsatsaronis, Production of hydrogen-rich fuels for pre-combustion carbon capture in power plants: A thermodynamic assessment, Int. J. Hydrogen Energy. 37 (2012) 7554–7564. https://doi.org/10.1016/j.ijhydene.2012.01.147.

[43] H.I. Velásquez-Arredondo, S. De Oliveira Junior, P. Benjumea, Exergy efficiency analysis of chemical and biochemical stages involved in liquid biofuels production processes, Energy. 41 (2012) 138–145. https://doi.org/10.1016/j.energy.2011.06.025.

[44] R. Palacios-Bereche, K.J. Mosqueira-Salazar, M. Modesto, A. V. Ensinas, S.A. Nebra, L.M. Serra, M.A. Lozano, Exergetic analysis of the integrated first- and second-generation ethanol production from sugarcane, Energy. 62 (2013) 46–61. https://doi.org/10.1016/j.energy.2013.05.010.

[45] H.T. Tan, K.T. Lee, A.R. Mohamed, Second-generation bio-ethanol (SGB) from Malaysian palm empty fruit bunch: Energy and exergy analyses, Bioresour. Technol. 101 (2010) 5719–5727. https://doi.org/10.1016/j.biortech.2010.02.023.

[46] R. Saidur, G. Boroumandjazi, S. Mekhilef, H.A. Mohammed, A review on exergy analysis of biomass based fuels, Renew. Sustain. Energy Rev. 16 (2012) 1217–1222. https://doi.org/10.1016/j.rser.2011.07.076.

[47] S. Spyrakis, K.D. Panopoulos, E. Kakaras, Synthesis, Modeling and Exergy Analysis of Atmospheric Air Blown Biomass Gasification for Fischer-Tropsch Process*, Int. J. Thermodyn. 12 (2009) 187–192. www.icatweb.org/journal.htm (accessed March 12,

2021).

[48] K.J. Ptasinski, Thermodynamic efficiency of biomass gasification and biofuels conversion, Biofuels, Bioprod. Biorefining. 2 (2008) 239–253. https://doi.org/10.1002/bbb.65.

[49] M.J. Prins, K.J. Ptasinski, F.J.J.G. Janssen, Exergetic optimisation of a production process of Fischer-Tropsch fuels from biomass, Fuel Process. Technol. 86 (2005) 375–389. https://doi.org/10.1016/j.fuproc.2004.05.008.

[50] J.F. Peters, F. Petrakopoulou, J. Dufour, Exergetic analysis of a fast pyrolysis process for bio-oil production, Fuel Process. Technol. 119 (2014) 245–255. https://doi.org/10.1016/j.fuproc.2013.11.007.

[51] J. Szargut, D. Morris, F. Steward, Exergy analysis of thermal, chemical, and metallurgical processes, Hemisphere Publishing Corporation, 1988.

[52] M.A. Rubio Rodríguez, J. De Ruyck, P.R. Díaz, V.K. Verma, S. Bram, An LCA based indicator for evaluation of alternative energy routes, Appl. Energy. 88 (2011) 630–635. https://doi.org/10.1016/j.apenergy.2010.08.013.

[53] M.B.B. Michael J. Moran, Howard N. Shapiro, Daisie D. Boettner, Fundamentals of Engineering Thermodynamics, 9th Edition | Wiley, Wiley. John Wiley and Sons, Inc., NewYork, 2018.

[54] G. Song, L. Shen, J. Xiao, Estimating specific chemical exergy of biomass from basic analysis data, Ind. Eng. Chem. Res. 50 (2011) 9758–9766. https://doi.org/10.1021/ie200534n.

[55] J. Szargut, T. Styrylska, Approximate evaluation of the exergy of fuels, Brennst. Waerme Kraft. 16 (1964) 589–596.

[56] I. Barin, Thermochemical Data of Pure Substances, 3rd ed., Wiley, New York, 1995. https://doi.org/10.1002/9783527619825.

[57] M.N. Islam, F.N. Ani, Techno-economics of rice husk pyrolysis, conversion with catalytic treatment to produce liquid fuel, Bioresour. Technol. 73 (2000) 67–75. https://doi.org/10.1016/S0960-8524(99)00085-1.

[58] M. Shemfe, S. Gu, B. Fidalgo, Techno-economic analysis of biofuel production via

bio-oil zeolite upgrading: An evaluation of two catalyst regeneration systems, Biomass and Bioenergy. 98 (2017) 182–193. https://doi.org/10.1016/j.biombioe.2017.01.020.

[59] M.M. Wright, D.E. Daugaard, J.A. Satrio, R.C. Brown, Techno-economic analysis of biomass fast pyrolysis to transportation fuels, Fuel. 89 (2010) S2–S10. https://doi.org/10.1016/j.fuel.2010.07.029.

[60] A. Dutta, J.A. Schaidle, D. Humbird, F.G. Baddour, A. Sahir, Conceptual Process Design and Techno-Economic Assessment of Ex Situ Catalytic Fast Pyrolysis of Biomass: A Fixed Bed Reactor Implementation Scenario for Future Feasibility, Top. Catal. 59 (2016) 2–18. https://doi.org/10.1007/s11244-015-0500-z.

[61] S. Wijeyekoon, K. Torr, H. Corkran, P. Bennett, Commercial status of direct thermochemical liquefaction technologies, 2020.

[62] R.E.W. Max S. Peters, Klaus D. Timmerhaus, Plant design and economics for chemical engineers, 5th ed., McGraw-Hill, 2003.

[63] S. Mani, L.G. Tabil, S. Sokhansanj, Grinding performance and physical properties of wheat and barley straws, corn stover and switchgrass, Biomass and Bioenergy. 27 (2004) 339–352. https://doi.org/10.1016/j.biombioe.2004.03.007.

[64] A. Dutta, A.H. Sahir, E. Tan, D. Humbird, L.J. Snowden-Swan, P.A. Meyer, J. Ross, D. Sexton, R. Yap, J. Lukas, Process Design and Economics for the Conversion of Lignocellulosic Biomass to Hydrocarbon Fuels: Thermochemical Research Pathways with In Situ and Ex Situ Upgrading of Fast Pyrolysis Vapors, Richland, WA (United States), 2015. https://doi.org/10.2172/1238302.

[65] C. Chang, X. Chen, Y. Wang, X. Feng, An efficient optimization algorithm for waste Heat Integration using a heat recovery loop between two plants, Appl. Therm. Eng. 105 (2016) 799–806. https://doi.org/10.1016/j.applthermaleng.2016.04.079.

[66] A.K. Kralj, P. Glavič, M. Krajnc, Waste heat integration between processes, Appl. Therm. Eng. 22 (2002) 1259–1269. https://doi.org/10.1016/S1359-4311(02)00047-9.

[67] A. Anastasovski, P. Rasković, Z. Guzović, A review of heat integration approaches for organic rankine cycle with waste heat in production processes, Energy Convers. Manag. 221 (2020) 113175. https://doi.org/10.1016/j.enconman.2020.113175.

[68] C. Song, Y. Qiu, Q. Liu, N. Ji, Y. Zhao, Y. Kitamura, X. Hou, Process intensification

of cellulosic ethanol production by waste heat integration, Chem. Eng. Res. Des. 132 (2018) 115–122. https://doi.org/10.1016/j.cherd.2018.01.016.

[69] G.A. Florides, S.A. Kalogirou, S.A. Tassou, L.C. Wrobel, Modelling and simulation of an absorption solar cooling system for Cyprus, Sol. Energy. 72 (2002) 43–51. https://doi.org/10.1016/S0038-092X(01)00081-0.

[70] C.D. Moné, D.S. Chau, P.E. Phelan, Economic feasibility of combined heat and power and absorption refrigeration with commercially available gas turbines, Energy Convers. Manag. 42 (2001) 1559–1573. https://doi.org/10.1016/S0196-8904(00)00157-6.

[71] R.M. Lazzarin, A. Gasparella, G.A. Longo, Ammonia-water absorption machines for refrigeration: Theoretical and real performances, Int. J. Refrig. 19 (1996) 239–246. https://doi.org/10.1016/0140-7007(96)00016-3.

[72] G. Grossman, A. Zaltash, ABSIM - Modular simulation of advanced absorption systems, Int. J. Refrig. 24 (2001) 531–543. https://doi.org/10.1016/S0140-7007(00)00051-7.

[73] M.H. Beitelmal, C.D. Patel, Model-Based Approach for Optimizing a Data Center Centralized Cooling System, 2006.

[74] Engineering Equation Solver, F-chart software, (n.d.).

[75] H. Yin, C. Volker Hartkopf, D. Archer, D. Claridge, An Absorption Chiller in a Micro BCHP Application: Model based Design and Performance Analysis, 2006.

[76] X. Liao, P. Garland, R. Radermacher, The modeling of air-cooled absorption chiller integration in CHP system, in: Am. Soc. Mech. Eng. Adv. Energy Syst. Div. AES, American Society of Mechanical Engineers (ASME), 2004: pp. 371–378. https://doi.org/10.1115/IMECE2004-60308.

[77] C. Somers, A. Mortazavi, Y. Hwang, R. Radermacher, P. Rodgers, S. Al-Hashimi, Modeling water/lithium bromide absorption chillers in ASPEN Plus, Appl. Energy. 88 (2011) 4197–4205. https://doi.org/10.1016/j.apenergy.2011.05.018.

[78] R. Reid, J. Prausnitz, B. Poling, The Properties of Gases & Liquids, 4th Edition (R. C. Reid, J. M. Prausnitz & B. E. Poling), 4th ed., McGraw-Hill, 1988.

[79] L. Haar, J.S. Gallagher, G.S. Kell, NBS/NRC steam tables thermodynamic and

transport properties and computer programs for vapor and liquid states of water in SI units, Hemisphere Publishing Corporation,New York, NY, 1984.

[80] R. Mansouri, I. Boukholda, M. Bourouis, A. Bellagi, Modelling and testing the performance of a commercial ammonia/water absorption chiller using Aspen-Plus platform, Energy. 93 (2015) 2374–2383. https://doi.org/10.1016/j.energy.2015.10.081.

[81] N.A. Darwish, S.H. Al-Hashimi, A.S. Al-Mansoori, Performance analysis and evaluation of a commercial absorption-refrigeration water-ammonia (ARWA) system, Int. J. Refrig. 31 (2008) 1214–1223. https://doi.org/10.1016/j.ijrefrig.2008.02.005.

[82] G. Bailey, P.J. Joyce, D. Schrijvers, R. Schulze, A.M. Sylvestre, B. Sprecher, E. Vahidi, W. Dewulf, K. Van Acker, Review and new life cycle assessment for rare earth production from bastnäsite, ion adsorption clays and lateritic monazite, Resour. Conserv. Recycl. 155 (2020) 104675. https://doi.org/10.1016/J.RESCONREC.2019.104675.

[83] J. Pérez, J. Lumbreras, E. Rodríguez, Life cycle assessment as a decision-making tool for the design of urban solid waste pre-collection and collection/transport systems, Resour. Conserv. Recycl. 161 (2020) 104988. https://doi.org/10.1016/J.RESCONREC.2020.104988.

[84] H. Jin, K. Frost, I. Sousa, H. Ghaderi, A. Bevan, M. Zakotnik, C. Handwerker, Life cycle assessment of emerging technologies on value recovery from hard disk drives, Resour. Conserv. Recycl. 157 (2020) 104781. https://doi.org/10.1016/J.RESCONREC.2020.104781.

[85] Y. Wang, Y. Du, J. Wang, J. Zhao, S. Deng, H. Yin, Comparative life cycle assessment of geothermal power generation systems in China, Resour. Conserv. Recycl. 155 (2020) 104670. https://doi.org/10.1016/J.RESCONREC.2019.104670.

[86] S. Temizel-Sekeryan, A.L. Hicks, Global environmental impacts of silver nanoparticle production methods supported by life cycle assessment, Resour. Conserv. Recycl. 156 (2020) 104676. https://doi.org/10.1016/J.RESCONREC.2019.104676.

[87] D. Maga, M. Hiebel, N. Thonemann, Life cycle assessment of recycling options for polylactic acid, Resour. Conserv. Recycl. 149 (2019) 86–96. https://doi.org/10.1016/J.RESCONREC.2019.05.018.

[88] H. Baumann, A.-M. Tillman, The Hitch Hiker's Guide to LCA- An orientation in LCA methodology and application, Studentlitteratur, Lund 2004, 2004.

[89] G. Finnveden, M.Z. Hauschild, T. Ekvall, J. Guinée, R. Heijungs, S. Hellweg, A. Koehler, D. Pennington, S. Suh, Recent developments in Life Cycle Assessment, J. Environ. Manage. 91 (2009) 1–21. https://doi.org/10.1016/J.JENVMAN.2009.06.018.

[90] United NationsFramework Convention on Climate Change.... - Google Scholar, (n.d.). https://scholar.google.com/scholar?q=United NationsFramework Convention on Climate Change. Adoption of the Paris Agreement. 21st Conf. Parties, Paris: United Nations; 2015. (accessed October 29, 2021).

[91] M. Tabatabaei, M. Aghbashlo, M. Dehhaghi, H.K.S. Panahi, A. Mollahosseini, M. Hosseini, M.M. Soufiyan, Reactor technologies for biodiesel production and processing: A review, Prog. Energy Combust. Sci. 74 (2019) 239–303. https://doi.org/10.1016/J.PECS.2019.06.001.

[92] R. Luque, L. Herrero-Davila, J.M. Campelo, J.H. Clark, J.M. Hidalgo, D. Luna, J.M. Marinas, A.A. Romero, Biofuels: a technological perspective, Energy Environ. Sci. 1 (2008) 542–564. https://doi.org/10.1039/B807094F.

[93] B.D. Solomon, Biofuels and sustainability, Ann. N. Y. Acad. Sci. 1185 (2010) 119–134. https://doi.org/10.1111/J.1749-6632.2009.05279.X.

[94] M.D.-A. energy, undefined 2009, Biorefineries for biofuel upgrading: a critical review, Elsevier. (n.d.). https://www.sciencedirect.com/science/article/pii/S0306261909001676?casa_token=o4tFpsNnhjcAAAAA:4JynTlPA7h29IIRKUVIbCg9kjHrpM5Kj_goXinmxL-87QBwaYhqsLSSl81PkncgfBf8medRB6g (accessed November 2, 2021).

[95] J. Dong, Y. Tang, A. Nzihou, Y. Chi, E. Weiss-Hortala, M. Ni, Life cycle assessment of pyrolysis, gasification and incineration waste-to-energy technologies: Theoretical analysis and case study of commercial plants, Sci. Total Environ. 626 (2018) 744–753. https://doi.org/10.1016/J.SCITOTENV.2018.01.151.

[96] B.H. Gebreslassie, M. Slivinsky, B. Wang, F. You, Life cycle optimization for sustainable design and operations of hydrocarbon biorefinery via fast pyrolysis, hydrotreating and hydrocracking, Comput. Chem. Eng. 50 (2013) 71–91. https://doi.org/10.1016/J.COMPCHEMENG.2012.10.013.

[97] Q. Dang, C. Yu, Z. Luo, Environmental life cycle assessment of bio-fuel production via fast pyrolysis of corn stover and hydroprocessing, Fuel. 131 (2014) 36–42. https://doi.org/10.1016/J.FUEL.2014.04.029.

[98] P. Steele, M.E. Puettmann, V.K. Penmetsa, J.E. Cooper, Life-Cycle Assessment of Pyrolysis Bio-Oil Production, For. Prod. J. 62 (2012) 326–334. https://doi.org/10.13073/FPJ-D-12-00016.1.

[99] J.F. Peters, D. Iribarren, J. Dufour, Simulation and life cycle assessment of biofuel production via fast pyrolysis and hydroupgrading, Fuel. 139 (2015) 441–456. https://doi.org/10.1016/J.FUEL.2014.09.014.

[100] J. Fan, T.N. Kalnes, M. Alward, J. Klinger, A. Sadehvandi, D.R. Shonnard, Life cycle assessment of electricity generation using fast pyrolysis bio-oil, Renew. Energy. 36 (2011) 632–641. https://doi.org/10.1016/J.RENENE.2010.06.045.

[101] F. Cherubini, A.H. Strømman, Life cycle assessment of bioenergy systems: State of the art and future challenges, Bioresour. Technol. 102 (2011) 437–451. https://doi.org/10.1016/J.BIORTECH.2010.08.010.

[102] O. Jolliet, M. Saadé-Sbeih, P. Crettaz, N. Jolliet-Gavin, S. Shaked, G. Soucy, G. Houillon, Analyse du cycle de vie : comprendre et réaliser un écobilan, 2017.

[103] T. Ekvall, G. Finnveden, Allocation in ISO 14041—a critical review, J. Clean. Prod. 9 (2001) 197–208. https://doi.org/10.1016/S0959-6526(00)00052-4.

[104] K.A. de, O.L. van, W.A. Sleeswijk, U.H. de Haes, B.H. de, D.R. van, H. Maj, Handbook on life cycle assessment operational guide to the ISO standards, Int. J. Life Cycle Assess. 2002 75. 7 (2002) 311–313. https://doi.org/10.1007/BF02978897.

[105] AspenTech, Aspen Plus user models, (n.d.). https://www.aspentech.com/en.

[106] A.T. Talwalkar, IGT/DOE coal-conversion systems technical data book, 1981.

[107] R.L. Diaz, J C; Braun, Process simulation model for a staged, fluidized-bed oil-shale retort with lift-pipe combustor (Technical Report) | OSTI.GOV, 1984.

[108] AspenTech, Aspen Plus model for oil shale retorting process, (2010).

[109] V. V. Kelkar, K.M. Ng, Development of fluidized catalytic reactors: Screening and scale-up, AIChE J. 48 (2002) 1498–1518. https://doi.org/10.1002/AIC.690480714.

[110] M. Rüdisüli, T.J. Schildhauer, S.M.A. Biollaz, J.R. Van Ommen, Scale-up of bubbling fluidized bed reactors — A review, Powder Technol. 217 (2012) 21–38. https://doi.org/10.1016/J.POWTEC.2011.10.004.

[111] S.M. Walas, J.R. Couper, Chemical Process equipment, Second, Elsevier Ltd, 2005.

[112] M. Ringer, V. Putsche, J. Scahill, Large-Scale Pyrolysis Oil Production: A Technology Assessment and Economic Analysis, 2006. NREL/TP-510-37779.

[113] O. Williams, C. Eastwick, S. Kingman, D. Giddings, S. Lormor, E. Lester, Investigation into the applicability of Bond Work Index (BWI) and Hardgrove Grindability Index (HGI) tests for several biomasses compared to Colombian La Loma coal, Fuel. 158 (2015) 379–387. https://doi.org/10.1016/J.FUEL.2015.05.027.

[114] D. Kunii, O. Levenspiel, Fluidization Engineering, 2nd ed., Butterworth-Heinemann, 1991.

[115] H.S. Fogler, Elements of chemical engineering, 2020. http://websites.umich.edu/~elements/12chap/html/12prof2a.htm (accessed August 17, 2021).

[116] T.E. Broadhurst, H.A. Becker, Onset of fluidization and slugging in beds of uniform particles, AIChE J. 21 (1975) 238–247. https://doi.org/10.1002/AIC.690210204.

[117] C.Y. Wen, Y.H. Yu, A generalized method for predicting the minimum fluidization velocity, AIChE J. 12 (1966) 610–612. https://doi.org/10.1002/aic.690120343.

[118] F. Nugrahany, Modelling of Biomass Pyrolysis with Ex-situ Catalytic Upgrading for Bio-crude Production, (2018). http://urn.kb.se/resolve?urn=urn:nbn:se:kth:diva-231489 (accessed October 18, 2021).

[119] P. Srikhirin, S. Aphornratana, S. Chungpaibulpatana, A review of absorption refrigeration technologies, Renew. Sustain. Energy Rev. 5 (2000) 343–372. https://doi.org/10.1016/S1364-0321(01)00003-X.

[120] P.A. Domanski, A. Prabhakar, Theoretical Evaluation of the Vapor Compression Cycle With a Liquid-Line/ Suction-Line Heat Exchanger, Economizer, and Ejector, 1995. https://citeseerx.ist.psu.edu/viewdoc/download?doi=10.1.1.600.603&rep=rep1&type=pdf (accessed May 27, 2021).

[121] G.G. Maidment, R.M. Tozer, Combined cooling heat and power in supermarkets, in: Appl. Therm. Eng., Pergamon, 2002: pp. 653–665. https://doi.org/10.1016/S1359-4311(01)00117-X.

[122] N. Grioui, K. Halouani, A. Zoulalian, F. Halouani, Thermochemical modeling of isothermal carbonization of thick wood particle - Effect of reactor temperature and wood particle size, Energy Convers. Manag. 48 (2007) 927–936. https://doi.org/10.1016/j.enconman.2006.08.003.

[123] France electricity prices, September 2020 | GlobalPetrolPrices.com, (n.d.). https://www.globalpetrolprices.com/France/electricity_prices/ (accessed April 26, 2021).

[124] H. Yang, S. Kudo, H.-P. Kuo, K. Norinaga, A. Mori, O. Mašek, J. Hayashi, Estimation of Enthalpy of Bio-Oil Vapor and Heat Required for Pyrolysis of Biomass, Energy and Fuels. 27 (2013) 2675–2686. https://doi.org/10.1021/EF400199Z.

Annex I

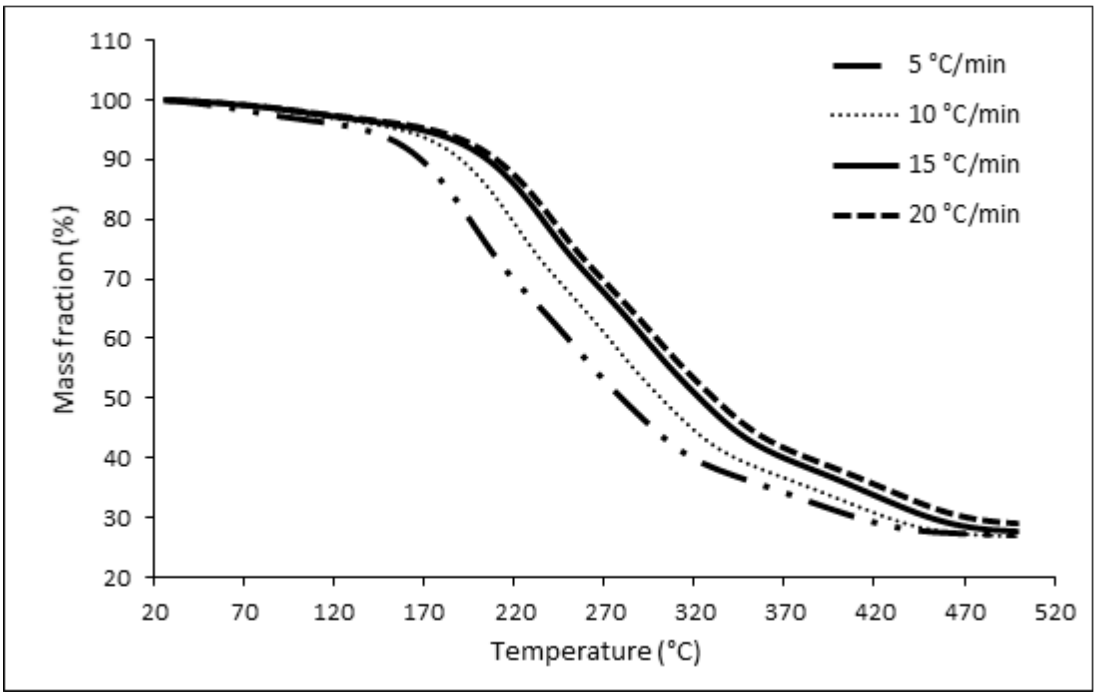

TG curve

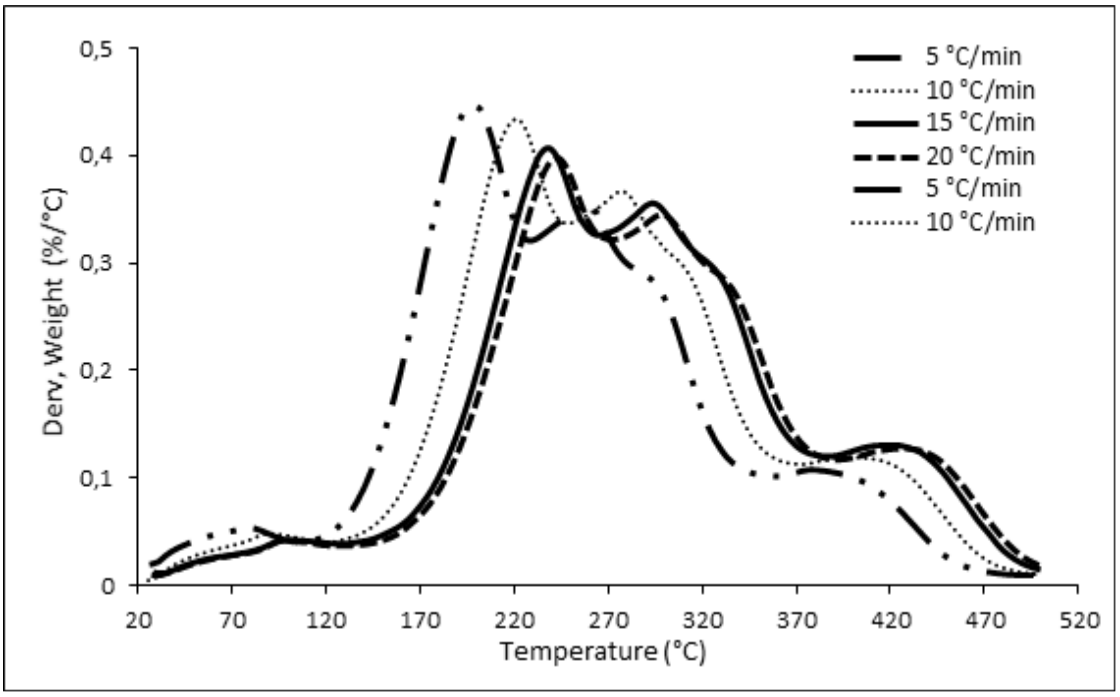

DTG curve

Annex II

```
C     User Kinetics Subroutine for RCSTR.


      SUBROUTINE PYROLKIN (SOUT,   NSUBS,  IDXSUB,   ITYPE,  NINT,
     2                     INT,    NREAL,  REAL,     IDS,    NPO,
     3                     NBOPST, NIWORK, IWORK,    NWORK,  WORK,
     4                     NC,     NR,     STOIC,    RATES,  FLUXM,
     5                     FLUXS,  XCURR,  NTCAT,    RATCAT, NTSSAT,
     6                     RATSSA, KCALL,  KFAIL,    KFLASH, NCOMP,
     7                     IDX,    Y,      X,        X1,     X2,
     8                     NRALL,  RATALL, NUSERV,   USERV,  NINTR,
     9                     INTR,   NREALR, REALR,    NIWR,   IWR,
     *                     NWR,    WR,     NRL,      RATEL,  NRV,
     1                     RATEV)


C-----------------------------------------------------------------------
C     OMWS pyrolysis is expressed as a single nth-order reaction:
C
C                  RK = K * FK0 * (FK/FK0)**N
C
C     Where:
C     RK   = OMWS reaction rate, kg/m**3·s.
C     K    = reaction rate, 1/s. In this model, K = 2.55E4*EXP(-8367.09/T),
C                               where T is temperature in kelvin.
C     FK0 = original OMWS concentration, kg/m**3.
C      FK   = OMWS concentration, kg/m**3 .
C     N    = reaction order. N = 1.0 in this model.
C
C
C     The subsequent production of each product from OMWS pyrolysis is
```

```
C     calculated by means of stoichiometric factors:
C
C                  Ri = Fi * RK
C
C     Where:
C     Fi  = stoichiometric factor of ith product, kg of ith product/kg OMWS.
C     Ri  = reaction rate of ith product, kg of ith product/m**3·s.
C
C
C     The Fi for each product used in this model is modified based on the data
C     reported by Agblevor et. al.:
C
C
C-----------------------------------------------------------------------

      IMPLICIT NONE
C
C     DECLARE VARIABLES USED IN DIMENSIONING
C
      INTEGER NSUBS, NINT,   NPO,   NIWORK, NWORK,
     +        NC,    NR,     NTCAT, NTSSAT, NCOMP,
     +        NRALL, NUSERV, NINTR, NREALR, NIWR,
     +        NWR
C
#include "ppexec_user.cmn"
      EQUIVALENCE (RMISS, USER_RUMISS)
      EQUIVALENCE (IMISS, USER_IUMISS)
#include "dms_ncomp.cmn"
#include "rxn_rcstrr.cmn"
#include "rxn_rprops.cmn"
      EQUIVALENCE (TEMP,  RPROPS_UTEMP )
      EQUIVALENCE (PRES,  RPROPS_UPRES )
      EQUIVALENCE (VFRAC, RPROPS_UVFRAC)
      EQUIVALENCE (BETA,  RPROPS_UBETA )
      EQUIVALENCE (VVAP,  RPROPS_UVVAP )
```

```
      EQUIVALENCE (VLIQ,  RPROPS_UVLIQ )
      EQUIVALENCE (VLIQS, RPROPS_UVLIQS)
       EQUIVALENCE (B(1),  IB(1)        )
C
#include "pputl_ppglob.cmn"
#include "dms_maxwrt.cmn"
#include "dms_plex.cmn"

C     DECLARE ARGUMENTS
C
      INTEGER IDXSUB(NSUBS), ITYPE(NSUBS),  INT(NINT),  IDS(2),
     +        NBOPST(6,NPO), IWORK(NIWORK), IDX(NCOMP), INTR(NINTR),
     +        IWR(NIWR),     NREAL,         KCALL,      KFAIL,
     +        KFLASH,        NRL,           NRV,        I,
     +        IMISS,         KDIAG,         KV,         KER,
     +        DMS_IFCMNC,    LMW,           LMWI
C
      REAL*8  SOUT(1),       WORK(NWORK),   STOIC(NC,NSUBS,NR),
     +        RATES(1),      FLUXM(1),      FLUXS(1),   RATCAT(NTCAT),
     +        RATSSA(NTSSAT),Y(NCOMP),      X(NCOMP),   X1(NCOMP),
     +        X2(NCOMP)
C
      REAL*8  RATALL(NRALL), USERV(NUSERV), REALR(NREALR),
     +        WR(NWR),       RATEL(1),      RATEV(1),   XCURR,
     +        XMW(1),        B(1),          TEMP,       PRES
C
      REAL*8  REAL(NREAL),   RMISS,         XLEN,       DIAM,
     +        VFRAC,         BETA,          VVAP,       VLIQ,
     +        VLIQS,         VMXV,          DVMX
C
      REAL*8  FACTH2,    FACTH2O,   FACTH2S,   FACTNH3,   FACTCO,
     +        FACTCO2,   FACTCH4,   FACTC2H6,  FACTC3H8,  FACTC4H10,
     +        FACTDOD,   FACTCHAR,  FKO,       CKO,       T,
     +        FK,        VBED,      VOLR,      K,         ROMWS,
     +        FACTDEC,   FACTCRE,   FACTCEN,   FACTCAN,   FACTPHE,
```

```
     +        FACTNOL,   FACTHEX,   FACTTET,   FACTRAD,   FACTPEN,
     +        FACTTRI,   FACTHEP,   FACTTAD,   FACTNAD,   FACTPAL,
     +        FACTTRC,   FACTETH,   FACTBUT,   FACTHED,
C
      REAL*8  RH2,       RH2O,      RH2S,      RNH3,      RCO,
     +        RCO2,      RCH4,      RC2H6,     RC3H8,     RC4H10,
     +        RDOD,      RCHAR,     RDEC,      RCRE,      RCEN,
     +        RCAN,      RPHE,      RTRI,      RNOL,      RHEX,
     +        RTET,      RRAD,      RPEN,      RHEP,      RTAD
     +        RNAD,      RPAL,      RTRC,      RETH,      RBUT
     +        RHED

C
C     BEGIN EXECUTABLE CODE

C-------------------------------------------------------------------------------
C     INPUT DATA

C     STOICHIOMETRIC FACTOR FOR EACH PYROLYSIS COMPONENT (KG EACH COMPONENT/KG OMWS)
      FACTH2   = 0.005569
       FACTH2O  = 0.088
       FACTH2S  = 0
       FACTNH3  = 0
       FACTCO   = 0.015385
       FACTCO2  = 0.203082
       FACTCH4  = 0.004144
       FACTC2H6 = 0.01295
       FACTC3H8 = 0.01295
       FACTC4H10= 0.004921
       FACTDOD  = 0.0076
      FACTDEC  = 0.0075
      FACTCRE  = 0.0053
      FACTCEN  = 0.013
      FACTCAN  = 0.0092
      FACTPHE  = 0.0059
```

```
      FACTTRI  = 0.013
       FACTNOL  = 0.027
       FACTHEX  = 0.0177
       FACTTET  = 0.027
       FACTRAD  = 0.012
       FACTPEN  = 0.01
       FACTHEP  = 0.048
       FACTTAD  = 0.037
       FACTNAD  = 0.021
       FACTPAL  = 0.01
       FACTTRC  = 0.03
       FACTETH  = 0.028
       FACTBUT  = 0.007
       FACTHED  = 0.01
       FACTCHAR = 0.299


       FKO      = 0.0192
       CKO      = 850
C-------------------------------------------------------------------------------


C     RETRIEVE REACTION TEMPERATURE (K) AND LEFT OMWS FLOW RATE (KG/S)
       T        = SOUT(IDXSUB(1)-1+NCOMP_NCC+2)
       FK       = SOUT(IDXSUB(3)-1+1)


C     RETRIEVE VOID FRACTION AND REACTOR VOLUME (M**3)
      VBED     = RCSTRR_VFRRC
      VOLR     = RCSTRR_VOLRC


C      RETRIVE MOLECULAR WEIGHT OF EACH COMPONENT (KG/KMOL)
       LMW      =  DMS_IFCMNC('MW')
       DO I     =  1,NCOMP_NCC
```

```
          LMWI   =  LMW+I
          XMW(I) =  B(LMWI)
         END DO


C      TOTAL PYROLYSIS RATE OF OMWS (KG OMWS/M**3 SHALE/S)
       K        = 2.55E4*EXP(-8367.09/T)
        ROMWS = K * CKO * (FK/FKO)**1


C      REACTION RATE OF EACH COMPONENT (CONVENTIONAL: KMOL/S; NONCONVENTIONAL: KG/S)
        RH2      =  ROMWS * FACTH2    / XMW(3)  * (1.0-VBED) * VOLR
        RH2O     =  ROMWS * FACTH2O   / XMW(4)  * (1.0-VBED) * VOLR
        RH2S     =  ROMWS * FACTH2S   / XMW(6)  * (1.0-VBED) * VOLR
        RNH3     =  ROMWS * FACTNH3   / XMW(7)  * (1.0-VBED) * VOLR
        RCO      =  ROMWS * FACTCO    / XMW(9)  * (1.0-VBED) * VOLR
        RCO2     =  ROMWS * FACTCO2   / XMW(10) * (1.0-VBED) * VOLR
        RCH4     =  ROMWS * FACTCH4   / XMW(11) * (1.0-VBED) * VOLR
        RC2H6    =  ROMWS * FACTC2H6  / XMW(12) * (1.0-VBED) * VOLR
        RC3H8    =  ROMWS * FACTC3H8  / XMW(13) * (1.0-VBED) * VOLR
        RC4H10   =  ROMWS * FACTC4H10 / XMW(14) * (1.0-VBED) * VOLR
        RDOD     =  ROMWS * FACTDOD   / XMW(15) * (1.0-VBED) * VOLR
        RDEC     =  ROMWS * FACTDEC   / XMW(16) * (1.0-VBED) * VOLR
        RCRE     =  ROMWS * FACTCRE   / XMW(17) * (1.0-VBED) * VOLR
        RCEN     =  ROMWS * FACTCEN   / XMW(18) * (1.0-VBED) * VOLR
        RCAN     =  ROMWS * FACTCAN   / XMW(19) * (1.0-VBED) * VOLR
        RPHE     =  ROMWS * FACTPHE   / XMW(20) * (1.0-VBED) * VOLR
        RTRI     =  ROMWS * FACTTRI   / XMW(21) * (1.0-VBED) * VOLR
        RNOL     =  ROMWS * FACTNOL   / XMW(22) * (1.0-VBED) * VOLR
        RHEX     =  ROMWS * FACTHEX   / XMW(23) * (1.0-VBED) * VOLR
        RPEN     =  ROMWS * FACTPEN   / XMW(24) * (1.0-VBED) * VOLR
        RHEP     =  ROMWS * FACTHEP   / XMW(25) * (1.0-VBED) * VOLR
        RTAD     =  ROMWS * FACTTAD   / XMW(26) * (1.0-VBED) * VOLR
        RNAD     =  ROMWS * FACTNAD   / XMW(27) * (1.0-VBED) * VOLR
        RPAL     =  ROMWS * FACTPAL   / XMW(28) * (1.0-VBED) * VOLR
```

```
      RTRC     =  ROMWS * FACTTRC   / XMW(29) * (1.0-VBED) * VOLR
      RETH     =  ROMWS * FACTETH   / XMW(30) * (1.0-VBED) * VOLR
      RBUT     =  ROMWS * FACTBUT   / XMW(31) * (1.0-VBED) * VOLR
      RHED     =  ROMWS * FACTHED   / XMW(32) * (1.0-VBED) * VOLR
      RTRI     =  ROMWS * FACTTRI   / XMW(33) * (1.0-VBED) * VOLR
      RTRI     =  ROMWS * FACTTRI   / XMW(34) * (1.0-VBED) * VOLR
      RCHAR    =  ROMWS * FACTCHAR * (1.0-VBED) * VOLR
      ROMWS = -ROMWS * (1.0-VBED) * VOLR

C     WRITE(MAXWRT_MAXBUF(1),200) XMW(15)
C 200 FORMAT(1X,"XMW=",F11.5)
C     CALL DMS_WRTTRM(1)


C     INITIALIZE RATES
      DO 100 I = 1, NC
        RATES(I) = 0D0
 100  CONTINUE


C     REACTION RATE OF COMPONENTS

C     MIXED COMPONENTS
       RATES(1)  = 0.0D0

       RATES(2)  = 0.0D0

       RATES(3)  = RH2

       RATES(4)  = RH2O

       RATES(5)  = 0.0D0

       RATES(6)  = RH2S
```

```
 RATES(7)  = RNH3

 RATES(8)  = 0.0D0

 RATES(9)  = RCO

 RATES(10) = RCO2

 RATES(11) = RCH4

 RATES(12) = RC2H6

 RATES(13) = RC3H8

 RATES(14) = RC4H10

 RATES(15) = RDOD

RATES(16) = RDEC

RATES(17) = RCRE

RATES(18) = RCEN

RATES(19) = RCAN

RATES(20) = RPHE

RATES(21) = RTRI

RATES(22) = RNOL

RATES(23) = RHEX

RATES(24) = RTET
```

```
      RATES(25) = RRAD

      RATES(26) = RPEN

      RATES(27) = RHEP

      RATES(28) = RTAD

      RATES(29) = RNAD

      RATES(30) = RPAL

      RATES(31) = RTRC

      RATES(32) = ETH

      RATES(33) = RBUT

      RATES(34) = RHED


C     CISOLID COMPONENTS
       RATES(NCOMP_NCC+35)  = 0.0D0

       RATES(NCOMP_NCC+36)  = 0.0D0

       RATES(NCOMP_NCC+37)  = 0.0D0

       RATES(NCOMP_NCC+38)  = 0.0D0

       RATES(NCOMP_NCC+39)  = 0.0D0

       RATES(NCOMP_NCC+40)  = 0.0D0

       RATES(NCOMP_NCC+41)  = 0.0D0
```

```
      RATES(NCOMP_NCC+42)  = 0.0D0

      RATES(NCOMP_NCC+43)  = 0.0D0

      RATES(NCOMP_NCC+44)  = 0.0D0

      RATES(NCOMP_NCC+45)  = 0.0D0

C     NONCONVENTIONAL COMPONENTS
      RATES(NCOMP_NCC*2+1) = ROMWS

      RATES(NCOMP_NCC*2+2) = RCHAR

      RETURN
      END
```

Annex III

Dryer

Mass flow rate of dry solids (W_s)	=	1.04	(kg/s)
Moisture content of entering solids, dry basis (X_i)	=	0.11	kg/kg
Moisture content of exiting solids, dry basis	=	0.042	kg/kg
Inlet temperature of solids	=	20	℃
Outlet temperature of solids	=	50	℃
Mass flow rate of dry gas	=	5.56	kg/s
Absolute humidity of inlet gas	=	0.01	kg/kg
Inlet temperature of gas	=	120	℃
Outlet temperature of gas	=	70	℃
Ambient Temperature	=	20	℃
Specific heat of gas	=	1.01	kJ/kg.K
Specific heat of vapor in gas	=	1.9	kJ/kg.K
Specific heat of dry solids	=	1.5	kJ/kg.K
Specific heat of liquid (moisture) in solids	=	4.18	kJ/kg.K

From eq. 2.9, absolute humidity of exhaust gas can be calculated as

Absolute humidity of exhaust gas (Y_o)	=	0.023	kg/kg

From eq. 2.11 and 2.12, enthalpy of solids and gases can be calculated as

Enthalpy of inlet of gas	=	150.50	kJ/kg
Enthalpy of outlet gas	=	132.94	kJ/kg
Enthalpy of gas at ambient	=	47.49	kJ/kg
Enthalpy of inlet solids	=	59.28	kJ/kg
Enthalpy of outlet solids	=	133.86	kJ/kg

Eq. 2.10 gives the wall heat losses

Wall heat loss (Q_{wl})	=	20.07	kW

Finally, minimum heat provided by heater can be calculated from equation 2.13.

Minimum heat provided by heater (Q_h)	=	486.58	kW

Annex IV

Enthalpy of LiBr-water solution

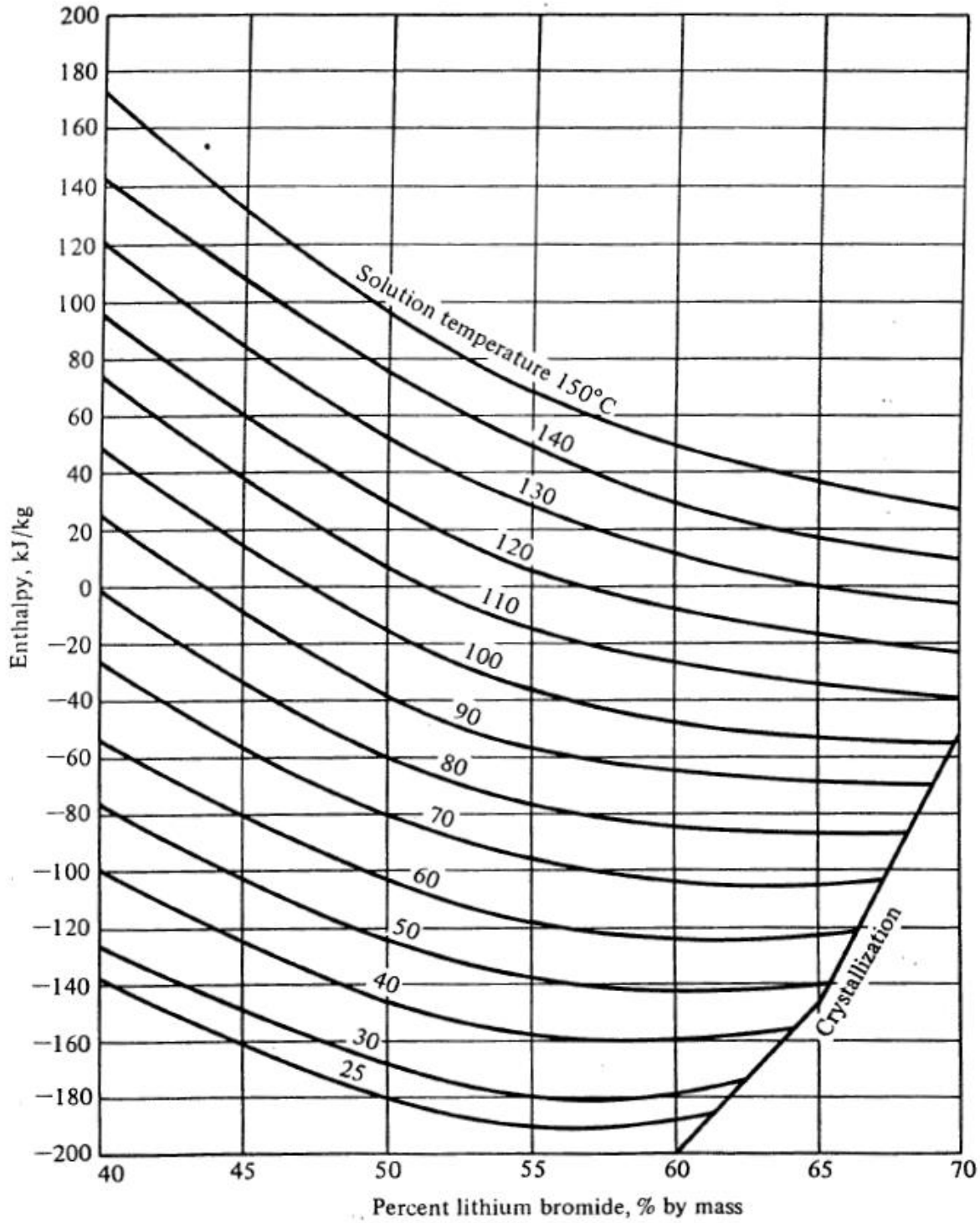

Annex V

Thermal properties of bio-oil at 40°C (liquid), 400°C (vapor) and 1 bar

Formula	Name	MW	Latent heat of vaporization	C_p (Liquid)	C_p (Vapor)	Boiling Point
		g/mol	kJ/mol	kJ/kg.K	kJ/kg.K	°C
$C_{10}H_{20}$-5	1-DECENE	140.27	39.60	2.07	2.93	170.60
C_7H_8O-5	P-CRESOL	108.14	47.67	1.79	2.17	201.98
$C_{11}H_{22}$-2	1-UNDECENE	154.30	41.92	2.06	2.93	192.67
$C_{11}H_{24}$	N-UNDECANE	156.31	41.90	2.11	3.04	195.93
$C_8H_{10}O$-3	P-ETHYLPHENOL	122.17	50.87	1.79	2.26	217.99
$C_{13}H_{26}$-2	1-TRIDECENE	182.35	46.31	2.06	2.95	232.84
$C_{13}H_{28}O$	1-TRIDECANOL	200.36	52.50	2.03	2.90	280.25
$C_{16}H_{34}$	N-HEXADECANE	226.45	51.85	2.07	3.04	286.86
$C_{14}H_{28}$-2	1-TETRADECENE	196.38	48.47	2.05	2.95	251.10
$C_{14}H_{30}$	N-TETRADECANE	198.39	48.16	2.08	3.04	253.58
$C_{15}H_{32}O$	1-PENTADECANOL	228.42	54.82	2.02	2.91	310.75
$C_{17}H_{36}$	N-HEPTADECANE	240.47	54.01	2.07	3.03	302.15
$C_{17}H_{34}$-D_1	1-HEPTADECENE	238.46	51.88	2.03	2.97	300.33
$C_{19}H_{40}O$	1-NONADECANOL	284.53	59.86	2.00	2.93	361.95
$C_{16}H_{31}N$	PALMITONITRILE	237.43	57.60	1.98	2.86	344.87
$C_{18}H_{33}N$	TRICYCLOHEXYLAMINE	263.47	57.30	1.70	2.81	344.28
$C_{20}H_{38}O_2$-N_1	ETHYL-OLEATE	310.52	60.40	1.90	2.73	352.95
$C_{22}H_{42}O_2$-N_5	BUTYL-OLEATE	338.57	66.80	1.88	2.80	379.67
$C_{17}H_{34}O$	9-HEPTADECANONE	254.46	56.50	2.05	2.90	313.72

Specific heat capacity of gases at 40°C, 400°C and 1 bar

Formula	Name	C_p 40°C	C_p 400°C
		kJ/kg.K	kJ/kg.K
H_2	HYDROGEN	14.125	14.675
CO	CARBON MONOXIDE	1.04	1.1
CO_2	CARBON DIOXIDE	0.86	1.11
CH_4	METHANE	2.25	3.50
C_2H_6	ETHANE	1.83	3.20
C_3H_8	PROPANE	1.75	3.17
C_4H_{10}	BUTANE	1.75	3.15